PROGRESS REPORT SUBMITTED BY SJ GATLEY FOR GRANT TITLED

RADIOTRACERS FOR LIPID SIGNALING PATHWAYS IN BIOLOGICAL SYSTEMS

AWARDED BY THE US DEPARTMENT OF ENERGY

PERSONNEL

Northeastern University

SJ Gatley, PhD
RD Duclos, PhD
K Hu (nee Qian) (PhD program completed August 2016)
S Sonti (PhD program to be completed Dec 2016)

B&W Hospital, Boston MA; later, Mayo Clinic, Rochester MN

TR DeGrado, PhD
M Pandey, PhD

Peer-reviewed publications

Johnston M, Bhatt SR, Sikka S, Mercier RW, West JM, Makriyannis A, Gatley SJ, Duclos RI Jr. Assay and inhibition of diacylglycerol lipase activity. Bioorg Med Chem Lett. 2012 Jul 15;22(14):4585-92.

Duclos RI, Gatley SJ, Bhatt SR, Johnston M. The preparation of 2-O-[1'-C]arachidonoyl-1-O-stearoyl-sn-glycerol. J Labelled Comp Radiopharm. 2009Jun 1;52(8):324-326.

Duclos RI Jr, Johnston M, Vadivel SK, Makriyannis A, Glaser ST, Gatley SJ. A methodology for radiolabeling of the endocannabinoid 2-arachidonoylglycerol(2-AG). J Org Chem. 2011 Apr 1;76(7):2049-55.

Pandey MK, DeGrado TR, Qian K, Jacobson MS, Hagen CE, Duclos RI Jr, Gatley SJ.Synthesis and preliminary evaluation of N-(16-^{18}F-fluorohexadecanoyl)ethanolamine(^{18}F-FHEA) as a PET probe of N-acylethanolamine metabolism in mouse brain. ACS Chem Neurosci. 2014 Sep 17;5(9):793-802.

Kun Hu, Shilpa Sonti, Sherrye Glaser, Richard Duclos, Samuel Gatley. BRAIN UPTAKE AND METABOLISM OF THE ENDOCANNABINOID ANANDAMIDE LABELED IN EITHER THE ARACHIDONOYL OR ETHANOLAMINE MOIETY. (submitted to Nuclear Medicine and Biology, Aug 2016)

Meeting abstracts

Gatley SJ et al. Brain transport and metabolism studies with 2-arachidonoylethanolamine and fatty acid ethanolamides. International Cannabinoid Research Society. Geneva, Illinois, July 2011.

Pandy M et al. Design and synthesis of N-(16-[^{18}F]fluorohexadecanoyl)ethanolamide as an endocannabinoid PET probe in animals and plants. Society for Nuclear Medicine (Abstract #1327147) Miami Beach, FL 2012.

Sonti, S, Gatley SJ et al. Brain regional uptake of radiolabel from carbon-14 labeled endocannabinoids. Abstract # 404.19/GGG19. Society for Neurosciences, Annual Meeting 2012, New Orleans, October 13-17.

Qian, K, Gatley SJ et al. A potential PET radiotracer for fatty acid amide hydrolase activity in the brain. Abstract # 639.25/C26. Society for Neurosciences, Annual Meeting 2012, New Orleans, October 13-17.

Gatley SJ et al. Fluoropalmitoylethanolamine distribution and its potential as a PET tracer. SFN, 2014.

Sonti S et al. Docosahexaenoic acid and its ethanolamide in the brain: possible role in early development and neuroprotection of the dopaminergic system. SFN, 2014.

Qian K et al. Brain Distribution Pattern of Radiolabel from Carbon-14 Labeled Anandamide SFN, 2014.

General.

The primary focus of this project continues to be the development of radiotracers and radiotracer methodology for studying physiology and biochemistry. The compounds that have been labeled areacylethanolamines and acylglycerols that are, as classes, represented in both in plants and in animals. In the latter, some of these act as ligands for cannabinoid receptors and they are therefore known as endocannabinoids. Cannabinoid receptors are not found in plant genomes so that plants must contain other receptors and signaling systems that use acylethanolamines. Relatively little work has been done on that issue, though acylethanolamines do modulate plant growth and stress resistance, thus possessing obvious relevance to agriculture and energy production.

Progress has been described in five peer-reviewed papers and seven meeting abstracts.

Preparation of 2-acylglycerol lipid messengers in high purity.

A novel enzymatic synthesis was developedthat gave pure 2-acylglycerols free of any rearrrangement to the thermodynamically more stable 1(3)-acylglycerol byproducts. The method utilized 1,3-dibutyryl-2-acylglycerol substrate ethanolysis by a resinimobilized lipase. Thus, pure radiolabeled 2-acylglycerols can now be conveniently prepared just prior to their utilization. These synthetic studies were published in the Journal of Medicinal Chemistry, 2011. Diacylglycerol lipase assay methodology. Diacylglycerol lipases (DAGLs) generate 2-acylglycerols, and are thus potential targets for disease- or growth-modifying agents, by means of reducing formation of 2-acylglycerols. A radioTLC assay of the hydrolysis of radiolabeled diglyceride substrate [1''-carbon-14]2-arachidonoyl-1-stearoyl-sn-glycerol has been implemented, and used to validate a novel, potentially highthroughput fluorescence resonance energy transfer (FRET) based assay. A number of new DAGL inhibitors that have selectivity for DAGLs were synthesized and screened. This work was very recently published in Bioorganic and Medicinal Chemistry Letters.Acylethanolamines. The work initially focused on myristoylethanolamine (MEA) labeled in the acyl moiety with tritium and with carbon-14. Standard coupling conditions were used and gave the desired radiotracers in decent yields. Tritiated product was needed for the search for binding sites of this signaling messenger, and C-14 labeled product for imaging using phosphorimaging screens. Additionally, C-14 MEA was prepared labeled in the ethanolamine moiety.

Fluorine-18 labeled acylethanolamines.

A multi-step synthesis was performed to obtain unlabeled N-(16-fluorohexadecanoyl)ethanolamide for an HPLC standard via the precursor 16-bromo-N-[2[(tetrahydro-2Hpyran-2-yl)oxy]ethyl]hexadecanoylamide. Near-anhydrous F-18 and the bromo precursor (approximately 2-3 mg) in acetonitrile (0.5 ml) were heated with a PETWave microwave reactor for 10 min at 80 °C. F-18 incorporation was checked using silica-gel TLC (8:92 methanol/chloroform). Deprotection was carried out using TFA. The crude product was purified by semi-preparative ODS HPLC (80:20 AcN/ H2O). The product peak was diluted in water, concentrated on an SPE column, and eluted in 1 mL EtOH. F-18 incorporation to form the THP protected product was >90% with negligible side products observed. Deprotection and HPLC purification proceeded successfully with >99% radiochemical l purity. Brain distribution studies were done in mice. This work was presented at the Society of Nuclear Medicine meeting in June 2012.

Subsequent more detailed studies including whole body tissue distribution studies, microPET experiments and radiochromatographic studies were published in ACS Chemical Neurosciences in 2014.

Iodine-125 labeled acylethanolamines.

The precursor 12-bromo-N-[2[(tetrahydro-2H-pyran-2-yl)oxy]ethyl]dodecanoylamide was prepared and a 1 mg sample was subject to exchange labeling withradioiodide in refluxing acetonitrile for 1 hour. HPLC analysis as above indicated incorporation of about10% of the radioactivity into a compound with the expected retention time of the corresponding iodocompound. Treatment with TFA converted the radioactivity into a compound with the expected retentiontime of 12-iododododenanoyl ethanolamine.

Radiotracer studies in plants.

One of the aims of this funding was to follow up the studies of Tripathy et al. (Plant Physiol., 2003) who first reported high affinity binding sites for tritiated myristoylethanolamine in plants, and also reported blockage of these sites by the cannabinoid receptor antagonist AM281. Because plant genomes do not contain genes for cannabinoid receptors, this was an intriguing report. I-125 labeled AM281 was therefore prepared, to facilitate identification of binding sites for this compound in Arabodopsis thaliana plants. However, such sites could not be found, the binding studies were repeated in tobacco plants. Again, binding sites for AM281 were not found. Additionally, it has become evident that clear demonstration of binding sites for tritiated MEA is obscured by metabolic incorporation of radioactivity into plant tissues. Studies on this issue are being aggressively pursued. Binding methodologies used in experiments with animal tissues require modification for their optimal use with plant tissues.

Detailed studies of [^{14}C]myristoylethanolamine isotopomers and of [^{14}C]arachidonoylethanolamine isotopomers

Since the labeled compounds being prepared for experiments with plants may have utility in Nuclear Medicine, studies were conducted with some of these compounds in mice. The brain uptake of C-14 MEA labeled in either acyl or ethanolamine moiety was 3-4 fold higher than uptake of C-14 myristic acid or C-14 ethanolamine. Carrier MEA increased brain uptake. Autoradiographs of MEA showed regionally specific uptake, with somewhat different patterns for acyl and ethanolamine isotopomers. It is hypothesized that these labeled compounds might form the basis of autoradiographic imaging of regional activity of enzymes such as fatty acid amide hydrolase, which may regulate endocannabinoid tone in animals. Early results were presented at the 2011 ICRS meeting, and at the 2012 Society for Neurosciences. N-arachidonoylethanolamine is an endocannabinoid signaling messenger in animals and is known as “anandamide”. It is one of several families of signaling molecules derived from arachidonic acid, the principal omega-6 polyunsaturated fatty acids (PUFA’s) in animal species. Other derivatives of arachidonic acid include thromboxanes and prostaglandins. Full details of the studies with the ethanolamide isotopomers were a part of the PhD dissertation of Kun Hu (nee Qian), and were submitted for publication to Nuclear Medicine and Biology in August 2016.

Syntheses of [^{14}C]docosahexanoylethanolamine isotopomers and preliminary biological investigations

Docosahexaenoic acid (DHA) is the omega-3 PUFA that can be regarded in some respects as the counterpart of arachidonic acid in the omega-6 series. While arachidonic acid is pro-

inflammatory, DHA is anti-inflammatory, and foods high in DHA (or artificially enriched in DHA) are commonly regarded as promoting health. In contrast to the large literature on the N-ethanolamide of arachidonic acid (i.e. the endocannabinoid anandamide) as of now (9/25/2016) there are only six papers on the corresponding ethanolamide of DHA, and when our studies under this grant began there were none. Beneficial actions of endogenously produced DHAethanolamine ("synaptamide") have been indicated, and to help elucidate the possible roles of synaptamide, we have synthesized this molecule for the first time labeled with C-14 in either the ethanolamine moiety or the fatty acid moiety. Studies of the disposition of endogenously administered isotopomers of DHA-ethanolamine are in progress, to complement tissue culture experiments evaluation hypothesized protective effects of this DHA derivative.

ACS Chemical Neuroscience

Research Article

pubs.acs.org/chemneuro

Synthesis and Preliminary Evaluation of *N*-(16-^{18}F-Fluorohexadecanoyl)ethanolamine (^{18}F-FHEA) as a PET Probe of *N*-Acylethanolamine Metabolism in Mouse Brain

Mukesh K. Pandey,[†,§] Timothy R. DeGrado,*[,†,§] Kun Qian,[∥] Mark S. Jacobson,[†] Clinton E. Hagen,[‡] Richard I. Duclos, Jr.,[∥] and S. John Gatley*[,∥]

[†]Division of Nuclear Medicine, Department of Radiology, and [‡]Division of Biomedical Statistics and Informatics, Mayo Clinic, Rochester, Minnesota 55905, United States

[§]Brigham and Women's Hospital, Harvard Medical School, Boston, Massachusetts 02115, United States

[∥]Department of Pharmaceutical Sciences, Northeastern University, Boston, Massachusetts 02115, United States

Supporting Information

ABSTRACT: *N*-Acylethanolamines are lipid signaling molecules found throughout the plant and animal kingdoms. The best-known mammalian compound of this class is anandamide, *N*-arachidonoylethanolamine, one of the endogenous ligands of cannabinoid CB1 and CB2 receptors. Signaling by *N*-acylethanolamines is terminated by release of the ethanolamine moiety by hydrolyzing enzymes such as fatty acid amide hydrolase (FAAH) and *N*-acylethanolamine-hydrolyzing amidase (NAAA). Herein, we report the design and synthesis of *N*-(16-^{18}F-fluorohexadecanoyl)-ethanolamine (^{18}F-FHEA) as a positron emission tomography (PET) probe for imaging the activity of *N*-acylethanolamine hydrolyzing enzymes in the brain. Following intravenous administration of ^{18}F-FHEA in Swiss Webster mice, ^{18}F-FHEA was extracted from blood by the brain and underwent hydrolysis at the amide bond and incorporation of the resultant ^{18}F-fluorofatty acid into complex lipid pools. Pretreatment of mice with the FAAH inhibitor URB-597 (1 mg/kg IP) resulted in significantly slower ^{18}F-FHEA incorporation into lipid pools, but overall ^{18}F concentrations in brain regions were not altered. Likewise, pretreatment with a NAAA inhibitor, (*S*)-*N*-(2-oxo-3-oxytanyl)biphenyl-4-carboxamide (30 mg/kg IV), did not significantly affect the uptake of ^{18}F-FHEA in the brain. Although evidence was found that ^{18}F-FHEA behaves as a substrate of FAAH in the brain, the lack of sensitivity of brain uptake kinetics to FAAH inhibition discourages its use as a metabolically trapped PET probe of *N*-acylethanolamine hydrolyzing enzyme activity.

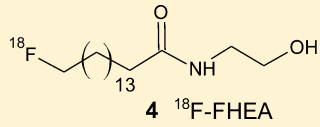

4 ^{18}F-FHEA

KEYWORDS: *Endocannabinoids, N-acylethanolamines, N-(16-^{18}F-fluorohexadecanoyl)ethanolamine, ^{18}F-FHEA, PET*

N-Acylethanolamines, including *N*-palmitoylethanolamine and *N*-arachidonoylethanolamine (anandamide), have diverse actions at cannabinoid receptors and other endocannabinoid systems. Their actions are terminated by fatty acid amide hydrolase (FAAH) and/or *N*-acylethanolamine-hydrolyzing amidase (NAAA). Changes in *N*-acylethanolamine levels and/or cannabinoid receptor (CB1/2) expression have been reported in many pathological states.[1,2] The three major areas of endocannabinoid actions are stress recovery and behavior,[1,2] energy balance through food regulation,[3] and immune and inflammatory regulation.[4] Endocannabinoid signaling may be dysregulated in a number of mental disorders, including bipolar disorder, depression, anxiety disorders, and dysfunctional response to chronic stress.[1,2,5−8] A noninvasive imaging method for monitoring *N*-acylethanolamine kinetics in the brain could have potential utility to help in our understanding of endocannabinoid processing. Of particular interest would be the potential for mapping of activity of *N*-acylethanolamine hydrolyzing enzymes (FAAH and NAAA) in various psychiatric and neurological disorders.

Wyffels et al.[9] reported development of single photon emission computed tomography (SPECT) imaging agents for evaluation of FAAH activity, whereby ^{123}I was substituted for the ethanolic hydroxyl group on *N*-linoleoylethanoamine and *N*-arachidonoylethanolamine (anandamide). The highest uptake values for ^{123}I-labeled *N*-(2-iodoethyl)linoleoylamide and *N*-(2-iodoethyl)arachidonylamide were reported to be 1.23% ID/g at 3 min and 0.58%ID/g at 10 min post-injection in brain, respectively, but no retention of radioactivity was observed.[9] These authors explained the lower uptake and poor retention in brain due to instability of the tracer. The same group modified their molecules to develop a series of compounds as aryl anandamide analogues.[10] Among those, two of them were labeled with ^{11}C to achieve positron emission tomography (PET) imaging agents.[10] On careful analysis, it is noted that these authors have again replaced the hydroxyl group of the ethanolamine component with substituents to develop aryl analogues of *N*-linoleoylethanoamine and *N*-arachidonoylethanolamine (anandamide). The highest brain uptake value was 1.44 ± 0.02%ID/g at 1 min post-injection, with continuous washout over time.[10] Furthermore, Wyffels et al.[11] labeled an

Received: December 4, 2013
Revised: July 8, 2014
Published: July 8, 2014

Scheme 1. Synthesis of *N*-(16-^{18}F-Fluorohexadecanoyl)ethanolamine (^{18}F-FHEA)[a]

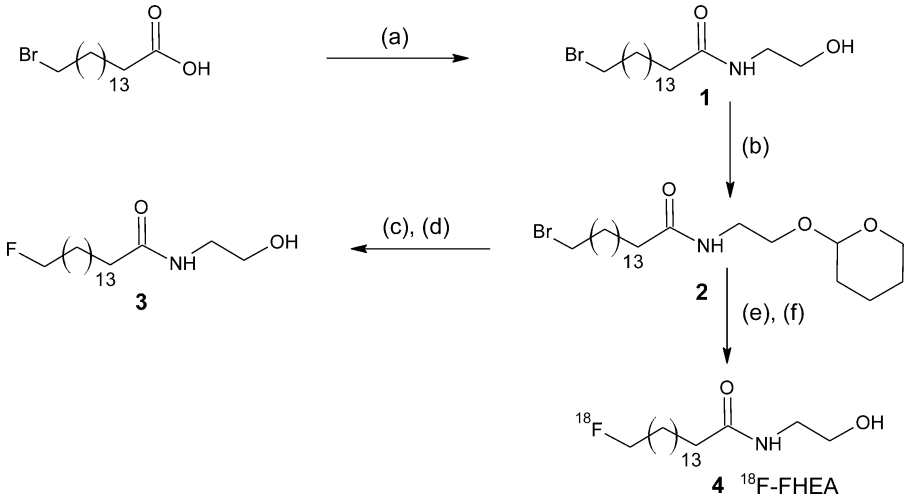

[a](a) Methyl chloroformate, ethanolamine, triethylamine, dichloromethane, 0 °C to RT; (b) 3,4-dihydro-2*H*-pyran, *p*-toluenesulfonic acid, dichloromethane, 12 h; (c) tetra-*n*-butylammonium fluoride, tetrahydrofuran; (d) aq methanol, *p*-toluenesulfonic acid; (e) K2.2.2, K^{18}F, K_2CO_3, microwave; (f) 15% trifluoroacetic acid solution, microwave.

analogue of the FAAH inhibitor URB-597 to map FAAH activity but the compound suffered extremely poor retention in brain. On the other hand, Glaser et al.[12] using ^{3}H-labeled anandamide found a brain uptake of 2.38 ± 0.22%ID at 5 min with retention in overall activity (both unmetabolized and metabolized) over time, indicating the importance of labeling position on the resulting brain kinetics following radiolabeled *N*-acylethanolamine hydrolysis.[12] In contrast to the work of Wyffels and co-workers[9,10] that labeled the ethanolamine component, we anticipated that labeling of the fatty acyl component would increase brain retention due to incorporation of the liberated fatty acid into various complex lipid pools. To support this notion, a different analogue of URB-597, [^{11}C]CURB, was developed by Wilson et al.,[13] which was labeled in a different position from that of Wyffels et al.[11] [^{11}C]CURB showed excellent preclinical in vivo results and is currently in human trials as [^{11}C]CURB.[13] [^{11}C]CURB is thought to be useful to measure the overall expression of FAAH in brain, as its metabolism by NAAA is relatively insignificant.

In the present approach, we anticipated that a radiotracer based on a close structural analogue of *N*-palmitoylethanolamine would be a substrate for both FAAH and NAAA.[14−17] FAAH has been studied in great detail,[1,18−20] but NAAA is relatively poorly understood.[15,16] NAAA was first reported in 1999, but in recent years it is being seen as an important enzyme in *N*-acylethanolamine metabolism.[15,16] NAAA is a lysosomal enzyme and shows highest activity at pH 4.5−5.0, whereas FAAH is a membrane-bound protein and exhibits highest activity at pH 8.5−10.[15] The Michaelis constant (K_m) for *N*-palmitoylethanolamine (PEA) against targeting enzymes FAAH and NAAA is 1.5 and 97 μM, respectively.[21,22]

We have previously conducted autoradiographic studies in mouse brain using ^{3}H-arachidonoylethanolamine (anandamide), and shown that regional disposition of label reflects incorporation into phospholipids of arachidonic acid liberated by FAAH.[12] To translate this methodology to PET, we have prepared and evaluated *N*-(16-^{18}F-fluorohexadecanoyl)-ethanolamine (^{18}F-FHEA), a structurally simpler compound than anandamide. While previous biological data on the nonradioactive form of FHEA itself is lacking, *N*-hexadecanoylethanolamine (palmitoylethanolamine) is a well-known FAAH substrate.[23,24] It has a very low affinity for cannabinoid receptors compared with anandamide, but higher affinity for peroxisome proliferator-activated receptor alpha (PPAR-alpha).[25,26] It possesses analgesic properties and is consumed as a "nutraceutical" for pain relief. In this study, we report on the radiosynthesis of ^{18}F-FHEA and initial brain uptake, biodistribution and metabolite analysis studies in mice.

RESULTS

Synthesis of ^{18}F-FHEA. Scheme 1 describes the synthesis of ^{18}F-FHEA (**4**). To synthesize the labeling precursor for ^{18}F-FHEA, 16-bromohexadecanoic acid was activated using methyl chloroformate and then reacted with ethanolamine in the presence of triethylamine to get *N*-(16-bromohexadecanoyl)-ethanolamine (**1**).[27] The obtained bromo-*N*-acylethanolamine **1** was treated with 3,4-dihydro-2*H*-pyran in the presence of *p*-toluenesulfonic acid in dichloromethane to obtain 16-bromo-*N*-[2[(tetrahydro-2*H*-pyran-2-yl)oxy]ethyl]hexadecanoylamide (**2**) as precursor for radiofluorination. The compound **2** served as precursor for radiofluorination. Before radiofluorination, compound **2** was treated with tetra-*n*-butylammonium fluoride in acetonitrile followed by deprotection using *p*-toluenesulfonic acid to obtain nonradioactive ^{19}F-FHEA (**3**) as a reference standard for HPLC.

The radiofluorination of the 16-bromo-*N*-[2[(tetrahydro-2*H*-pyran-2-yl)oxy]ethyl]hexadecanoylamide (**2**) using cyclotron-produced K^{18}F was carried out under microwave heating at 80 °C, 10 min as described previously.[28,29] Our recent use of a microwave reactor in nucleophilic radiofluorination of fatty acids[28,29] showed enhanced product yield with significant reduction in reaction time and side products.[29] Structural similarity of FHEA to those of the fatty acids gave us confidence on the application of radiofluorination of FHEA by incorporating a PETWave microwave reactor (CEM Corporation, Mathews NC) into a TRACERlab FXN Pro (GE HealthCare, Waukesha WI) radiosynthesis module during productions of ^{18}F-FHEA. Radiofluorination proceeded efficiently, with >90% incorporation of ^{18}F-fluoride into the corresponding amide. ^{18}F-Fluoro-*N*-[2[(tetrahydro-2*H*-pyran-

dx.doi.org/10.1021/cn400214j | ACS Chem. Neurosci. 2014, 5, 793−802

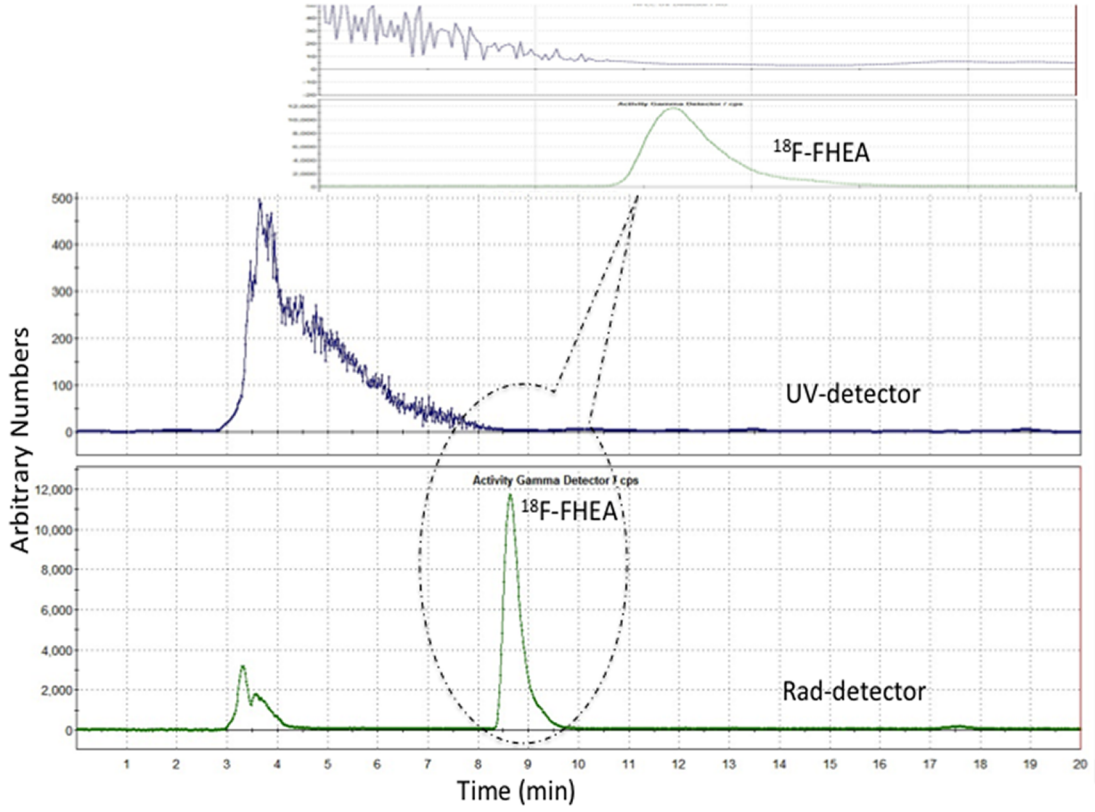

Figure 1. Preparative HPLC chromatogram of ^{18}F-FHEA.

2-yl)oxy]ethyl]hexadecanoylamide was quantitatively hydrolyzed by addition of 0.45 mL of 15% TFA (trifluoroacetic acid) aqueous solution and microwave heating (60 °C) for 5 min. The deprotected ^{18}F-FHEA product **4** was purified by semipreparative C-18 HPLC (80:20 ACN/H_2O, t_R = 7.3 min). Overall radiochemical yields after semipreparative HPLC isolation was in the range 12−21% decay-corrected. Radiochemical purity of the product (**4**) was >99% by radio-HPLC (Figure 1). The specific activity was estimated by measuring the minimum detection limit for nonradioactive FHEA as 5.2 μg using the preparative HPLC system. Based on this finding, we estimated the specific activity of ^{18}F-FHEA to be in the range of 1.4−5.1 Ci/μmol. The product was formulated in saline solution and passed through a sterile filter before administration to mice by tail-vein injection.

Synthesis of Nonradioactive Standards. The details for the synthesis of nonradioactive standards are described in the Supporting Information (Scheme SS1). The synthesized nonradioactive standards were utilized to identify possible labeled metabolites by HPLC/TLC. A separate synthetic route (Scheme SS1, Supporting Information) starting with omega hydroxy fatty ester was utilized because of two reasons: (1) to avoid use of the bromo precursor **2** for multiple step synthesis of nonradioactive standards and (2) to avoid the poor product yield of bromo to fluoro conversion.

Synthesis of NAAA Inhibitor. Due to the absence of a commercial source for a potent and selective NAAA inhibitor, we chose (*S*)-*N*-(2-oxo-3-oxytanyl)biphenyl-4-carboxamide (Compound 7h) as one of the most potent NAAA inhibitor reported in the literature with IC_{50} value 115 ± 13 nm (Scheme 2).[30] A multistep synthesis and characterization was carried out following the literature method described by Solorzano et al.[30] The synthesized NAAA inhibitor was formulated in dimethyl

Scheme 2. Chemical Structures of FAAH and NAAA Inhibitors

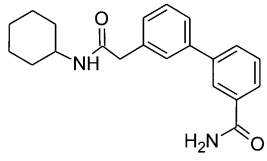

FAAH inhibitor URB597

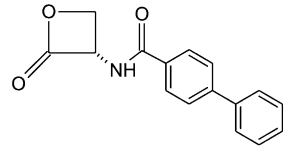

NAAA inhibitor- Compound 7h*

* Ref. 28, 29

sulfoxide/Cremophor/0.9% saline (20 μL/30 μL/150 μL) solutions. Each injection was 200 μL having 0.75 mg of NAAA inhibitor (20 mg/kg, Compound 7h). Although the same authors reported limited stability of Compound 7h in buffer (half-life of 12.6 ± 1.4 min at pH 7.4),[31] we reasoned that there would be sufficient stability to allow inhibition of NAAA following intravenous administration in mice.

Biodistribution and Brain Uptake Studies in Mice with and without FAAH Inhibitor. ^{18}F-FHEA's role in lipid signaling pathways and imaging potential were evaluated by measuring biodistribution and brain uptake in Swiss Webster mice. ^{18}F-FHEA uptake in brain regions as well as blood and urine were evaluated at five different time points between 1 and 60 min (Tables 1−3). Regional brain uptake was fairly constant from 1 to 60 min with the exception of the cortex, which differed over time ($p < 0.05$). The uptake differed across brain regions at each time point (Table 1). Urinal clearance was evident over time, while ^{18}F-FHEA in blood and whole brain remained (Table 2). Standardized uptake across all brain regions was statistically different at each time point. Concentrations in the hypothalamus ($p < 0.002$), thalamus (p

dx.doi.org/10.1021/cn400214j | ACS Chem. Neurosci. 2014, 5, 793−802

Table 1. Biodistribution (% ID/g) of ^{18}F-FHEA in Swiss Webster Mice Following Intravenous Administration[a]

tissue	1 min	5 min	15 min	30 min	60 min	*p*-value[b]
hypothalamus	2.88 ± 0.63	3.05 ± 0.47	2.04 ± 0.30[e]	2.13 ± 0.07	2.83 ± 0.90[e]	0.1276
ophthalmic tubules	3.21 ± 0.59	3.05 ± 0.43	2.54 ± 0.14[e]	2.55 ± 0.28	3.50 ± 1.33[e]	0.2261
hippocampus	2.55 ± 0.65[e]	2.52 ± 0.33	2.18 ± 0.03[e]	2.15 ± 0.35	3.09 ± 0.094[e]	0.3300
striatum	3.17 ± 0.55	2.92 ± 0.47	2.57 ± 0.23[e]	2.54 ± 0.35	3.78 ± 0.88[e]	0.1050
cerebellum	3.57 ± 0.69	3.42 ± 0.50	2.98 ± 0.22[e]	3.01 ± 0.37	4.21 ± 1.23[e]	0.1207
brain stem	3.63 ± 0.72	3.58 ± 0.56	2.95 ± 0.18[e]	2.66 ± 0.29	3.78 ± 1.18[e]	0.1011
cortex	3.61 ± 0.57	3.39 ± 0.52	2.87 ± 0.16[e]	2.90 ± 0.45	4.32 ± 1.37[e]	0.0455[d]
thalamus	3.30 ± 0.64	3.53 ± 0.47	2.64 ± 0.38[e]	2.45 ± 0.36	3.60 ± 0.99[e]	0.0697
whole brain	3.16 ± 0.76	3.14 ± 0.40	2.68 ± 0.22[e]	2.64 ± 0.30	3.69 ± 1.08[e]	0.2172
p-value[c]	<0.0001[d]	<0.0001[d]	<0.0001[d]	<0.0001[d]	<0.0001[d]	**overall model** <0.0001[d]

[a]Values are listed as mean ± standard deviation. There were 4 measurements for each time by body region category unless otherwise indicated. A random effects ANOVA was used to account for the repeated measurements (a measurement for each region) on each animal. Time was modeled as a between subject factor. There was a significant region by time interaction. [b]*p*-Values represent tests for differences in biodistribution across times. *p*-Values are not adjusted for multiple comparisons. [c]*p*-Values represent tests for differences in biodistribution across body regions. *p*-Values are not adjusted for multiple comparisons. [d]Statistically significant *p*-value. [e]$n = 3$.

Table 2. Comparison of Uptake (% ID/g) of ^{18}F-FHEA in Whole Brain, Blood, and Urine of the Swiss Webster Mice Following Intravenous Administration at Different Time Points[a]

tissue	1 min	5 min	15 min	30 min	60 min	*p*-value[b]
whole brain	3.16 ± 0.76	3.14 ± 0.40	2.68 ± 0.22[e]	2.64 ± 0.30	3.69 ± 1.08[e]	0.9997
blood	2.80 ± 0.77[e]	1.72 ± 0.20	1.43 ± 0.38[f]	2.29 ± 0.16	1.79 ± 0.16[e]	0.9994
urine	1.00 ± 1.95	29.83 ± 7.05	28.06 ± 1.59[f]	35.90 ± 12.44	43.60 ± 32.99[f]	<0.0001[d]
p-value[c]	0.8992	<0.0001[d]	0.0004[d]	<0.0001[d]	<0.0001[d]	**overall model** <0.0001[d]

[a]Values are listed as mean ± standard deviation. There were four measurements for each time by body region category unless otherwise indicated. A random effects ANOVA was used to account for the repeated measurements (a measurement for each region) on each animal. Time was modeled as a between subject factor. There was a significant region by time interaction. [b]*p*-Values represent tests for differences in biodistribution across times. *p*-Values are not adjusted for multiple comparisons. [c]*p*-Values represent tests for differences in biodistribution across body regions. *p*-Values are not adjusted for multiple comparisons. [d]Statistically significant *p*-value. [e]$n = 3$. [f]$n = 2$.

Table 3. Tissue/Whole Brain Ratios (T/WB) of uptake (% ID/g) of F-FHEA of the Swiss Webster Mice Following Intravenous Administration[a]

tissue	1 min	5 min	15 min[e]	30 min	60 min[e]	*p*-value[b]
hypothalamus	0.92 ± 0.08	0.97 ± 0.06	0.76 ± 0.06	0.81 ± 0.07	0.79 ± 0.27	0.0013[d]
ophthalmic tubules	1.03 ± 0.07	0.97 ± 0.06	0.95 ± 0.03	0.97 ± 0.04	0.93 ± 0.08	0.5597
hippocampus	0.75 ± 0.04[e]	0.80 ± 0.02	0.82 ± 0.05	0.81 ± 0.06	0.84 ± 0.01	0.9334
striatum	1.02 ± 0.14	0.93 ± 0.06	0.96 ± 0.03	0.96 ± 0.04	1.04 ± 0.06	0.2817
cerebellum	1.14 ± 0.07	1.09 ± 0.03	1.12 ± 0.01	1.14 ± 0.03	1.14 ± 0.03	0.8404
brain stem	1.16 ± 0.12	1.14 ± 0.06	1.10 ± 0.05	1.01 ± 0.02	1.02 ± 0.03	0.0219[d]
cortex	1.16 ± 0.10	1.08 ± 0.06	1.08 ± 0.07	1.09 ± 0.05	1.17 ± 0.10	0.3153
thalamus	1.05 ± 0.10	1.12 ± 0.04	0.99 ± 0.06	0.93 ± 0.07	0.98 ± 0.02	0.0059[d]
p-value[c]	<0.0001[d]	<0.0001[d]	<0.0001[d]	<0.0001[d]	<0.0001[d]	**overall model** <0.0001[d]

[a]Values are listed as mean ± standard deviation. There were four measurements for each time by body region category unless otherwise indicated. A random effects ANOVA was used to account for the repeated measurements (a measurement for each region) on each animal. Time was modeled as a between subject factor. There was a significant region by time interaction. [b]*p*-Values represent tests for differences in biodistribution across times. *p*-Values are not adjusted for multiple comparisons. [c]*p*-Values represent tests for differences in biodistribution across body regions. *p*-Values are not adjusted for multiple comparisons. [d]Statistically significant *p*-value. [e]$n = 3$.

< 0.006), and brain stem ($p < 0.03$) were different across time points (Table 3). The biodistribution data obtained at 30 min after intravenous administration of ^{18}F-FHEA are listed in Table 4. The effect of FAAH inhibitor on ^{18}F-FHEA uptake was evaluated by intraperitoneal administration of URB 597 (1 mg/kg) 60 min prior to the intravenous injection of ^{18}F-FHEA to the mice. Uptakes were examined by measuring percentage of injected dose per gram of the tissue (% ID/g) and standard uptake value (SUV). The biodistribution data showed that ^{18}F-FHEA was widely distributed throughout the body (Table 4). The only region that showed a significant effect of URB-597 was the bone: bone uptake in animals pretreated with URB-597 was significantly higher than that in controls (6.24 ± 11.30 SUV versus 0.62 ± 0.10, $p < 0.0001$). Typically, higher bone uptake of metabolizable ^{18}F-labeled radiotracers signifies higher metabolic release of free ^{18}F-fluoride.

To determine whether pretreatment with a FAAH-inhibitor altered the chemical form of ^{18}F in the brain, we conducted chloroform/methanol extractions (Folch-type)[28,32] of cerebellar tissue 5 min after administration of FHEA, followed by radio-TLC analysis of the chloroform fractions (Figure 2). There was no significant difference in the fraction of extracted ^{18}F-radioactivity found in the chloroform layer (80 ± 4% for controls, 86 ± 3% for URB-597 treated; $p = 0.07$, $n = 4$). The

dx.doi.org/10.1021/cn400214j | ACS Chem. Neurosci. 2014, 5, 793−802

Table 4. Uptake (% ID/g) and SUV of ^{18}F-FHEA in Swiss Webster Mice at 30 min Post-Injection[a]

tissue	%ID/g control mice	%ID/g URB treated Mice	%ID/g p-value[b]	SUV control mice	SUV URB treated mice	SUV p-value[b]
cortex	3.50 ± 0.82	2.89 ± 0.28	0.9039	0.90 ± 0.17	0.77 ± 0.10	0.9231
cerebellum	2.75 ± 1.73	2.68 ± 0.41	0.9899	0.70 ± 0.43	0.71 ± 0.08	0.9962
brain stem	3.04 ± 0.87	2.69 ± 0.42	0.9442	0.78 ± 0.20	0.71 ± 0.11	0.9595
thalamus	3.06 ± 0.63	2.68 ± 0.33	0.9401	0.79 ± 0.13	0.71 ± 0.08	0.9540
hypothalamus	2.85 ± 1.08	2.41 ± 0.29	0.9298	0.73 ± 0.24	0.64 ± 0.09	0.9468
olfactory tubercle	2.72 ± 0.61	2.60 ± 0.65	0.9809	0.70 ± 0.14	0.69 ± 0.19	0.9944
hippocampus	2.68 ± 0.72	2.16 ± 0.25	0.9176	0.69 ± 0.18	0.57 ± 0.08	0.9318
striatum	3.26 ± 0.79	2.45 ± 0.29	0.8710	0.84 ± 0.18	0.65 ± 0.10	0.8901
whole brain	2.83 ± 1.29	2.69 ± 0.20	0.9841	0.72 ± 0.30[d]	0.71 ± 0.06	0.9985
blood	2.32 ± 0.47	2.19 ± 0.31	0.9798	0.60 ± 0.12	0.58 ± 0.07	0.9876
urine	10.91 ± 4.78[d]	20.46 ± 17.99	0.0859	2.90 ± 1.26[d]	5.57 ± 5.01	0.0818
heart	5.19 ± 1.23	5.20 ± 1.87	0.9981	1.35 ± 0.32	1.37 ± 0.45	0.9865
lung	9.83 ± 3.84	5.13 ± 0.64[d]	0.3725	2.53 ± 0.90	1.33 ± 0.14[d]	0.4229
liver	15.07 ± 4.86	15.19 ± 1.86	0.9807	3.88 ± 1.07	4.04 ± 0.54	0.9119
spleen	2.94 ± 0.21	2.47 ± 0.22	0.9259	0.76 ± 0.03	0.66 ± 0.06	0.9386
kidney	12.89 ± 2.31	11.08 ± 1.64	0.7172	3.34 ± 0.45	2.93 ± 0.38	0.7728
testis	1.17 ± 0.27	0.80 ± 0.15	0.9418	0.30 ± 0.07	0.21 ± 0.05	0.9490
fat	3.14 ± 1.76	3.41 ± 1.74	0.9582	0.81 ± 0.43	0.91 ± 0.47	0.9421
bone	2.39 ± 0.48	22.56 ± 40.59	<0.0001[c]	0.62 ± 0.10	6.24 ± 11.30	<0.0001[c]
muscle	2.50 ± 0.40	2.74 ± 0.96	0.9621	0.65 ± 0.08	0.72 ± 0.23	0.9572
skin	1.29 ± 0.19	1.40 ± 0.22	0.9818	0.33 ± 0.04	0.37 ± 0.05	0.9785
overall model p-value		%ID/g URB < 0.0001[c]			SUV URB < 0.0001[c]	

[a]Values are listed as mean ± standard deviation. There were 4 measurements for each time by body region category unless otherwise indicated. [b]p-Value represents tests for differences in biodistribution across treatment groups. p-Values are not adjusted for multiple comparisons. [c]Statistically significant p-value. [d]n = 3.

chloroform fractions were subjected to silica gel TLC analysis using two different solvent systems to analyze both polar and nonpolar metabolites. The nonpolar solvent system comprised petroleum ether/diethyl ether/acetic acid (70:30:1, v/v), whereas the polar solvent system was made up of chloroform/methanol/ammonium hydroxide (60:30:1, v/v). In the nonpolar system, there was a large peak at the origin, and several smaller peaks, at Rf values of 0.16, 0.29, 0.36−0.37 (Figure 2a). On the basis of TLCs of nonradioactive standards and synthesized metabolites, the peaks were assigned as (1) polar lipid (PL) and FHEA, (2) diglyceride (DG), (3) fatty acid (FA), (4) triglyceride (TG), and (5) cholesterol ester (CE) (Figure 2a). In the polar solvent system, there was a small peak at the origin, and peaks at about 0.02, 0.05, 0.2, 0.25, 0.44−0.47, 0.83−0.86, and 0.97 Rf (Figure 2b). Based on reference standards, the metabolites 1−7 were assigned as (1) lysophosphatidyl choline (LPC) and lysophosphatidyl ethanolamine (LPE), (2) phosphatidyl choline (PC), (3) phosphatidyl ethanolamine (PE), (4) unknown (UNK), (5) fatty acid (FA), (6) FHEA, (7) diglyceride (DG) and triglyceride (TG) and cholesterol ester (CE) (Figure 2b). In the vehicle-treated animals, the peak at 0.05 Rf (PC) was most prominent, whereas in the FAAH inhibitor-treated animals nonmetabolized ^{18}F-FHEA was most prominent.

Biodistribution and Brain Uptake of *N*-(16-^{18}F-Fluorohexadecanoyl)ethanolamine (^{18}F-FHEA) in Swiss Webster Mice with and without NAAA Inhibitor. The effect of a NAAA inhibitor on ^{18}F-FHEA uptake was evaluated by intravenous administration of Compound 7h (30 mg/kg) 15 min prior to the retro-orbital administration of ^{18}F-FHEA to the mice. Uptake values at 30 min after ^{18}F-FHEA administration are presented in Table 5. The biodistribution data showed that ^{18}F-FHEA was widely distributed throughout the body (Table 5). The highest uptake was found in liver, followed by lung and kidney in both control and NAAA inhibitor treated mice group. Among brain regions, the highest uptake was found in cerebellum followed by brain stem and thalamus. Uptake levels across brain regions were found to be similar and not statistically different in both control and NAAA inhibitor treated mice (Table 5). The representative micro-PET images of ^{18}F-FHEA with and without NAAA inhibitor were acquired, and but no significant difference was noticed on treatment with NAAA inhibitor (Figure S6, Supporting Information).

Measurement of IC_{50} for Inhibition of Anandamide Hydrolysis in Mouse Brain Homogenate. Competitive inhibition measurements using unlabeled *N*-palmitoylethanolamine (PEA) and *N*-fluorohexadecanoylethanolamine (FHEA) with ^{14}C-labeled anandamide in mouse brain homogenates were performed. FHEA (IC_{50} = 220 ± 33 μM, n=5) showed more potent inhibition of anandamide hydrolysis than PEA (IC_{50} = 443 ± 45 μM, n=3) (p < 0.01).

DISCUSSION

We synthesized and evaluated the ^{18}F-labeled palmitoylethanolamine analogue ^{18}F-FHEA to understand its potential as a PET tracer for *N*-acylethanolamine metabolism catalyzed by FAAH and/or NAAA. Biodistribution (Tables 1−5) and PET imaging (Figure S6, Supporting Information) studies showed that ^{18}F-FHEA crossed the blood-brain barrier and distributed rather homogeneously throughout the mouse brain. However, no differences in either global brain concentration of ^{18}F or of uptake in individual brain regions were observed between control mice and those treated with a dose of the FAAH inhibitor URB-597 (Table 4) shown by previous workers to block FAAH.[33]

The analysis of radiolabeled lipophilic ^{18}F-FHEA metabolites in the cerebellum at 5 min post-administration showed a

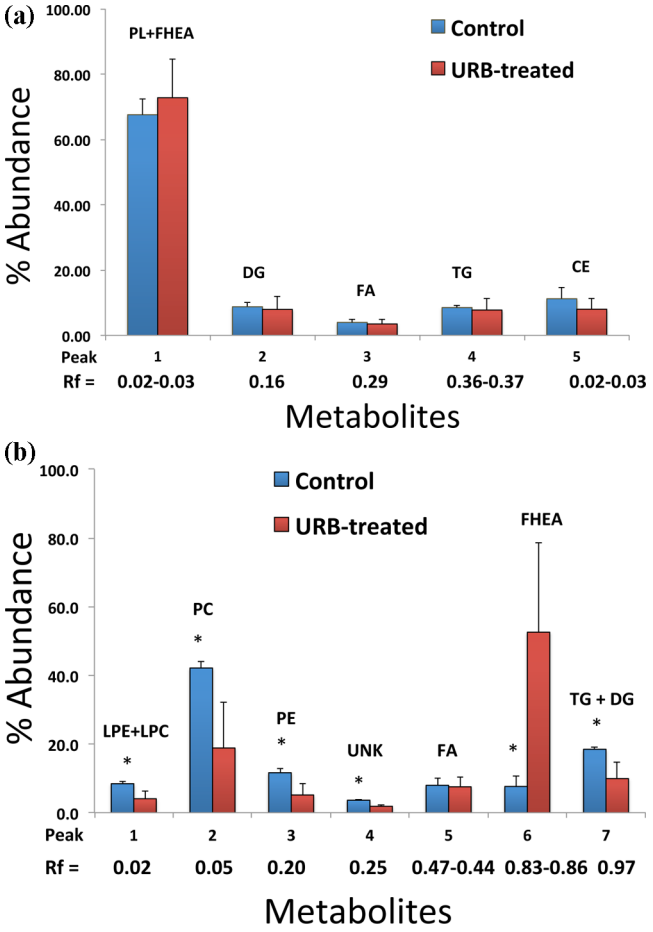

Figure 2. (a) Metabolite analysis of cerebellum by r-TLC measurement in a nonpolar solvent system (petroleum ether/diethyl ether/acetic acid, 70:30:1) after 5 min post-injection of *N*-(16-^{18}F-fluorohexadecanoyl)ethanolamine (3) to both control and URB 597 treated Swiss Webster mice. (PL, phospholipid; FHEA, fluorohexadecanoylethanolamine; MG, momoglyceride; DG, diglyceride; TG, triglyceride; CE, cholesterol ester.) (b) Metabolite analysis of cerebellum by r-TLC measurement in a polar solvent system (chloroform/methanol/ammonium hydroxide, 60:30:1) after 5 min post-injection of *N*-(16-^{18}F-fluorohexadecanoyl)ethanolamine (3) to both control and URB 597 treated Swiss Webster mice (n = 3, *P value <0.05, one tail Student's t test). (LPE, lysophosphatidylethanolamine; LPC, lysophosphatidylcholine; PC, phosphatidylcholine; PE, phosphatidylethanolamine; DG, diglyceride; UNK, unknown; FA, fatty acid; TG, triglyceride; CE, cholesterol ester.)

significantly reduced degree of metabolism of ^{18}F-FHEA to labeled phospholipids (Figure 2). Whereas in control mice the largest labeled lipid component was phosphatidyl choline, in URB-597 treated animals the most abundant labeled species was ^{18}F-FHEA, which increased from about 10% of the organic-soluble ^{18}F-radioactivity in controls to about 50% in animals treated with inhibitor. The degree of conversion to phospholipids of ^{18}F-FHEA in control brains was similar to the 60−70% of total tissue radiolabel seen at 5 min with [^{3}H]anandamide by Glaser et al.[12] Inhibition of incorporation of ^{18}F from ^{18}F-FHEA into complex lipids by URB-597 confirms the expectation that FHEA is a substrate for FAAH, but it is possible that other hydrolases contribute to its metabolism. For example, the study by Sun et al.[14] in macrophages observed the role of NAAA on *N*-acylethaloamine hydrolysis including anandamide and palmitoylethanolamine (PEA) as substrates. Accordingly, we also investigated ^{18}F-FHEA biodistribution with and without pretreatment with a known NAAA inhibitor. Since no inhibitors of NAAA are available commercially, we synthesized one of the most potent inhibitors described in the literature, "Compound **7h**" of Solorzano et al.[30] The potency of Compound 7h was established by in vitro inhibition of NAAA against PEA hydrolysis (IC_{50} = 115 nM);[30] however, data is lacking on the efficacy of Compound 7h as an in vivo inhibitor. In mice pretreated with Compound 7h, we did not measure any significant difference in uptake of ^{18}F-FHEA in brain and other organs at 30 min post-injection (Table 5). Since we have no firm evidence that NAAA was inhibited by Compound 7h at the levels administered in this study, these data remain inconclusive. However, the predominance of radioactivity in the form of nonmetabolized ^{18}F-FHEA in the cerebellum after specific FAAH inhibition by URB-597 argues that NAAA plays a relatively minor role in ^{18}F-FHEA metabolism in brain. Indeed, others have measured relatively low levels of NAAA in mouse brain.[34]

The finding that URB-597 did not significantly alter the brain regional concentration of ^{18}F-radioactivity after administration of FHEA, in spite of the fact that the lipid metabolites of ^{18}F-FHEA were dramatically changed, requires explanation. The transfer of ^{18}F-FHEA between blood and brain appears to be nearly unidirectional, so that while ^{18}F-FHEA can undergo rapid metabolism within the brain, unmetabolized ^{18}F-FHEA is also retained over the 30−60 min time period of our biodistribution measurements. Reasons for this are presently unclear, but one possibility is that ^{18}F-FHEA is retained in brain tissue by fatty acid binding proteins.[35,36]

An alternative approach to imaging FAAH, using high affinity binding radioligands such as ^{11}C-CURB and related ^{11}C and ^{18}F labeled compounds,[37,38] also appears promising. However, information given by the radioligand approach relates to concentration of enzyme, whereas the metabolic trapping approach, which we have pursued can give information about flux through the enzyme. Other approaches to developing imaging agents for FAAH have involved substitutions at the −OH group of the ethanolamine moiety of acylethanolamines, and have not been encouraging.[9−11]

We would also note that use of the injection vehicle for the NAAA and control groups (Table 5, dimethyl sulfoxide/Cremophore/0.9% saline (20 μL/30 μL/150 μL) resulted 1.5−2.0 times higher uptake across brain regions. Due to the poor stability of the NAAA inhibitor, we chose not to administered the inhibitor Compound 7h intraperitoneally as done for URB-597. Instead, it was administered through a tail-vein, which precluded a second tail-vein injection. ^{18}F-FHEA was then administered retro-orbitally, which has become a commonly employed injection site in small animal PET studies. Thus, the higher brain uptake of ^{18}F-FHEA with Cremophore-containing vehicle could have resulted from enhanced blood-brain barrier penetration caused by the vehicle, or differences in the injection method.

■ CONCLUSION

An efficient synthesis of *N*-(16-^{18}F-fluorohexadecanoyl)-ethanolamine (^{18}F-FHEA) and nonradioactive standards has been achieved. The radiochromatographic experiments demonstrated that pretreatment of mice with URB-597 decreased conversion of ^{18}F-FHEA to free fatty acids and complex lipids. This is consistent with reports that URB-597 inhibits FAAH, an

dx.doi.org/10.1021/cn400214j | ACS Chem. Neurosci. 2014, 5, 793−802

Table 5. Uptake (% ID/g) and SUV of ^{18}F-FHEA in Swiss Webster Mice at 30 min Post-Injection Using NAAA Inhibitor[a]

tissue	%ID/g control (vehicle) mice	%ID/g NAAA inhibitor treated mice	%ID/g p-value[b]	SUV control (vehicle) mice	SUV NAAA inhibitor treated mice	SUV p-value[b]
cortex	8.87 ± 2.47	9.14 ± 1.63	0.8484	2.06 ± 0.57	2.11 ± 0.34	0.8748
cerebellum	9.05 ± 2.52	9.35 ± 1.80	0.8449	2.11 ± 0.59	2.15 ± 0.37	0.8850
brain stem	8.81 ± 2.48	9.46 ± 2.19	0.6912	2.05 ± 0.59	2.18 ± 0.46	0.7234
thalamus	8.42 ± 2.82	8.41 ± 1.99	0.9924	1.96 ± 0.66	1.94 ± 0.42	0.9508
hypothalamus	6.97 ± 2.12	8.06 ± 3.28	0.5906	1.62 ± 0.49	1.85 ± 0.71	0.6015
hippocampus	6.60 ± 1.51	7.73 ± 2.00	0.3899	1.53 ± 0.34	1.78 ± 0.42	0.3809
striatum	7.96 ± 1.83	8.24 ± 1.91	0.8349	1.85 ± 0.43	1.90 ± 0.41	0.8693
rest of brain	7.96 ± 1.91	8.24 ± 1.68	0.8210	1.85 ± 0.45	1.90 ± 0.35	0.8582
whole brain	8.21 ± 2.12	8.54 ± 1.80	0.8090	1.91 ± 0.50	1.97 ± 0.38	0.8554
blood	5.37 ± 1.05	5.42 ± 1.08	0.9492	1.25 ± 0.27	1.26 ± 0.27	0.9759
urine	59.03 ± 32.48	91.20 ± 97.27	0.5648	13.66 ± 7.32	21.06 ± 22.32	0.5635
heart	5.79 ± 2.28	4.65 ± 0.76	0.3381	1.35 ± 0.53	1.08 ± 0.18	0.3300
lung	14.00 ± 3.40	12.40 ± 4.99	0.6062	3.27 ± 0.83	2.88 ± 1.15	0.5913
liver	29.96 ± 3.84	26.75 ± 4.87	0.3250	6.98 ± 0.103	6.19 ± 1.09	0.3097
spleen	4.79 ± 1.14	4.47 ± 0.77	0.6404	1.12 ± 0.29	1.04 ± 0.18	0.6224
kidney	19.87 ± 5.66	19.48 ± 5.42	0.9189	4.64 ± 1.41	4.51 ± 1.22	0.8819
testis	2.05 ± 0.61	2.13 ± 0.41	0.8340	0.48 ± 0.15	0.49 ± 0.09	0.8712
fat	6.09 ± 3.06	2.88 ± 2.25	0.1133	1.42 ± 0.72	0.66 ± 0.52	0.1094
bone	5.09 ± 0.94	4.77 ± 0.90	0.6251	1.19 ± 0.24	1.10 ± 0.20	0.5949
muscle	1.87 ± 0.51	2.29 ± 0.88	0.4499	0.44 ± 0.13	0.53 ± 0.20	0.4685
skin	2.82 ± 0.74	3.00 ± 0.57	0.6971	0.66 ± 0.18	0.69 ± 0.12	0.7379

[a]Values are listed as mean ± standard deviation. There were 4 measurements for each time by body region category. [b]p-Value represents tests for differences in biodistribution across treatment groups. p-Values are not adjusted for multiple comparisons. [c]Statistically significant p-value.

enzyme that terminates signaling by the endocannabinoid anandamide, *N*-arachidonoylethanolamine. However, URB-597 did not significantly alter the brain regional concentration of ^{18}F-radioactivity after administration of ^{18}F-FHEA. Results with the NAAA inhibitor Compound 7h are inconclusive, although a predominant role of FAAH in ^{18}F-FHEA metabolism is implied by the large fraction of nonmetabolized ^{18}F-FHEA remaining in brain following URB-597 treatment. To conclude, ^{18}F-FHEA appears to behave as a good mimic of *N*-acylethanolamine uptake and FAAH-sensitive metabolism in brain but its utility as a PET probe of FAAH activity in the brain may be compromised by the lack of sensitivity of total cerebral ^{18}F-radioactivity concentration to changes in *N*-acylethanolamine hydrolysis rate.

METHODS

Materials and Methods. All chemicals and solvents were purchased from Sigma-Aldrich and used as received. Anhydrous solvents were also purchased from Sigma-Aldrich in "sure seal" bottles. TLC analysis of reaction mixtures and products was performed on Merck silica gel 60 F254 TLC plates. Liquid chromatography was carried out on Merck 60 silica gel (32−63 μm). ^{1}H and ^{13}C NMR was recorded on a Varian 600 MHz spectrometer. Mass spectral data were obtained from the Mass Spectral Lab of School of Chemical Sciences, University of Illinois, Urbana, Illinois. Analytical HPLC was performed on a Phenomenex Luna C-18 column (5 μm, 4.6 × 250 mm) with a flow rate of 0.8 mL/min. Semipreparative HPLC was performed on the final ^{18}F-labeled product using a Phenomenex Luna C-18 column (5 μm, 10 × 250 mm) with a flow rate of 5.0 mL/min using 80:20 acetonitrile/water as an eluent at 220 nm UV wavelength. URB 597 was purchased from Merck Chemicals.

General Procedure for ^{18}F-Labeling. For ^{18}F-labeling, cyclotron-produced ^{18}F-fluoride (20 mCi) was dried down under nitrogen at 95 °C in a 3 mL glass vial containing Kryptofix 2.2.2 (10 mg), acetonitrile (0.8 mL), and K_2CO_3 (4 mg) solution in water (0.50 mL). The residue was further dried by azeotropic distillation with anhydrous acetonitrile (3 × 0.5 mL). The ^{18}F-fluoride residue was reconstituted in 0.5 mL of acetonitrile, and the bromo precursor (approximately 2−3 mg) in acetonitrile (0.5 mL) was added. The resultant reaction mixture was heated with a PETWave microwave reactor for 10 min at 80 °C. ^{18}F-fluoride incorporation was checked using silica-gel r-TLC (8:92 methanol/chloroform). Deprotection was carried out by addition of 0.45 mL of 15%TFA aqueous solution followed by heating in the microwave reactor for 5 min at 60 °C. After deprotection, the crude product was purified by using a semi-preparative C-18 HPLC (80:20 ACN/H_2O) system. The product peak was collected at 7.3 min retention time with >99% radiochemical purity, which was in complete agreement with the cold standard. The product peak was diluted in water, concentrated on a C-18 Sep-Pak column, and eluted in 1 mL of ethanol. The specific activity of the final product was found to be in the range of 1.4−5.1 Ci/μmol. Final product was formulated in 0.5−1% BSA in isotonic NaCl solution and filtered through a 0.22 μm filter before being administered to mice.

Biodistribution Method. Swiss Webster mice (body wt 24−28 g) were used in this study under approval of Institutional Animal Care and Use Committees (IACUCs) of Northeastern University and Mayo Clinic. The mice were anesthetized with isoflurane (3.0% induction, 2.0−2.5% maintenance) for imaging studies. For biodistribution studies, conscious mice were intravenously injected with 200 μL of ^{18}F-FHEA (0.37−0.74 MBq) formulated in 0.5−1% BSA in isotonic NaCl solution and filtered through a 0.22 μm filter (Millex-GS, Millipore, Bedford, MA). Radiochemical purity (>99%) was analyzed by radio-HPLC as described above. After 1−60 min administration, the animals were euthanized by cervical dislocation, and the brains dissected on a moist filter paper using forceps. Brain regions hypothalamus, olfactory tubercles, striatum, hippocampus, cerebellum, brain stem, cortex, thalamus, and rest-of-brain were rapidly weighed and then assayed for ^{18}F-radioactivity, together with injection standards, whereas rest-of-body biodistribution was performed by procurement of heart, liver, lung, spleen, kidney, testis, fat, skin, bone (femur) blood, urine, and skeletal muscle. Another set of Swiss Webster mice was used to examine the effect of FAAH inhibitor URB 597 on uptake and biodistribution of ^{18}F-FHEA. For this, animals were pretreated with 1 mg/kg of URB 597 dissolved in 75% DMSO solution and injected intraperitoneally 60 min prior to the ^{18}F-FHEA injection. The synthesized NAAA inhibitor is formulated in dimethyl

sulfoxide/Cremephore/0.9% saline (20 μL/30 μL/150 μL) solutions. Each injection was 200 μL having 0.75 mg of NAAA inhibitor (Compound 7h). The tissues were counted for ^{18}F-radioactivity and weighed. All ^{18}F-radioactivity measurements were corrected for radioactivity decay.

Following correction for background and physical decay, data were expressed as a percent of injected activity per gram of wet weight (% ID/g) and SUV (standard uptake value) using eqs 1 and 2, respectively.

$$\%\frac{\mathrm{ID}}{\mathrm{g}} = \frac{\mathrm{At}}{W_\mathrm{t}}\frac{1}{D_\mathrm{inj}} \times 100\ (\%/g) \tag{1}$$

where At = tissue activity, W_t = tissue weight, D_{inj} = dose injected.

$$\mathrm{SUV} = \left(\%\frac{\mathrm{ID}}{g}\right)W_\mathrm{a}/100 \tag{2}$$

where W_a = animal weight

Metabolite Analysis. Analysis of the metabolic fate of ^{18}F-FHEA in the brain was performed by using a Folch-type extraction procedure as described in literature.[19,21] Approximately 0.05 g of cerebellum was excised and thoroughly homogenized and sonicated (20 s) in 2.4 mL of chloroform/methanol (2:1) at 0 °C. Urea (40%, 0.6 mL) and 5% sulfuric acid (0.6 mL) were added, and the mixture was sonicated for an additional 20 s. After centrifugation for 10 min at 1800 rpm, aqueous and organic fractions were separated and counted for radioactivity. Organic fraction was concentrated under nitrogen and subjected on radio-thin layer chromatographic (r-TLC) studies. Silica coated glass TLC plate and petroleum ether/diethyl ether/acetic acid as (v/v) 70:30:1 as mobile phase were used for the analysis of the metabolites formed after 5 min of injection of ^{18}F-FHEA. Cyclone Plus Phosphor Imager by PerkinElmer was used to analyze the r-TLC plate.

We did not include the radioactivity associated with the protein pellet in this study. In pilot studies using [arachidonoyl-^{14}C]-anandamide, this fraction represented <10% of total radioactivity without further extraction of the pellet. The obtained mean activity distributions were (n = 4) organic or chloroform layer = 89.2%, aqueous layer = 1.3%, and protein pellet = 9.5%.

Measurement of IC_{50} for Inhibition of Anandamide Hydrolysis in Mouse Brain Homogenate. Mouse forebrain homogenates (n = 4) were prepared using a Polytron-type homogenizer and ice-cold buffer (10 mL) as previously described.[39] The buffer was tris/magnesium chloride/EDTA (100/5/1 in mM) containing 2.5% bovine serum albumin. To 0.1 mL of buffer containing [ethanolamine-^{14}C]anandamide (10 nCi/tube) and non-radioactive *N*-acylethanolamines (100−600 μM) was added 0.1 mL of pooled brain homogenates (equivalent of ∼0.5 mg of brain wet weight), and incubated at 25 °C for 10 min. The reactions were terminated by addition of 0.5 mL of 2 N HCl and 0.5 mL of chloroform. After vortexing and centrifuging the sample, 0.25 mL of the acid layer was removed for liquid scintillation counting. Since the anandamide substrate concentration (2 μM) used in the assays was much lower than the inhibitor concentrations, IC_{50} values were determined on the basis of the equation:

$$\mathrm{IC}_{50} = C_\mathrm{i}\mathrm{CPM}_\mathrm{i}/(\mathrm{CPM}_\mathrm{c} - \mathrm{CPM}_\mathrm{i}) \tag{3}$$

where C_i is the inhibitor concentration, CPM_i is count rate in the presence of inhibitor, and CPM_c is control count rate in the absence of inhibitor.

Statistical Analysis. Results are expressed as mean ± SD. Mean values were compared by using repeated measures ANOVA in SAS PROC Mixed (SAS/STAT version 12.1, Cary, NC). This analysis accounted for the repeated measurements within animal and the between subject effect of either time or treatment. Reported p-values have not been adjusted for multiple comparisons. Fisher's least significant difference was used to control the overall experiment-wise error rate, and as such $p < 0.05$ was interpreted as statistically significant only if the overall model was statistically significant, which was the case for the data presented in Tables 1−4.

Synthesis of *N*-(16-Bromohexadecanoyl)ethanolamine (1). Synthesis of *N*-(16-bromohexadecanoyl)ethanolamine (**1**) was achieved by stirring of 16-bromo hexadecanoic acid (2.00 g, 5.97 mmol), methyl chloroformate (1.128 g, 11.94 mmol), and triethylamine (1.204 g, 11.94 mmol) in dichloromethane at 0 °C for 30 min and then at room temperature for another 1.5 h. After 2 h, reaction temperature was further lowered to 0 °C for addition of ethanolamine (0.728 g, 11.94 mmol), and the resultant reaction mixture was stirred at room temperature overnight. After completion, solvent was removed under vacuum and cold water was poured into the flask containing residue with constant stirring for additional 10 min. Solid obtained was filtered and dried. TLC was re-examined for desired product in 8:92 methanol/chloroform as a solvent system. The residue was subjected to column chromatography using silica gel as an adsorbent and 5:95 methanol/chloroform as solvent to yield compound **1** (1.96 g, 87% yield, mp 90 ± 1 °C) as a white solid. ^{1}H NMR (25 °C, 599.77 MHz, $CDCl_3$) δ ppm: 5.88 (brs, 1H, NH), 3.66 (t, 2H, $J_{1,2}$ = 6.0 Hz, CH_2), 3.34 (m, 4H, 2 × CH_2), 2.14 (t, 2H, J = 6.0 Hz, CH_2), 1.78 (m, 2H, CH_2), 1.56 (m, 2H, CH_2), 1.35 (m, 2H, CH_2), 1.23−1.18 (brs, 20H, 10 ×CH_2). ^{13}C NMR (25 °C, 150.81 MHz, $CDCl_3$) δ ppm: 177.2 (CONH), 65.3 (CH_2OH), 45.1, 39.3, 36.7, 35.4, 32.3−31.9 (CH_2 × 9), 31.4, 30.8, 28.3. HRMS (ES) calcd for $C_{18}H_{36}O_2NBr$ (M^+), 377.19293; found, 377.19241 and (M+2) at 379.1 (due to isotopic abundance).

Synthesis of 16-Bromo-*N*-[2[(tetrahydro-2*H*-pyran-2-yl)oxy]-ethyl]hexadecanoylamide (2). Synthesis of 16-bromo-*N*-[2-[(tetrahydro-2*H*-pyran-2-yl)oxy]ethyl]hexadecanoylamide (**2**) was achieved by stirring of *N*-(16-bromohexadecanoyl)ethanolamine (**1**) (1.00 g, 2.65 mmol), 3,4-dihydro-2*H*-pyran (0.29 g, 3.44 mmol) in dichloromethane using *p*-toluenesulfonic acid as catalyst (0.548 g, 3.18 mmol). The mixture was stirred for 24 h at room temperature and quenched with water. After extraction with the chloroform, organic layer was dried over Na_2SO_4 and solvent was evaporated under vacuum. The residue was subjected to column chromatography (2:98 methanol: chloroform) to yield **2** (0.93 g, 76% yield, mp 60 ± 1 °C) as a white solid. ^{1}H NMR (25 °C, 599.77 MHz, $CDCl_3$) δ ppm: 6.00 (brs, 1H, NH), 4.55 (t, 1H), 3.88 (m, 1H), 3.76 (m, 1H), 3.61 (m, 1H), 3.55 (m, 1H), 3.47 (m, 2H), 3.41 (t, 2H, $J_{1,2}$ = 6.0 Hz, CH_2Br), 2.17 (t, 2H, J = 6.0 Hz, CH_2), 1.86 (m, 2H, CH_2), 1.62 (m, 2H, CH_2), 1.53 (m, 2H, CH_2), 1.41 (m, 2H, CH_2), 1.29−1.25 (brs, 24H, 12× CH_2). ^{13}C NMR (25 °C, 150.81 MHz, $CDCl_3$) δ ppm: 173.1 (CONH), 99.7 (OCHO), 67.1, 63.2, 39.4, 36.8, 34.0, 32.8, 30.7, 29.6−29.3 (CH_2 × 9), 28.7, 28.1, 25.7, 25.2, 20.0. HRMS (ES) calcd for $C_{23}H_{44}O_3NBr$ (M^+), 461.24263; found, 461.24182 and (M+2) at 463.3 (due to isotopic abundance).

Synthesis of *N*-(16-Fluorohexadecanoyl)ethanolamine (3). Synthesis of *N*-(16-fluorohexadecanoyl)ethanolamine (**3**) was achieved by stirring 16-bromo-*N*-[2[(tetrahydro-2*H*-pyran-2-yl)oxy]-ethyl]hexadecanoylamide (**2**) (0.50 g, 1.08 mmol) and 1 M THF solution tetra-*n*-butylammonium fluoride (1.2 mL) in acetonitrile. The resulting solution was stirred for 72 h at room temperature with two subsequent additions of 0.5 mL of 1 M tetra-*n*-butylammonium fluoride in THF after 24 and 48 h. TLC was used to monitor the progress of reaction; after completion, solvent was removed under vacuum. The obtained residue was dissolved in methanol with few drops of water, a catalytic amount of *p*-toluenesulfonic acid (100 mg, 0.58 mmol) was added, and the mixture was stirred for 2 h at room temperature. After 2 h, TLC was re-examined for deprotection of tetrahydropyranyl group. Subsequently, solvent was removed under vacuum and residue was extracted against water in dichloromethane. Thereafter, the organic layer was dried over Na_2SO_4, and solvent was evaporated under vacuum. The obtained residue was subjected to column chromatography (5:95 methanol/chloroform) to yield compound **3** (0.175g, 51% yield, mp 97 ± 1 °C) as a white solid. ^{1}H NMR (25 °C, 399.62 MHz, $CDCl_3$) δ ppm: 5.87 (brs, 1H, NH), 4.43−4.31 (dt, 2H, J_1 = 48.0 Hz, J_2 = 6.0 Hz, CH_2F), 3.66 (t, 2H, $J_{1,2}$ = 4.0 Hz CH_2OH), 3.36 (m, 2H, CH_2NH), 2.64 (brs, 1H, OH), 2.13 (m, 2H), 1.65 (m, 2H, CH_2), 1.57 (m, 2H, CH_2), 1.31 (m, 2H, CH_2), 1.28−1.19 (brs, 20H, 10 × CH_2). ^{13}C NMR (25 °C, 100.48 MHz, $CDCl_3$) δ ppm: 174.5 (CONH), 85.0−83.4 (d, J = 160 Hz, **C**H_2F),

dx.doi.org/10.1021/cn400214j | ACS Chem. Neurosci. 2014, 5, 793−802

62.6, 42.4, 36.6, 30.4, 30.2, 29.6−29.3 (CH_2 × 10), 25.7, 25.2−25.0 (d, J = 20 Hz). ^{19}F NMR (25 °C, 376.02 MHz, $CDCl_3$) δ ppm: −218 (m, 1F, CH_2**F**). HRMS (ES) calcd for $C_{18}H_{36}O_2NF$ (M^+), 317.27300; found, 317.27254.

■ ASSOCIATED CONTENT

Supporting Information

Synthesis of nonradioactive standards and their spectrascopic characterization, radio-TLC of compounds 4 and 8, and micro-PET images of 18F-FHEA in mice. This material is available free of charge via the Internet at http://pubs.acs.org.

■ AUTHOR INFORMATION

Corresponding Authors

*E-mail: degrado.timothy@mayo.edu. Phone: 507-538-4319. Fax 507-293-2235.

*E-mail: s.gatley@neu.edu. Phone: 617.373.3306. Fax: 617-373-8886.

Author Contributions

M.K.P. performed the synthesis, purification, and chemical characterization of compounds **1**−**8** and NAAA inhibitor. M.K.P and T.R.D. developed the initial radiosynthesis, whereas M.K.P and M.S.J. did the microwave-assisted automation of the radiosynthesis using TRACERLab FXN Pro synthetic module and routinely produced the tracer for biological evaluations. J.S.G., T.R.D., and M.K.P. did the biological evaluation in Swiss Webster mice. K.Q., J.S.G., and R.I.D. performed TLC of nonradioactive standards of various lipids and also performed the competitive inhibition measurements. Statistical analysis was carried out by C.E.H., T.R.D., and M.K.P. The manuscript was prepared by M.K.P and edited by T.R.D., J.S.G., and R.I.D. All authors have given approval to the final version of the manuscript.

Funding

Present work was financially supported by the Department of Energy, Office of Science, DER, Biological and Environmental Research Grant to J.S.G. (DE SC0005251) and Mayo Clinic's "Radiology Advance Award" to M.K.P. and T.R.D.

Notes

The authors declare no competing financial interest.

■ ABBREVIATIONS

CB, cannabinoid; FAAH, fatty acid amide hydrolase; CB1/2, cannabinoid receptor1/2; ^{18}F-FHEA, *N*-(16-^{18}F-fluorohexadecanoyl)ethanolamine; URB-597, FAAH inhibitor, [3-(3-carbamoylphenyl)phenyl] *N*-cyclohexylcarbamate, also known as KDS-4103; MBq, megabecquerel; DMSO, dimethyl sulfoxide; ACN, acetonitrile; DCM, dichloromethane; *p*-TsCl, *p*-toluene sulfonyl chloride; DHP, dihydropyran; TBAF, *n*-butylammoniumfluoride; TFA, trifluoroacetic acid; *p*-TSA, *p*-toluene sulfonic acid; K2.2.2, Kryptofix chemically known as 4,7,13,16,21,24-hexaoxa-1,10-diazabicyclo[8.8.8]hexacosane; anandamide, also known as *N*-arachidonoylethanolamine, AEA, an endogenous cannabinoid neurotransmitter; TLC, thin layer chromatography; r-TLC, radioactive thin layer chromatography; IACUC, Institutional Animal Care and Use Committee; PETwave Microwave, a microwave unit produced by CEM corporation; TRACERLab FXN Pro, a radiosynthetic module produced by General Electric Healthcare; PET, positron emission tomography; NAAA, *N*-acylethanolamine-hydrolyzing acid amidase; SPECT, single photon emission computed tomography; IC_{50}, half-maximal inhibitory concentration

■ REFERENCES

(1) Hillard, C. J., Weinlander, K. M., and Stuhr, K. L. (2012) Contributions of endocannabinoid signaling to psychiatric disorders in humans: Genetic and biochemical evidence. *Neuroscience 204*, 207−229.

(2) Hill, M. N., Patel, S., Campolongo, P., Tasker, J. G., Wotjak, C. T., and Bains, J. S. (2010) Functional interactions between stress and the endocannabinoid system: From synaptic signaling to behavioral output. *J. Neurosci. 30*, 14980−14986.

(3) Di Marzo, V., Ligresti, A., and Cristino, L. (2009) The endocannabinoid system as a link between homoeostatic and hedonic pathways involved in energy balance regulation. *Int. J. Obes. 33*, S18−S24.

(4) Pacher, P., and Mechoulam, R. (2011) Is lipid signaling through cannabinoid 2 receptors part of a protective system? *Prog. Lipid Res. 50*, 193−211.

(5) Hill, M. N., Kumar, S. A., Filipski, S. B., Iverson, M., Stuhr, K. L., Keith, J. M., Cravatt, B. F., Hillard, C. J., Chattarji, S., and McEwen, B. S. (2013) Disruption of fatty acid amide hydrolase activity prevents the effects of chronic stress on anxiety and amygdalar microstructure. *Mol. Psychiatry 18*, 1125−1135.

(6) Conzelmann, A., Reif, A., Jacob, C., Weyers, P., Lesch, K. P., Lutz, B., and Pauli, P. (2012) A polymorphism in the gene of the endocannabinoid-degrading enzyme FAAH (FAAH C385A) is associated with emotional-motivational reactivity. *Psychopharmacology (Berlin, Ger.) 224*, 573−579.

(7) Choi, K., Le, T., McGuire, J., Xing, G., Zhang, L., Li, H., Parker, C. C., Johnson, L. R., and Ursano, R. J. (2012) Expression pattern of the cannabinoid receptor genes in the frontal cortex of mood disorder patients and mice selectively bred for high and low fear. *J. Psychiatr. Res. 46*, 882−889.

(8) Monteleone, P., Bifulco, M., Maina, G., Tortorella, A., Gazzerro, P., Proto, M. C., Di Filippo, C., Monteleone, F., Canestrelli, B., Buonerba, G., Bogetto, F., and Maj, M. (2010) Investigation of CNR1 and FAAH endocannabinoid gene polymorphisms in bipolar disorder and major depression. *Pharmacol. Res. 61*, 400−404.

(9) Wyffels, L., De Bruyne, S., Blanckaert, P., Lambert, D. M., and De Vos, F. (2009) Radiosynthesis, in vitro and in vivo evaluation of ^{123}I-labeled anandamide analogues for mapping brain faah. *Bioorg. Med. Chem. 17*, 49−56.

(10) Wyffels, L., Muccioli, G. G., De Bruyne, S., Moerman, L., Sambre, J., Lambert, D. M., and De Vos, F. (2009) Synthesis, in vitro and in vivo evaluation, and radiolabeling of aryl anandamide analogues as candidate radioligands for in vivo imaging of fatty acid amide hydrolase in the brain. *J. Med. Chem. 52*, 4613−4622.

(11) Wyffels, L., Muccioli, G. G., Kapanda, C. N., Labar, G., De Bruyne, S., De Vos, F., and Lambert, D. M. (2010) PET imaging of fatty acid amide hydrolase in the brain: Synthesis and biological evaluation of an ^{11}C-labelled URB597 analogue. *Nucl. Med. Biol. 37*, 665−675.

(12) Glaser, S. T., Gatley, S. J., and Gifford, A. N. (2006) Ex vivo imaging of fatty acid amide hydrolase activity and its inhibition in the mouse brain. *J. Pharmacol. Exp. Ther. 316*, 1088−1097.

(13) Wilson, A. A., Garcia, A., Parkes, J., Houle, S., Tong, J., and Vasdev, N. (2011) [^{11}C]CURB: Evaluation of a novel radiotracer for imaging fatty acid amide hydrolase by positron emission tomography. *Nucl. Med. Biol. 38*, 247−253.

(14) Sun, Y. X., Tsuboi, K., Zhao, L. Y., Okamoto, Y., Lambert, D. M., and Ueda, N. (2005) Involvement of *N*-acylethanolamine-hydrolyzing acid amidase in the degradation of anandamide and other *N*-acylethanolamines in macrophages. *Biochim. Biophys. Acta 1736*, 211−220.

(15) Ueda, N., Tsuboi, K., and Uyama, T. (2010) *N*-acylethanolamine metabolism with special reference to *N*-acylethanolamine-hydrolyzing acid amidase (NAAA). *Prog. Lipid Res. 49*, 299−315.

(16) Ueda, N., Tsuboi, K., and Uyama, T. (2013) Metabolism of endocannabinoids and related *N*-acylethanolamines: Canonical and alternative pathways. *FEBS J. 280*, 1874−1894.

(17) Tsuboi, K., Takezaki, N., and Ueda, N. (2007) The *N*-acylethanolamine-hydrolyzing acid amidase (NAAA). *Chem. Biodiversity 4*, 1914−1925.
(18) Snider, N. T., Walker, V. J., and Hollenberg, P. F. (2010) Oxidation of the endogenous cannabinoid arachidonoyl ethanolamide by the cytochrome P450 monooxygenases: Physiological and pharmacological implications. *Pharmacol. Rev. 62*, 136−154.
(19) Ueda, N., Puffenbarger, R. A., Yamamoto, S., and Deutsch, D. G. (2000) The fatty acid amide hydrolase (FAAH). *Chem. Phys. Lipids 108*, 107−121.
(20) McKinney, M. K., and Cravatt, B. F. (2005) Structure and function of fatty acid amide hydrolase. *Annu. Rev. Biochem. 74*, 411−432.
(21) Fowler, C. J., Borjesson, M., and Tiger, G. (2000) Differences in the pharmacological properties of rat and chicken brain fatty acid amidohydrolase. *Br. J. Pharmacol. 131*, 498−504.
(22) Tsuboi, K., Sun, Y. X., Okamoto, Y., Araki, N., Tonai, T., and Ueda, N. (2005) Molecular characterization of *N*-acylethanolamine-hydrolyzing acid amidase, a novel member of the choloylglycine hydrolase family with structural and functional similarity to acid ceramidase. *J. Biol. Chem. 280*, 11082−11092.
(23) Jonsson, K. O., Vandevoorde, S., Lambert, D. M., Tiger, G., and Fowler, C. J. (2001) Effects of homologues and analogues of palmitoylethanolamide upon the inactivation of the endocannabinoid anandamide. *Br. J. Pharmacol. 133*, 1263−1275.
(24) Ho, W. S. V., Barrett, D. A., and Randall, M. D. (2008) "Entourage" effects of *N*-palmitoylethanolamide and *N*-oleoylethanolamide on vasorelaxation to anandamide occur through trpv1 receptors. *Br. J. Pharmacol. 155*, 837−846.
(25) O'Sullivan, S. E. (2007) Cannabinoids go nuclear: Evidence for activation of peroxisome proliferator-activated receptors. *Br. J. Pharmacol. 152*, 576−582.
(26) Lo Verme, J., Fu, J., Astarita, G., La Rana, G., Russo, R., Calignano, A., and Piomelli, D. (2005) The nuclear receptor peroxisome proliferator-activated receptor-alpha mediates the anti-inflammatory actions of palmitoylethanolamide. *Mol. Pharmacol. 67*, 15−19.
(27) Guan, L. P., Zhao, D. H., Xiu, J. H., Sui, X., Piao, H. R., and Quan, Z. S. (2009) Synthesis and anticonvulsant activity of *N*-(2-hydroxyethyl)amide derivatives. *Arch. Pharm. 342*, 34−40.
(28) Pandey, M. K., Belanger, A. P., Wang, S., and DeGrado, T. R. (2012) Structure dependence of long-chain [^{18}F]fluorothia fatty acids as myocardial fatty acid oxidation probes. *J. Med. Chem. 55*, 10674−10684.
(29) Belanger, A. P., Pandey, M. K., and DeGrado, T. R. (2011) Microwave-assisted radiosynthesis of [^{18}F]fluorinated fatty acid analogs. *Nucl. Med. Biol. 38*, 435−41.
(30) Solorzano, C., Antonietti, F., Duranti, A., Tontini, A., Rivara, S., Lodola, A., Vacondio, F., Tarzia, G., Piomelli, D., and Mor, M. (2010) Synthesis and structure-activity relationships of *N*-(2-oxo-3-oxetanyl)-amides as *N*-acylethanolamine-hydrolyzing acid amidase inhibitors. *J. Med. Chem. 53*, 5770−5781.
(31) Duranti, A., Tontini, A., Antonietti, F., Vacondio, F., Fioni, A., Silva, C., Lodola, A., Rivara, S., Solorzano, C., Piomelli, D., Tarzia, G., and Mor, M. (2012) *N*-(2-oxo-3-oxetanyl)carbamic acid esters as *N*-acylethanolamine acid amidase inhibitors: Synthesis and structure-activity and structure-property relationships. *J. Med. Chem. 55*, 4824−4836.
(32) DeGrado, T. R., Bhattacharyya, F., Pandey, M. K., Belanger, A. P., and Wang, S. (2010) Synthesis and preliminary evaluation of 18-[^{18}F]-fluoro-4-thia-oleate as a pet probe of fatty acid oxidation. *J. Nucl. Med. 51*, 1310−1317.
(33) Rapoport, S. I. (2005) In vivo approaches and rationale for quantifying kinetics and imaging brain lipid metabolic pathways. *Prostaglandins Other Lipid Mediators 77* (1−4), 185−96.
(34) Tai, T., Tsuboi, K., Uyama, T., Masuda, K., Cravatt, B. F., Houchi, H., and Ueda, N. (2012) Endogenous molecules stimulating *N*-acylethanolamine-hydrolyzing acid amidase (NAAA). *ACS Chem. Neurosci. 3* (5), 379−85.
(35) Kaczocha, M., Rebecchi, M. J., Ralph, B. P., Teng, Y. H., Berger, W. T., Galbavy, W., Elmes, M. W., Glaser, S. T., Wang, L., Rizzo, R. C., Deutsch, D. G., and Ojima, I. (2014) Inhibition of Fatty Acid binding proteins elevates brain anandamide levels and produces analgesia. *PLoS One 9* (4), e94200.
(36) Fowler, C. J. (2013) Transport of endocannabinoids across the plasma membrane and within the cell. *FEBS J. 280* (9), 1895−904.
(37) Sadovski, O., Hicks, J. W., Parkes, J., Raymond, R., Nobrega, J., Houle, S., Cipriano, M., Fowler, C. J., Vasdev, N., and Wilson, A. A. (2013) Development and characterization of a promising fluorine-18 labelled radiopharmaceutical for in vivo imaging of fatty acid amide hydrolase. *Bioorg. Med. Chem. 21* (14), 4351−7.
(38) Hicks, J. W., Parkes, J., Sadovski, O., Tong, J., Houle, S., Vasdev, N., and Wilson, A. A. (2013) Synthesis and preclinical evaluation of [^{11}C-carbonyl] PF-04457845 for neuroimaging of fatty acid amide hydrolase. *Nucl. Med. Biol. 40* (6), 740−746.
(39) Omeir, R. L., Chin, S., Hong, Y., Ahern, D. G., and Deutsch, D. G. (1995) Arachidonoyl ethanolamide-[1, 2-^{14}C] as a substrate for anandamide amidase. *Life Sci. 56* (23/24), 1999−2005.

Manuscript Details

Manuscript number	NUCMEDBIO_2016_222
Title	BRAIN UPTAKE AND METABOLISM OF THE ENDOCANNABINOID ANANDAMIDE LABELED IN EITHER THE ARACHIDONOYL OR ETHANOLAMINE MOIETY
Article type	Research Paper

Abstract

Introduction. Anandamide (N-arachidonoylethanolamine) is a retrograde neuromodulator that activates cannabinoid receptors. The concentration of anandamide in the brain is controlled by fatty acid amide hydrolase (FAAH), which has been the focus of recent drug discovery efforts. Previous studies in C57BL/6 mice using [3H-arachidonoyl] anandamide demonstrated deposition of tritium in thalamus and cortical areas that was blocked by treatment with a FAAH inhibitor and that was not seen in FAAH-knockout mice. This suggested that long chain fatty acid amides radiolabeled in the fatty acid moiety might be useful as ex vivo and in vivo radiotracers for FAAH, since labeled fatty acid released by hydrolysis would be rapidly incorporated into phospholipids with long metabolic turnover periods. Methods. Radiotracers were administered intravenously to conscious Swiss-Webster mice, and radioactivity concentrations in brain areas was quantified and radiolabeled metabolites determined by radiochromatography. Results. [14C]Arachidonic acid, [14C-arachidonoyl]anandamide and [14C-ethanolamine]anandamide, and also [14C] myristic acid, [14C-myristoyl]myristoylethanolamine and [14C-ethanolamine]myristoyl-ethanolamine all had very similar distribution patterns, with whole brain radioactivity concentrations of 2-4% injected dose per gram. Pretreatment with the potent selective FAAH inhibitor URB597 did not significantly alter distribution patterns although radiochromatography demonstrated that the rate of incorporation of label from [14C]anandamide into phospholipids was decreased. Pretreatment with the muscarinic agonist arecoline which increases cerebral perfusion increased brain uptake of radiolabel from [14C]arachidonic acid and [14C-ethanolamine]anandamide, and (in dual isotope studies) from the unrelated tracer [125I]RTI-55. Conclusions. Together with our previously published study with [18F-palmitoyl]16-fluoro-palmitoylethanolamine, the data show that the primary determinant of brain uptake for these tracers in Swiss-Webster mice is initial distribution according to blood flow. It is possible that recently reported strain differences in long chain fatty acid trafficking between C57BL/6 and Swiss Webster mice are responsible for the differences between our results using [14C]anandamide and the earlier studies using [3H]anandamide.

Corresponding Author	Samuel Gatley
Corresponding Author's Institution	Northeastern University
Order of Authors	Kun Hu, Shilpa Sonti, Sherrye Glaser, Richard Duclos, Samuel Gatley

Submission Files Included in this PDF

File Name [File Type]

cover letter Hu NMB- Dr Eckelman.docx [Cover Letter]

Hu et al. NMB submission main text.docx [Manuscript File]

Hu Figure 1.jpg [Figure]

Hu Figure 2.jpg [Figure]

Hu Figure 3.jpg [Figure]

Hu Figure 4.jpg [Figure]

Hu Figure 5A.jpg [Figure]

Hu Figure 5B.jpg [Figure]

Hu Figure 5C.jpg [Figure]

Hu Table 1.docx [Figure]

Hu Table 2.docx [Figure]

To view all the submission files, including those not included in the PDF, click on the manuscript title on your EVISE Homepage, then click 'Download zip file'.

Dear Dr Eckelman:

I would be grateful if you could consider our manuscript entitled: BRAIN UPTAKE AND METABOLISM OF THE ENDOCANNABINOID ANANDAMIDE LABELED IN EITHER THE ARACHIDONOYL OR ETHANOLAMINE MOIETY
publication in Nuclear Medicine and Biology.

The experiments described in the manuscript were largely conducted by my PhD student Kun Hu. This work began as a project to extend previous studies conducted by Dr Sherrye Glaser, on an autoradiographic method using [^{3}H-arachidonoyl]-anandamide for assessing fatty acid hydrolase activity. She used C57 mice. We were unable to demonstrate these finding using Swiss-Webster mice and [^{14}C]anandamide. We present Kun's studies that attempted to repeat the earlier observations, and together with Dr Glaser discuss possible reasons, such as a strain differences, for the discrepancy.

Sincerely,

S John Gatley
Department of Pharmaceutical Sciences
Northeastern University
Boston, MA 02360

BRAIN UPTAKE AND METABOLISM OF THE ENDOCANNABINOID ANANDAMIDE LABELED IN EITHER THE ARACHIDONOYL OR ETHANOLAMINE MOIETY

Kun Hu, Shilpa Sonti, Sherrye T Glaser, Richard I Duclos Jr and Samuel J Gatley

Department of Pharmaceutical Sciences
Northeastern University
360 Huntington Avenue
Boston, MA 02115

Department of Biological Sciences
Kingsborough Community College
2001 Oriental Boulevard
Brooklyn, NY 11235

Brain Uptake and Metabolism of [^{14}C]anandamide

KEYWORDS

Endocannabinoid, radiotracer, lipophilicity,

CORRESPONDING AUTHOR: Samuel John Gatley, Department of Pharmaceutical Sciences, Northeastern University, Boston MA 02115. Email: s.gatley@neu.edu. Phone: 617-373.3306

FUNDING

This work was supported by the Office of Science (BER), U.S. Department of Energy.

ABSTRACT

Introduction. Anandamide (N-arachidonoylethanolamine) is a retrograde neuromodulator that activates cannabinoid receptors. The concentration of anandamide in the brain is controlled by fatty acid amide hydrolase (FAAH), which has been the focus of recent drug discovery efforts. Previous studies in C57BL/6 mice using [^{3}H-arachidonoyl]anandamide demonstrated deposition of tritium in thalamus and cortical areas that was blocked by treatment with a FAAH inhibitor and that was not seen in FAAH-knockout mice. This suggested that long chain fatty acid amides radiolabeled in the fatty acid moiety might be useful as *ex vivo* and *in vivo* radiotracers for FAAH, since labeled fatty acid released by hydrolysis would be rapidly incorporated into phospholipids with long metabolic turnover periods. Methods. Radiotracers were administered intravenously to conscious Swiss-Webster mice, and radioactivity concentrations in brain areas was quantified and radiolabeled metabolites determined by radiochromatography. Results. [^{14}C]Arachidonic acid, [^{14}C-arachidonoyl]anandamide and [^{14}C-ethanolamine]anandamide, and also [^{14}C]myristic acid, [^{14}C-myristoyl]myristoylethanolamine and [^{14}C-ethanolamine]myristoyl-ethanolamine all had very similar distribution patterns, with whole brain radioactivity concentrations of 2-4% injected dose per gram. Pretreatment with the potent selective FAAH inhibitor URB597 did not significantly alter distribution patterns although radiochromatography demonstrated that the rate of incorporation of label from [^{14}C]anandamide into phospholipids was decreased. Pretreatment with the muscarinic agonist arecoline which increases cerebral perfusion increased brain uptake of radiolabel from [^{14}C]arachidonic acid and [^{14}C-ethanolamine]anandamide, and (in dual isotope studies) from the unrelated tracer [^{125}I]RTI-55. Conclusions. Together with our previously published study with [^{18}F-palmitoyl]16-fluoro-palmitoylethanolamine, the data show that the primary determinant of brain uptake for these tracers in Swiss-Webster mice is initial distribution according to blood flow. It is possible that recently reported strain differences in long chain fatty acid trafficking between C57BL/6 and Swiss Webster mice are responsible for the differences between our results using [^{14}C]anandamide and the earlier studies using [^{3}H]anandamide.

INTRODUCTION

Anandamide (*N*-arachidonoylethanolamine) is a lipid signaling molecule that is an agonist at cannabinoild and vanilloid receptors [1]. In the brain endocannabinoid system it acts as a retrograde neuromodulator, being produced post-synaptically and activating presynaptic cannabinoid CB1 receptors that control release of classical neurotransmitters [2]. Fatty acid amide hydrolase (FAAH) is primarily responsible for terminating actions of anandamide and other fatty acid ethanolamides) in the brain [3]. Potent and selective inhibitors of this serine hydrolase have been developed, including [3-(3-carbamoylphenyl)phenyl] N-cyclohexylcarbamate (URB597) [4], and the enzyme has been the subject of much drug discovery effort [5,6]. It is possible that an inhibitor of FAAH, by raising cannabinergic tone only in brain regions that are producing anandamide, might provide some of the therapeutic actions ascribed to delta-9 tetrahydrocannabinol (the principal active component of cannabis) without its undesirable psychoactive effects. Interest in the therapeutic potential of FAAH inhibitors for indications such as pain and psychiatric disorders has led to the development of radiolabeled analogs of these compounds that can be used to examine the distribution of FAAH in brains of living humans and other animals, so that the relationship between dose regimens and in vivo binding of candidate drugs to FAAH activity can be imaged [7,8]. A potential alternative approach to the use of radiolabeled irreversibly binding FAAH inhibitors would be the use of labeled substrates of FAAH that yielded metabolically trapped labeled products. These might give complementary information, related to flux through FAAH rather than the concentration of FAAH, to that obtained using the radioligand approach. Glaser and co-workers provided evidence that this approach was feasible [9]. They administered anandamide labeled with tritium on the arachidonic acid moiety to C57BL/6 mice, and found that the brain concentration of tritium was about 2.5% ID/g at euthanasia times between 5 and 60 min; this was 3-4 times higher than seen when [^{3}H]arachidonic acid was administered. Autoradiograms of sections prepared from brains of mice euthanized at 30 min, obtained using a Biospace beta-imager, revealed a pattern of tritium deposition for [^{3}H]anandamide that was distinct from that obtained with tritiated arachidonic acid, with highest radioactivity levels (30-40% higher than in striatum or hippocampus) in somatosensory and visual cortex and thalamus. Furthermore, in

FAAH knockout mice, selective uptake of radiolabel in cortex and thalamus was eliminated and at 30 min post injection tritium in the brain remained in the form of anandamide. Addition of the serine hydrolase inhibitor methyl arachidonoylfluorophospate (MAFP) to the intravenous injection mixture also reduced radiolabel in the brain and increased the fraction that was unmetabolized anandamide [9]. The trapping mechanism in these experiments is formation of glycerophospholipids from labeled arachidonic acid released from anandamide by the action of FAAH. Arachidonic acid is rapidly esterified at the 2-position of phospholipids, and is released from this pool quite slowly; the turnover time is 3-4 h [10]. The brain regional disposition of label from intravenously administered arachidonic acid in the rat brain has been evaluated in a series of publications from the Rapoport group [11-13].

We recently evaluated [^{18}F]16-fluorohexadecanoylethanolamine ([^{18}F]omega-fluoropalmitic acid; FHEA) as a positron labeled analog of labeled anandamide [14]. Palmitoylethanolamine is also a substrate for FAAH [15], is present in the brain in higher concentrations than anandamide [16], and is marketed as a nutraceutical [17]. Measuring ^{18}F in microdissected brain regions of Swiss-Webster after intravenous injection of FHEA, we found that: (1) brain concentration of ^{18}F was 3-4 %ID/g at all times evaluated (1, 5, 15, 30, 60 min), with no time-dependency; (2) ^{18}F concentrations in hippocampus were lower than those in striatum, cerebellum thalamus, cortex or brain stem at all times tested; (3) there were no significant differences in brain regional content of ^{18}F measured at 30 min between mice pretreated with the potent selective FAAH inhibitor URB597 and vehicle-pretreated mice; (4) radio thin-layer chromatography of brain tissue 30 min after euthanasia showed significantly higher intact FHEA and significantly lower phosphatidylcholine levels in URB597-pretreated animals compared with vehicle-treated animals. Thus while URB597 did inhibit FAAH in vivo, it did not reduce regional brain concentrations of radiolabel from a radioactive substrate of FAAH whose metabolic product was incorporated in phospholipids. These results with [^{18}F]fluoropalmitoylethanolamine [14] appear to stand in contrast to those of Glaser et al. [9] with [^{3}H-arachidonoyl]ethanolamine and are disappointing from the standpoint of developing a metabolically trapped PET tracer for FAAH.

In the present study, we evaluated the effects of URB597 on in vivo metabolism and brain regional deposition of [^{14}C]anandamide, with the radiolabel being either on the arachidonic acid moiety or the ethanolamine moiety. Similar studies were conducted with [^{14}C]myristoylethanolamine. We also evaluated the effects of the cholinergic muscarinic agonist arecoline on brain radioactivity concentrations at early times after administration of [^{14}C]arachidonic acid or [^{14}C]anandamide. Arecoline increases brain perfusion and also is reported to stimulate phospholipase A_2, the enzyme that mobilizes arachidonic acid from phospholipids [18-20]. In these experiments we included the labeled cocaine analog [^{125}I]RTI-55 (2-beta-carbomethoxy-3-beta-[4-iodophenyl]tropane) [21] in the injected material. While RTI-55 labeled with ^{125}I or ^{123}I is generally employed as a radiotracer for monoamine reuptake sites, it is well-extracted by the brain [22] and was used here at early experimental time-points to indicate changes is cerebral perfusion.

MATERIALS AND METHODS

Animals. Male Swiss-Webster mice (25g) were purchased from Tacomic Farms. They were maintained at the animal facility of Division of Laboratory Animal Medicine (DLAM) on 12 hour alternating light and dark periods, with access to food and water ad libitum. Mice were treated humanely in compliance with NIH guidelines for the use of laboratory animals, and according to a protocol approved by Northeastern University Institutional Animal Care and Use Committee (IACUC). They were housed in groups of 5 in a facility until used. Radiotracers were injected intravenously in a 0.2 mL volume of vehicle consisting of ethanol/emulphor/0.9% saline (1:1:18, v/v) after placement in a mouse holder (Braintree Scientific). At indicated times they were euthanized by cervical dislocation, following which the brain was rapidly removed.

Assay of brain-regional radioactivity after microdissection. In some experiments, the brain was dissected into major regions using the forceps method (Scheffel). Iodine-125 was assayed using a gamma-counter (COBRA). For assay of carbon-14 or tritium, brain regions were dissolved using "Solvable" (Perkin-Elmer) before addition of UltimaGold liquid scintillation fluid; samples were then counted using a Beckman 6500 instrument. Samples of whole blood were decolorized by addition of 50 microliters of hydrogen peroxide before addition of liquid scintillation fluid.

Autoradiography. Brains were placed in ice-cold saline, blotted, and after removal of the cerebellum and brain stem they were glued to the stage of a vibratome (World Precision Instruments) so that coronal sections of width 300 could be prepared. Sections were air-dried and then apposed to phosphorimaging plates. Plates were developed using a Cyclone system (Perkin-Elmer), and images were analyzed using the ImageQuant software supplied with the instrument.

Radiotracers. Carbon-14 and tritium labeled compounds were purchased from American Radiolabeled Chemicals or from Maravek. Fatty acid ethanolamides were prepared from

radioactive ethanolamine and appropriate carboxylic acids using 1-ethyl-3-(3-dimethylaminopropyl)-carbodiimide as a carboxyl activating agent and 4-dimethylaminopyridine as a catalyst. Dichloromethane was used as solvent and reactions were done under argon. Compounds were purified using silica gel chromatography.

Iodine-125 iodide was purchased from Perkin-Elmer; [^{125}I]RTI-55 was prepared by iododestannylation, using trimethyltin starting material purchased from ABX Advanced Biochemical Compounds. It was purified by reverse-phase HPLC. Radioactive peaks were collected and partitioned between ether and water. The ether layer was dried using anyhydrous sodium sulfate, and the solvent removed under a stream of argon. The residue was redissolved in ethanol and stored at -20 degrees until use.

Radioanalytical studies. A modified Folch procedure [24] was used to extract radioactive species from brain or blood. Organic fractions were analyzed using silica gel thin-layer chromatography. Aqueous fractions were analyzed using cation exchange HPLC.

RESULTS

Brain radioactivity from labeled long chain fatty acids and their ethanolamides. Initial studies demonstrated that radiolabel from [^{14}C-arachidonoyl]anandamide localized heterogeneously within the brain following intravenous administration, and that the regional brain concentrations achieved with labeled anandamide were higher than those seen after administration of equivalent activities of [^{14}C]arachidonic acid (Figure 1, Table 1). These findings are consistent with observations in Glaser et al. [9] using [^{3}H-arachdonoyl]anandamide and Pandey et al. [14] using [^{18}F]16-fluorohexadecanoylethanolamine. Since hippocampus had the lowest concentration of radioactivity, the regional brain concentrations at 10 and 100 min are presented normalized to hippocampus concentrations in Figure 2. At least as far as the larger brain regions (striatum, thalamus, cortex and hippocampus, and the ventricle area, are concerned, the patterns for [^{14}C]arachidonic acid and [^{14}C]anandamide are the same at both time-points.

A similar situation pertained when comparing brain uptake of [^{14}C]myristoylethanolamine and [^{14}C]myristic acid; the distribution pattern of the ethanolamide was similar to that of myristic acid (or of arachidonic acid) but the brain regional concentrations were 3-4 times higher (data not shown).

Brain radioactivity from [^{14}C]ethanolamine]anandamide, and effects of URB597. Administration of [^{14}C-ethanolamine]AEA gave a heterogeneous pattern similar to that obtained with [^{14}C-arachidonyl]anandamide with least uptake in hippocampus (Figure 3). There were only small changes in pattern after pretreatment of animals with URB597. However, at the 15 minutes time-point there was a small increase in whole brain radioactivity concentration, whereas at 100 minutes there was a small decrease. These changes are of marginal statistical significance, but are consistent with the idea that while [^{14}C]ethanolamine released by the action of FAAH is fixed in the brain as phospholipid, [^{14}C]anandamide is able very slowly to diffuse back to the blood.

In contrast to the lack of large effect of URB597 on total brain radioactivity, radio-chromatographic analysis of the lipid fraction of Folch extractions [24] showed that while residual intact anandamide amounted to 90% of brain radioactivity in URB597 treated animals at 15 min, it was only 20% in controls. At 100 min post-injection, anandamide was barely detectable in controls, but still accounted for almost 40% of brain activity after the inhibitor (Figure 4). HPLC analysis of the aqueous fraction of Folch extractions of brains from animals given [^{14}C-ethanolamine]anandamide showed the presence of [^{14}C]ethanolamine but it could not be accurately quantified and amounted to <5% of total extracted radioactivity (not shown).

Effects of the muscarinic agonist arecoline on brain uptake of [^{14}C]anandamide. Pretreatment of mice with the muscarinic cholinergic agonist arecoline increased brain disposition of label from [^{14}C]anandamide. This effect was not seen when the muscarinic antagonist atropine was given before arecoline. Atropine blocks both central and peripheral muscarinic receptors. Methylatropine, which cannot pass the blood brain barrier and so antagonizes only peripheral receptors, was given to controls. Thus the blocking effect of atropine on arecoline can be ascribed to a central action.

Effects on arecoline on brain uptake of other radiotracers. Figure 6 shows effects of arecoline on the brain uptake of [^{14}C]arachidonic acid and [^{14}C]anandamide in dual isotope experiments with the labeled cocaine analog [^{125}I]RTI-55. In agreement with previous reports, radioactivity from [^{14}C]arachidonic acid was significantly increased at a 1-minute time-point, as was radioactivity from [^{125}I]RTI-55 (Figure 6A). The net uptake of label from [^{14}C]anandamide at 15 min post injections was also increased, in concert with that of [^{125}I]RTI-55 (Figure 6B). The expected striatum-to-cerebellum ratio of about 2 at this time point was seen for [^{125}I]RTI-55, in both control and arecoline treated animals. RTI-55 readily crosses the blood brain barrier, so that immediately after injection its brain uptake reflects blood flow rather than the distribution of monoamine (largely dopamine) transporters as at later times. The effects of arecoline on

uptake of [^{14}C]anandamide and [^{125}I]RTI-55 were largely abolished by pretreatment of mice with the brain-permeable muscarinic antagonist, atropine (Figure 6C).

DISCUSSION

Our data using [^{14}C-arachidonoyl]anandamide in Swiss-Webster mice are similar to those of Glaser et al. using [^{3}H-arachidonoyl]anandamide in C57BL/6 mice in that brain radioactivity was of the order of 3% ID/g in 25g mice and was heterogeneously distributed. Also, inhibition of FAAH using MAFP or URB597 decreased the extent of metabolism of labeled anandamide and of formation of labeled phospholipids, as did knockout of the FAAH gene. However, while FAAH was inhibited in both studies, this was not associated with significant changes in local radioactivity deposition in the present study, in contrast to the findings of Glaser et al. [9]. Thus, there are no indications in our experiments with [^{14}C-arachidonoyl]anandamide that the autoradiograms contain information about regional FAAH activity. Two other sets of observations support this conclusion. Firstly, the autoradiographic pattern we observed using [^{14}C]arachidonic acid was not significantly different to that seen with [^{14}C-arachidonoyl]anandamide, although the brain concentrations using [^{14}C]arachidonic acid were lower (Figures, 1,2). This suggests that regional accumulation of radiolabel for both tracers is driven by the same process, possibly simply delivery of tracer, dissolution in brain lipids, and very slow washout. An alternative explanation, that FAAH activity is so high in all brain regions that it does not determine the rate of trapping of arachidonic acid derived from anandamide, can be discarded, since residual anandamide was measured in brain. Secondly, [^{14}C-ethanolamine]anandamide gave very similar ^{14}C deposition pattern to [^{14}C-arachidonoyl]anandamide in both control and URB597 pretreated mice (Figure 3), though FAAH activity produces labeled ethanolamine rather than labeled arachidonic acid with this isotopomer. Metabolic trapping in the case of [^{14}C-ethanolamine]anandamide involves largely [^{14}C]phosphatidylethanolamine, rather than [^{14}C]phosphatidylcholine (Figure 4), but [^{14}C]ethanolamine produced from labeled anandamide evidently has a much higher probability of conversion to complex lipids than of diffusing from the brain into the blood. Low activities of ^{14}C in the brain from [^{14}C]ethanolamine administered intravenously shows that ethanolamine also crosses the blood brain barrier poorly in the direction of blood to brain. This is not surprising, in view of the high polarity of ethanolamine (Table 2). The homogeneous (except for

ventricles) autoradiograms seen with [^{14}C]ethanolamine may in part reflect diffusion and redistribution of this very water-soluble compound during preparation and drying of sections, although [^{14}C]phosphatidylethanolamine was detected in brain extracts after administration of [^{14}C]ethanolamine.

It is not clear why the results of the present study with [^{14}C-arachidonoyl]anandamide are not in agreement with those obtained earlier using tritiated anandamide and arachidonic acid [9]. There were a number of technical differences: 1) we used Swiss-Webster mice rather than C57BL/6 mice; 2) we used ^{14}C rather than ^{3}H, and we imaged using a phosphor-imager rather than a beta-imager; 3) we cut sections of unfixed brain using a vibratome, whereas Glaser et al. used a rapid fixation technique followed by microtome sectioning; 4) we used tracers of higher specific radioactivity; 5) we used pretreatment with FAAH inhibitor rather than (intravenous) co-injection with tracer; 6) we did not use FAAH knockout mice in our experiments. Taking these six points in order, some possible explanations for discrepant results could in principle involve:

1) Mouse strain. A recent study [25] documented differences in tissue accumulation of fatty acids and their partitioning into lipid classes between the Swiss-Webster and C57BL/6 strains. In constant infusion experiments using ^{14}C-labeled palmitic, arachidonic and docosahexaenoic acids, the area under the plasma concentration-time curve with infusion of arachidonic acid was significantly lower for C57BL/6 mice. The curves for palmitic and docosahexaenoic acid, however, were not significantly different between the mouse strains. Additionally, incorporation of arachidonic acid but not the other fatty acids into diacylglycerols was significantly lower in C57BL/6 mice. These differences in arachidonic acid incorporation likely produce unique kinetics for trapping tracer in each strain, resulting in different timing requirements for visualizing FAAH activity in each mouse strain. More differences between the two mouse strains were noted for liver and especially heart, than for brain, but it is clear that conclusions drawn from one strain of mice do not necessarily apply to another.

2) Tritium vs carbon-14. Tritium is lost during oxidation of C-atoms bearing tritium, as ^{3}H-atoms abstracted by enzymatic cofactors then appear as H^{3}HO water. Thus regions found to have

relatively lower radioactivity after administration of tritium radiotracers may be regions where tritium has been lost in the absence of loss of the carbon skeleton. The tritium atoms on commercially available [^{3}H]arachidonic acid are located at the four double bonds. Some fraction of this label must be lost from [^{3}H]arachidonic acid in vivo, since an important function of arachidonic acid is to serve as the precursor of prostaglandins and related signaling molecules via cyclooxygenase-catalyzed oxidations and rearrangements [26,27]. Additionally, anandamide is a substrate of cyclooxygenases, forming eicosanoids that retain the ethanolamide moiety [28,29]. Thus it is possible that brain regional differences in metabolism of [^{3}H]anandamide, other than hydrolysis of the amide bond by FAAH could contribute to regional heterogeneity in autoradiograms.

3) Preparation of sections. In the study of Glaser et al. [9] brains: "were transferred into 2% paraformaldehyde plus 2% glutaraldehyde in phosphate buffer on ice for 1 h. The brains were then washed three times with iced PB, and cryoprotected overnight at 4°C in 30% sucrose in PB. Serial cryosections (40 microns) were made and promptly fixed for 5 min in 2% OsO4 in PB. The slides were rinsed in distilled water and desiccated for at least 3 days." It seems possible that the fixation process may have removed unmetabolized anandamide from the surface of the sections, but left in place labeled arachidonic acid (derived from anandamide) incorporated into phospholipids. The beta particles from tritium are very weak, and their range in tissue is <1 micron, so loss of unfixed anandamide from the top layer of cells would be sufficient to alter the appearance of autoradiograms. Also, it seems possible that physical changes in the surface associated with the fixation process might alter the efficiency with which the weak beta particles leave the section, possibly on a regionally selective basis.

4) Administration of serine hydrolase inhibitors. We pretreated animals by intraperitoneal injection of the selective FAAH inhibitor, URB597, 3h before administration of radiotracer. Thus immediate effects of administration of the FAAH-blocking drug on initial extraction of radiotracer by the brain should have been minimal. In contrast, Glaser et al. [9] working before the wide availability of specific inhibitors of FAAH, administered the relatively non-specific inhibitor MAFP and CAY10435, which is potent but of uncharacterized specificity [30] as mixtures with the radiotracer (plus non-radioactive anandamide—see point 5, below). It is

possible that co-injection may have reduced extraction of the tracer during passage through the brain vasculature, by acute pharmacological effects, rather than reducing the degree of hydrolysis of anandamide by FAAH.

5) Specific radioactivity of labeled anandamide. We, unlike Glaser et al. [9], did not dilute the radioactive anandamide with non-radioactive ("carrier") anandamide. Our decision on this point was motivated by the desire to avoid possible pharmacodynamics effects of carrier anandamide, in other words, to preserve the tracer principle (Hevesy 1923). In this we followed the usual practice in nuclear medicine, of using "no carrier added" radioactive probes, since ultimately one would want to evaluate FAAH activity in humans, and the practice avoids the possibility of physiological or toxicological actions, as well as fulfilling a requirement for tracer kinetic modeling. A 4 microcurie injection of [^{14}C]anandamide of specific activity 50 mCi/mmol corresponds to a concentration of 400 nM in the injection bolus, while injection of [^{3}H]anandamide with a loading dose of 10 mg/Kg body weight in a 25g mouse (i.e. 250 microgram) corresponds to a concentration of 5,000 nM in the injection bolus. Thus Glaser et al. [9] administered about 12 times the amount of anandamide as in the present study. Glaser and Kaczochka [31] used a loading dose of 1 mg/Kg, so the total dose of anandamide was very similar to ours.

Since we measured a brain uptake of [^{14}C]anandamide of about 2% injected radioactivity per gram of brain, one can estimate a brain concentration in our work of about 1.6 nmol/g (about 20 nmol/g for Glaser et al. [9]). Most measurements of the average concentration of anandamide in the brains of rodents are in the range 0.1-1 nmol/g (Fegley et al. 2005, Chen et al. 2009, Muccioli et al. 1998, Richardson et al. 2007), so that neither our autoradiographic studies nor those of Glaser et al. [9] appear to correspond to true tracer conditions. It is likely, however, that focal synaptic concentrations of anandamide can be much higher than average brain concentrations. A possible explanation for the discrepancy between our results and those of Glaser et al. [9] is the existence of a binding protein that is saturated under the conditions of Glaser et al. [9], so that most of the labeled anandamide is available for hydrolysis, but that binds essentially all the labeled anandamide under our conditions, so that there was no "free" anandamide. If so, the concentration (Bmax) of this hypothetical binding site would have to be

well above the 1.6 nmol/g calculated for our brain uptake of [^{14}C]anandamide, and the dissociation constant (Km) well below this value (or 1600 nM). Fatty acid binding proteins would appear to be a possibility, but do not seem to meet these criteria for Bmax and Km (Matsumata et al. [36] and references therein). We consider it more likely that the "stickiness" of [^{14}C]anandamide reflects its dissolution in the abundant structurally similar lipid pools of the brain, and its very poor solubility in aqueous compartments.

6) FAAH knockout mice. An important piece of evidence in support of the conclusion of Glaser et al. [9] that regional accumulation of [^{3}H]anandamide indicated relative FAAH activity was that autoradiograms from animals in which the FAAH gene was deleted showed less regional heterogeneity. A possible explanation for these observations is related to point #2, above. Cyclooxygenase activity is upregulated in animals lacking FAAH [37] and so the loss of tritium by oxidation of the arachidonic acid moiety might be responsible for reduced autoradiographic contrast.

Determinants of uptake of radiolabeled fatty acids and their ethanolamides in the brain. The finding of very similar distribution patterns for [^{14}C]arachidonic acid and [^{14}C]anandamide suggests that the same mechanism might be responsible for disposition of both tracers. An obvious possibility is that this pattern reflects the initial delivery of labeled compound to the brain, and that this is long-lasting for [^{14}C]anandamide because it is very lipophilic (Table 2) and therefore dissolves avidly in brain lipids, with very little back-diffusion to the blood. [^{14}C]arachidonic acid released from [^{14}C]anandamide by FAAH also has a very low probability of back diffusion compared with the probability of incorporation into PLs. When [^{14}C-ethanolamine]anandamide is used, then it is presumed that the [^{14}C]ethanolamine is also rapidly incorporated into phospholipids at the site of action of FAAH, since the heterogeneous disposition of label from [^{14}C-ethanolamine]anandamide is in sharp contrast to the homogeneous distribution pattern seen after administration of [^{14}C]ethanolamine. This picture is supported by the greatly increased level of labeled anandamide in brains of mice pretreated with FAAH inhibitor, after administration of either isotopomer of [^{14}C]anandamide, and by the fact that [^{14}C]phosphatidylethanolamine is a major radioactive species in the brains of mice given [^{14}C-ethanolamine]anandamide.

Stimulation of brain uptake of radiotracers by arecoline. We found that arecoline increased the brain uptake of several radiotracers in mice, including [^{14}C]arachidonic acid, for which enhanced brain uptake has previously been demonstrated in rats [38] (Figure 5). Effects of arecoline on brain perfusion have been noted previously [39.40]. Since the brain-permeable muscarinic antagonist atropine blocked increased radiotracer uptake after administration of arecoline, it is apparent that effects are mediated by central muscarinic receptors. DeGeorge et al. [38] suggested that increased deposition of labeled arachidonic acid after arecoline is due to stimulation of phospholipase A2 (PLA_2), and thus to increased turnover of phospholipid pools that incorporate arachidonic acid moieties. Although this mechanism of direct coupling to PLA_2 activity could not operate on the other radiotracers we evaluated, including [^{14}C-

ethanolamine]anandamide, we cannot exclude an indirect coupling to PLA_2 via increased production of vasoactive metabolites of arachidonic acid.

Brain permeability and lipophilicity. The general inverse relationship between logP (or logD) values and blood brain barrier permeability is well documented, and clearly dominant amongst the standard molecular metrics of the radiotracers used in this study (Table 2). RTI-55 has a logD(7.4) value between 1 and 2 where brain extraction for compounds that are neutral or weak bases is optimum [41]. Although clogD(7.4) values of long chain fatty acids are 1—2 units lower than those of the corresponding ethanolamides, their clogD values are nevertheless high and their brain uptake is lower. This suggests a possible role of ethanolamides as prodrugs for pharmacologically active compounds that are carboxylates.

REFERENCES

1. Devane, WA, Hanus L, Breuer A, Pertwee RG, Stevenson LA, Griffin G, Gibson D, Mandelbaum A, Etinger A and Mechoulam R. Isolation and structure of a brain constituent that binds to the cannabinoid receptor. Science 1992; 258: 1946-1949.

2. Kano M, Ohno-Shosaku T, Hashimotodani Y, Uchigashima M and Watanabe M. "Endocannabinoid-mediated control of synaptic transmission." Physiol Rev 2009 89: 309-380.

3. Ahn K, McKinney MK and Cravatt BF. "Enzymatic pathways that regulate endocannabinoid signaling in the nervous system." 2008 Chem Rev 108: 1687-1707.

4. Johnson DS, Stiff C, Lazerwith SE, Kesten SR, Fay LK, Morris M, Beidler D, Liimatta MB, Smith DE, Dudley DT, Sadagopan N, Bhattachar SN, Kesten SJ, Nomanbhoy TK, Cravatt BF and Ahn K. "Discovery of PF-04457845: A Highly Potent, Orally Bioavailable, and Selective Urea FAAH Inhibitor." 2005 ACS Med Chem Lett 2: 91-96.

5. Huggins JP, Smart TS, Langman S, Taylor L and Young T. "An efficient randomised, placebo-controlled clinical trial with the irreversible fatty acid amide hydrolase-1 inhibitor PF-04457845, which modulates endocannabinoids but fails to induce effective analgesia in patients with pain due to osteoarthritis of the knee." 2012; Pain 153: 1837-1846.

6. Bégaud B, Bousser MG, Cohen C, Diquet B, Duprat P, Janssens W, Mallaret M, Mazué G, Micallef J, Monneret C, Montastruc JM, Venance L. Report by the Temporary Specialist Scientific Committee (TSSC), "FAAH (Fatty Acid Amide Hydrolase)", on the causes of the accident during a Phase 1 clinical trial in Rennes in January 2016. Agence Nationale de Sécurité du Médicament et des produits de santé, 2016. (English version).

7. Wilson AA, Garcia A, Parkes P, Houle S, Tong J and Vasdev N. "[^{11}C]CURB: Evaluation of a novel radiotracer for imaging fatty acid amide hydrolase by positron emission tomography." 2012; Nucl Med Biol 38: 247-253.

8. Boileau I, Rusjan PM, Williams B, Mansouri E, Mizrahi R, De Luca V, Johnson DS, Wilson AA, Houle S, Kish SJ and Tong J. "Blocking of fatty acid amide hydrolase activity with PF-04457845 in human brain: a positron emission tomography study with the novel radioligand [(11)C]CURB." 2005; J Cereb Blood Flow Metab 35: 1827-1835.

9. Glaser ST, Gatley SJ and Gifford AN. "Ex vivo imaging of fatty acid amide hydrolase activity and its inhibition in the mouse brain." 2006; J Pharmacol Exp Ther 316: 1088-1097.

10. Rapoport SI "In vivo approaches to quantifying and imaging brain arachidonic and docosahexaenoic acid metabolism." 2003; J Pediatr 143(4 Suppl): S26-34.

11. Rapoport SI, Purdon D, Shetty HU, Grange E, Smith Q, Jones C and Chang MC. "In vivo imaging of fatty acid incorporation into brain to examine signal transduction and neuroplasticity involving phospholipids." 1997; Ann N Y Acad Sci 820: 56-73; discussion 73-54.

12. Robinson PJ, Noronha J, DeGeorge JJ, Freed LM, Nariai T and Rapoport SI. "A quantitative method for measuring regional in vivo fatty-acid incorporation into and turnover within brain phospholipids: review and critical analysis." 1992; Brain Res Brain Res Rev 17: 187-214.

13. Basselin M, Chang L., Bell JM and Rapoport SI. "Chronic lithium chloride administration to unanesthetized rats attenuates brain dopamine D2-like receptor-initiated signaling via arachidonic acid." 2005; Neuropsychopharmacology 30(6): 1064-1075.

14. Pandey MK, DeGrado TR, Qian K, Jacobson MS, Hagen CE, Duclos, Jr RI. and Gatley SJ. "Synthesis and preliminary evaluation of N-(16-18F-fluorohexadecanoyl)ethanolamine (18F-FHEA) as a PET probe of N-acylethanolamine metabolism in mouse brain." 2014; ACS Chem Neurosci 5(9): 793-802.

15. Hamtiaux L, Masquelier J, Muccioli GG, Bouzin C, Feron O, Gallez B, Lambert DM. The association of N-palmitoylethanolamine with the FAAH inhibitor URB597 impairs melanoma growth through a supra-additive action. 2012; BMC Cancer. 19;12:92.

16. Alhouayek M, Bottemanne P, Subramanian KV, Lambert DM, Makriyannis A, Cani PD and Muccioli GG. "N-Acylethanolamine-hydrolyzing acid amidase inhibition increases colon N-palmitoylethanolamine levels and counteracts murine colitis." 2015; FASEB J 2): 650-661.

17. Kopsky DJ, Hesselink JM. Multimodal stepped care approach with acupuncture and PPAR-α agonist palmitoylethanolamide in the treatment of a patient with multiple sclerosis and central neuropathic pain. 2012; Acupunct Med. 30:53-5.

18. Woelk H, Goracci G, Porcellati G. The action of brain phospholipases A2 on purified, specifically labelled 1,2-diacyl-, 2-acyl-1-alk-1'-enyl- and 2-acyl-1-alkyl-sn-glycero-3-phosphorylcholine. 1974; Hoppe Seylers Z Physiol Chem. 355(1):75-81.

19. Horrocks LA. Sources for brain arachidonic acid uptake and turnover in glycerophospholipids. 1989 Ann N Y Acad Sci. 559:17-24.

20. Sun GY, Xu J, Jensen MD, Simonyi A. Phospholipase A2 in the central nervous system: implications for neurodegenerative diseases. 2004; J Lipid Res. 45:205-13.

21. Boja JW, Patel A, Carroll FI, Rahman MA, Philip A, Lewin AH, Kopajtic TA, Kuhar MJ. [125I]RTI-55: a potent ligand for dopamine transporters. 1991; Eur J Pharmacol. 26;194:133-4.

22. Innis R, Baldwin R, Sybirska E, Zea Y, Laruelle M, al-Tikriti M, Charney D, Zoghbi S, Smith E, Wisniewski G, et al. Single photon emission computed tomography imaging of monoamine reuptake sites in primate brain with [^{123}I]CIT. 1991; Eur J Pharmacol. 6;200(2-3):369-70.

23. Hanson RN, Franke L, Lee SH, Seitz DE. Radioiododestannylation: preparation and evaluation of radioiodinated thienyl alcohols. 1987; Int J Rad Appl Instrum A. 38:641-5.

24. Folch J, Lees M, Sloane Stanley GH. A simple method for the isolation and purification of total lipides from animal tissues. 1957; J Biol Chem. 226:497-509.

25. Seeger DR and Murphy EJ . "Mouse Strain Impacts Fatty Acid Uptake and Trafficking in Liver, Heart, and Brain: A Comparison of C57BL/6 and Swiss Webster Mice." 2016; Lipids 51: 549-560.

26. Schneider C, Boeglin WE, Lai S, Cha JK and Brash AR. "Synthesis and applications of stereospecifically (3)H-labeled arachidonic acids as mechanistic probes for lipoxygenase and cyclooxygenase catalysis." 2000; Anal Biochem 284: 125-135.

27. FowlerCJ, Stenstrom A and Tiger G. "Ibuprofen inhibits the metabolism of the endogenous cannabimimetic agent anandamide." 2007; Pharmacol Toxicol 80: 103-107.

28. McGinley CM. and van der Donk WA. "Enzymatic hydrogen atom abstraction from polyunsaturated fatty acids." 2003; Chem Commun (Camb) 23: 2843-2846.

29. Hermanson DJ, Gamble-George JC, Marnett LJ and Patel S.. "Substrate-selective COX-2 inhibition as a novel strategy for therapeutic endocannabinoid augmentation." 2014; Trends Pharmacol Sci 35: 358-367.

30. Boger DL, Miyauchi H, Du W, Hardouin C, Fecik RA, Cheng H, Hwang I, Hedrick MP, Leung D, Acevedo O, Guimarães CR, Jorgensen WL, Cravatt BF. Discovery of a potent, selective, and efficacious class of reversible alpha-ketoheterocycle inhibitors of fatty acid amide hydrolase effective as analgesics. J Med Chem. 2005; 48:1849-56.

31. Glaser ST and Kaczocha M. "Temporal changes in mouse brain fatty acid amide hydrolase activity." 2009; Neuroscience 163: 594-600.

32. Fegley D, Gaetani S, Duranti A, Tontini A, Mor M, Tarzia G and Piomelli D. "Characterization of the fatty acid amide hydrolase inhibitor cyclohexyl carbamic acid 3'-carbamoyl-biphenyl-3-yl ester (URB597): effects on anandamide and oleoylethanolamide deactivation." 2005; J Pharmacol Exp Ther 313: 352-358.

33. Chen K, Paudel KS, Derbenev AV, Smith BN and Stinchcomb AL. "Simultaneous Quantification of Anandamide and Other Endocannabinoids in Dorsal Vagal Complex of Rat Brainstem by LC-MS." 2009; Chromatographia 69: 1-7.

34. Muccioli GG, and Stella S. "An optimized GC-MS method detects nanomolar amounts of anandamide in mouse brain." 2008; Anal Biochem 373: 220-228.

35. Richardson D, Ortori CA, Chapman V, Kendall DA and Barrett DA. "Quantitative profiling of endocannabinoids and related compounds in rat brain using liquid chromatography-tandem electrospray ionization mass spectrometry." 2007; Anal Biochem 360: 216-226.

36. Matsumata M, Inada H and Osumi N. "Fatty acid binding proteins and the nervous system: Their impact on mental conditions." 2016; Neurosci Res 102: 47-55.

37. Glaser ST and Kaczocha M. "Cyclooxygenase-2 mediates anandamide metabolism in the mouse brain." 2010; J Pharmacol Exp Ther 335: 380-388.

38. DeGeorge JJ, Noronha JG, Bell J, Robinson P and Rapoport SI. "Intravenous injection of [1-14C]arachidonate to examine regional brain lipid metabolism in unanesthetized rats." 1989; J Neurosci Res 24: 413-423.

39. Patil PN and Stearns R. "Mechanism of vascular relaxation by cholinomimetic drugs with special reference to pilocarpine and arecoline." 2002; J Ocul Pharmacol Ther 18: 25-34.

40. Maiese K, Holloway HH, Larson DM and Soncrant TT. "Effect of acute and chronic arecoline treatment on cerebral metabolism and blood flow in the conscious rat." 1994; Brain Res 641: 65-75.

41. Waterhouse RN. Determination of lipophilicity and its use as a predictor of blood-brain barrier penetration of molecular imaging agents. Mol Imaging Biol. 2003; 5:376-89.

Figure 1. Regional deposition of radiolabel in the brain following administration of [^{14}C]arachidonic acid and [^{14}C-arachidonoyl]anandamide. A) Representative autoradiographs prepared after injection of [^{14}C]arachidonic acid. B) Representative autoradiographs prepared after injection of [^{14}C-arachidonoyl]anandamide. Image were adjusted using the OptiQuant software to make the sections in (A) and (B) look similar in intesity, to stress the point that the patterns of deposition are very similar. C) Sample sections with circles drawn around regions of interest used for quantification of signal. Left-to-right: cortex, striatum, ventricles, hippocampus, thalamus.

Figure 2. Relative signal intensity of different brain regions quantified from autoradiographs of mice injected with [^{14}C]arachidonic acid and [^{14}C-arachidonyl]anandamide. The patterns of radiolabel disposition were not significantly different between 10 and 100 minutes and between [^{14}C]arachidonic acid and [^{14}C-arachidonoyl]anandamide. (n=4, student's t-test, $p>0.05$) CX, cortex; HP, hippocampus; VT, ventricular epithelium; TH, thalamus; ST, striatum.

Figure 3. Effects of URB597 pre-treatment on regional deposition and total amount of brain radioactivity in mice injected with [^{14}C-EA]anandamide. A) Autoradiographic intensity data for 4 conditions (euthanasia at 15 and 100 min in control mice, and 15 and 100 min in URB597 pretreated mice, as indicated) in 4 brain regions (black, cortex; white, striatum; grey, hippocampus, striped, thalamus). Data are normalized to intensities for control, 15 min animals. B) Data from graph (A) normalized to the hippocampus for each condition (black, 15 min control; white, 100 min control; grey, 15 min URB597 treated; striped, 100 min URB597 treated.

Figure 4. The effects of URB597 pre-treatment on the chemical form of ^{14}C in mice injected with [^{14}C-EA]anandamide. A) Representative 2D radio-thin layer chromatogram of a Folch extraction of cerebellum. Developing solvents were (first): chloroform/methanol/ammonium hydroxide = 65:35:5; (second): chloroform/acetone/methanol/acetic acid/water = 30:40:10:10:5. The dominant spot corresponded to standards of phosphatidylethanolamine. Representative 1D radio-thin layer chromatogram of a Folch extract of whole blood. The developing solvent was chloroform/methanol/ammonium hydroxide =60:30:1. The lanes were: control 15 min; control 100 min; URB597 treated 15 min; URB597 treated 100 min; [^{14}C]anandamide standard.
C) Unchanged [^{14}C]anandamide in extracts of cerebellum. Bars are the mean +/- standard deviation (n = 3, normalized to radioactivity applied to TLC plate) for mice corresponding to indicated times and treatments. D) Unchanged [^{14}C]anandamide in extracts of whole blood. Bars are the mean +/- standard deviation (n = 3, normalized to radioactivity applied to TLC plate) for mice corresponding to indicated times and treatments.

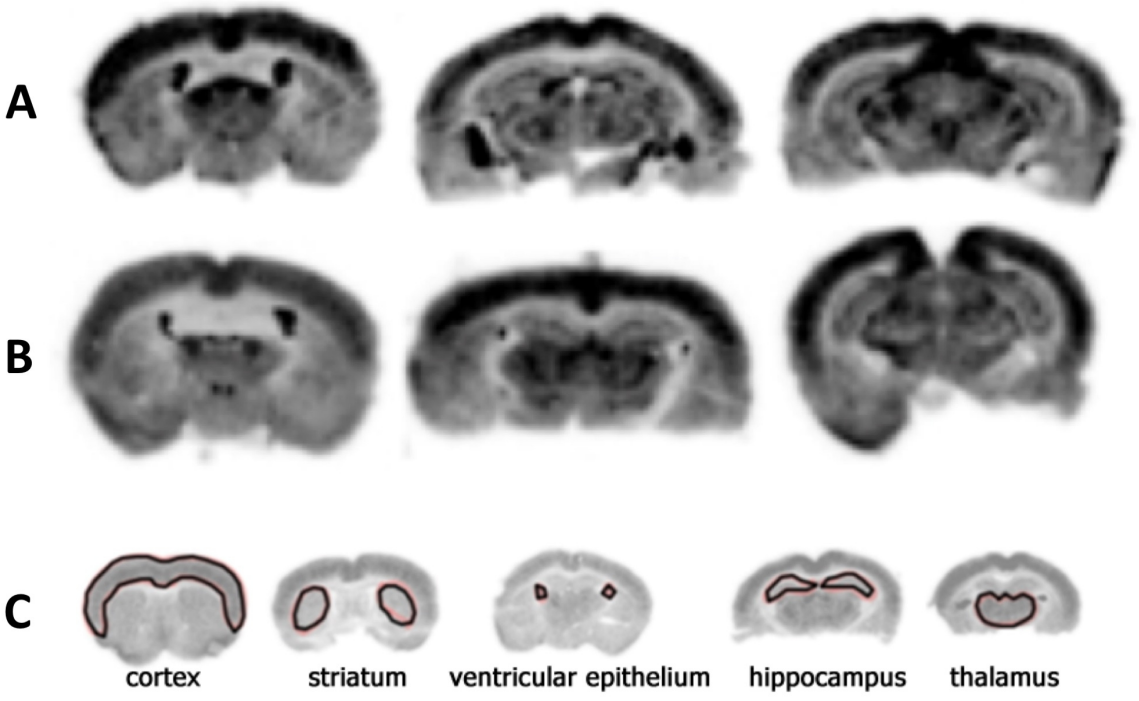
A
B
C
cortex
striatum
ventricular epithelium
hippocampus
thalamus

Hu Fig 1

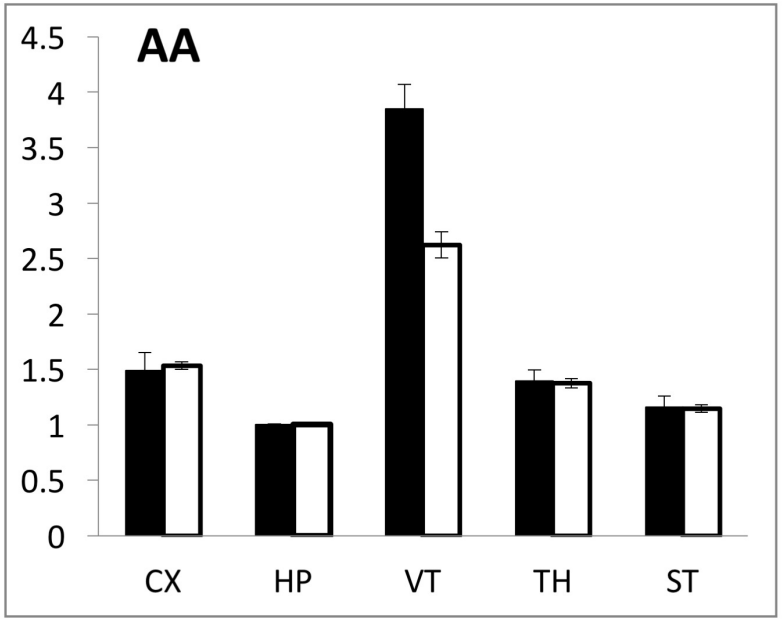
AA
4.5
4
3.5
3
2.5
2
1.5
1
0.5
0
CX
HP
VT
TH
ST

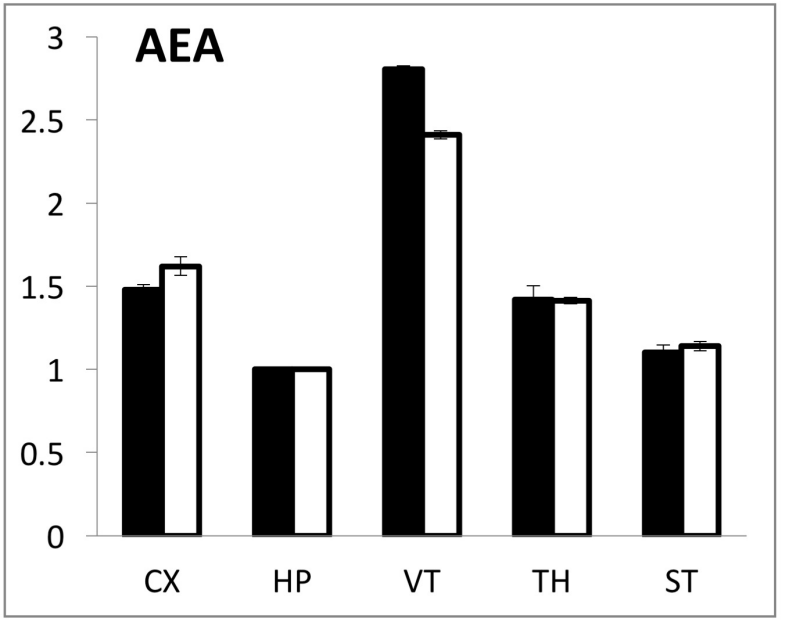
AEA
3
2.5
2
1.5
1
0.5
0
CX
HP
VT
TH
ST

Hu Fig 2

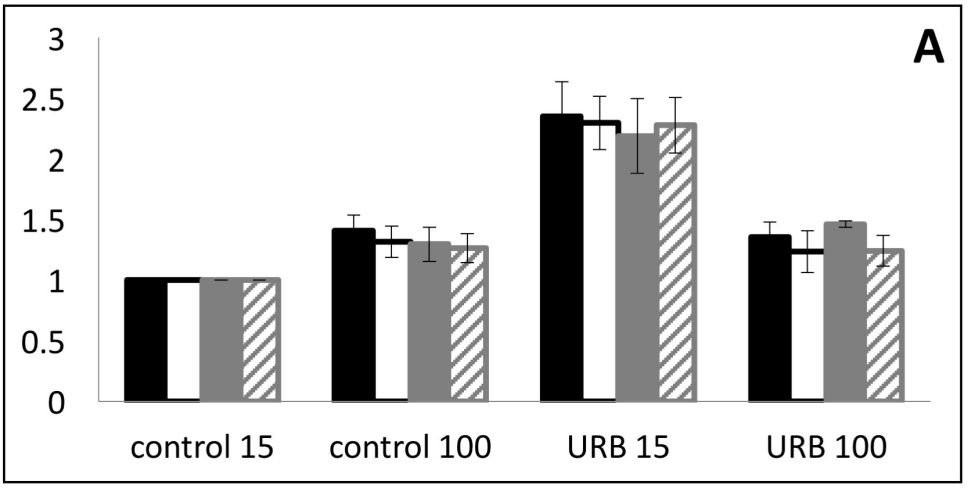
A
3
2.5
2
1.5
1
0.5
0
control 15
control 100
URB 15
URB 100

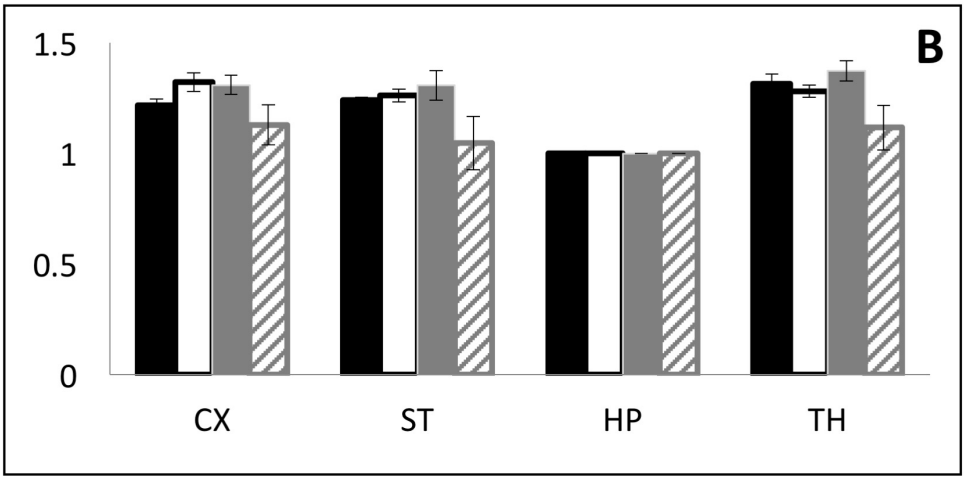
B
1.5
1
0.5
0
CX
ST
HP
TH

Hu Fig 3

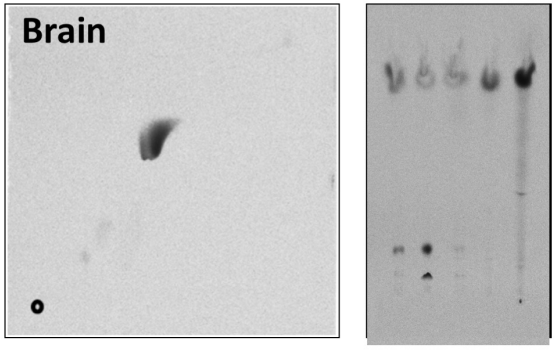
Brain

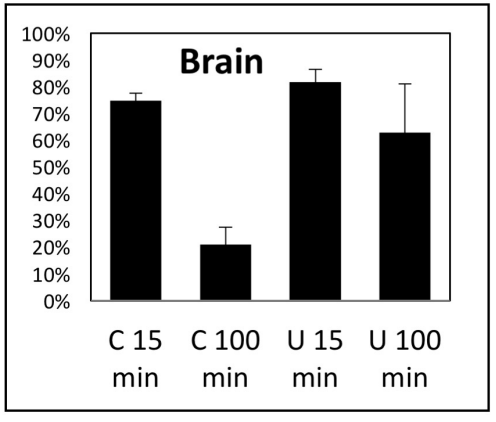
Brain
100%
90%
80%
70%
60%
50%
40%
30%
20%
10%
0%
C 15 min
C 100 min
U 15 min
U 100 min

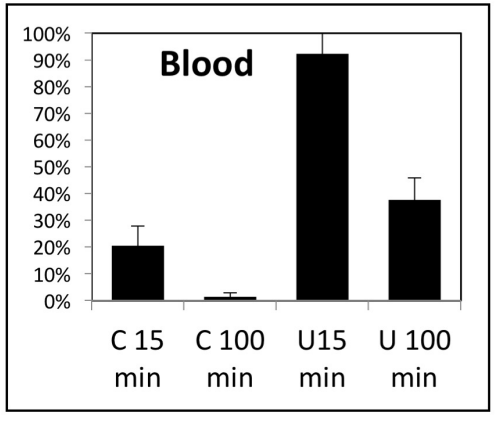
Blood
100%
90%
80%
70%
60%
50%
40%
30%
20%
10%
0%
C 15 min
C 100 min
U15 min
U 100 min

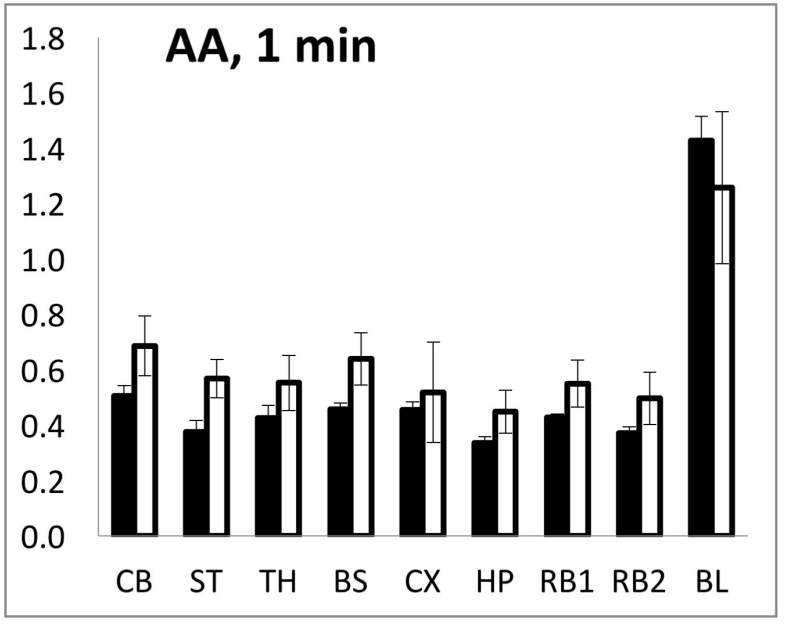
AA, 1 min
1.8
1.6
1.4
1.2
1.0
0.8
0.6
0.4
0.2
0.0
CB
ST
TH
BS
CX
HP
RB1
RB2
BL

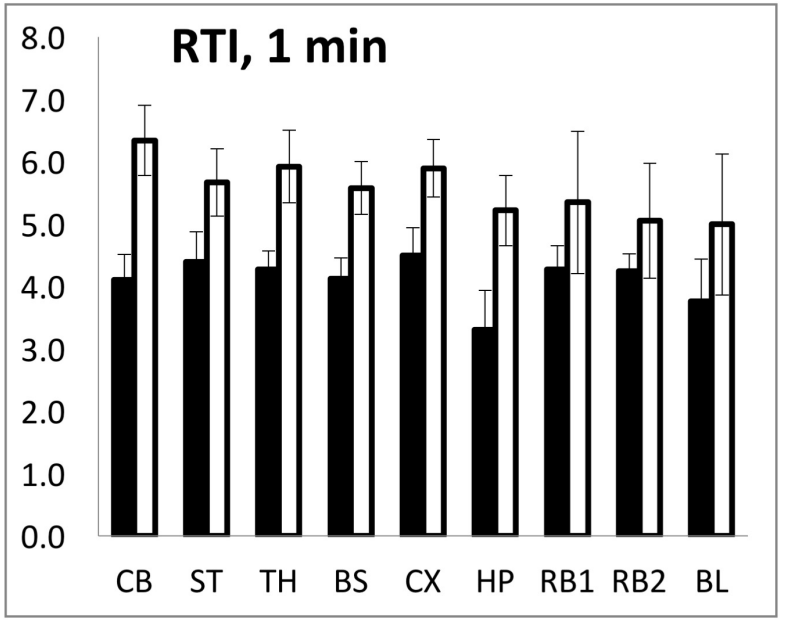
RTI, 1 min
8.0
7.0
6.0
5.0
4.0
3.0
2.0
1.0
0.0
CB
ST
TH
BS
CX
HP
RB1
RB2
BL

Hu Fig 5 A

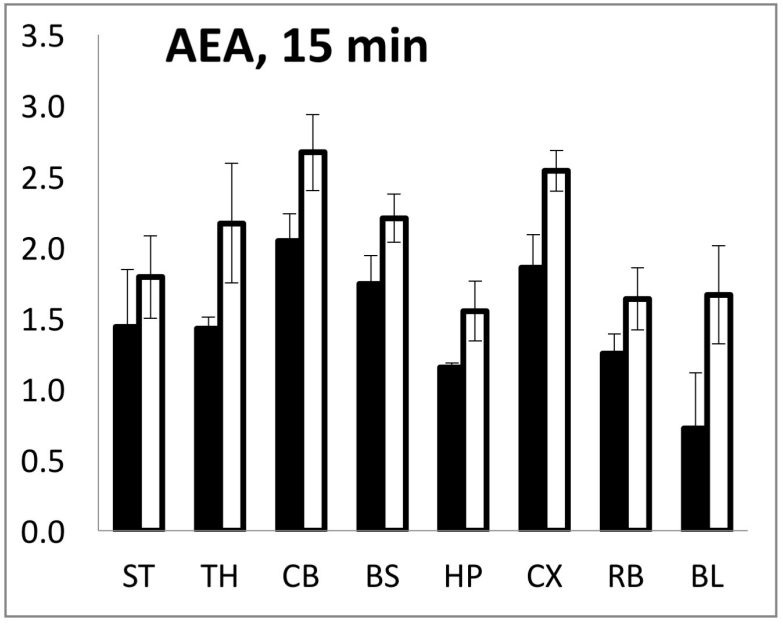
AEA, 15 min
3.5
3.0
2.5
2.0
1.5
1.0
0.5
0.0
ST
TH
CB
BS
HP
CX
RB
BL

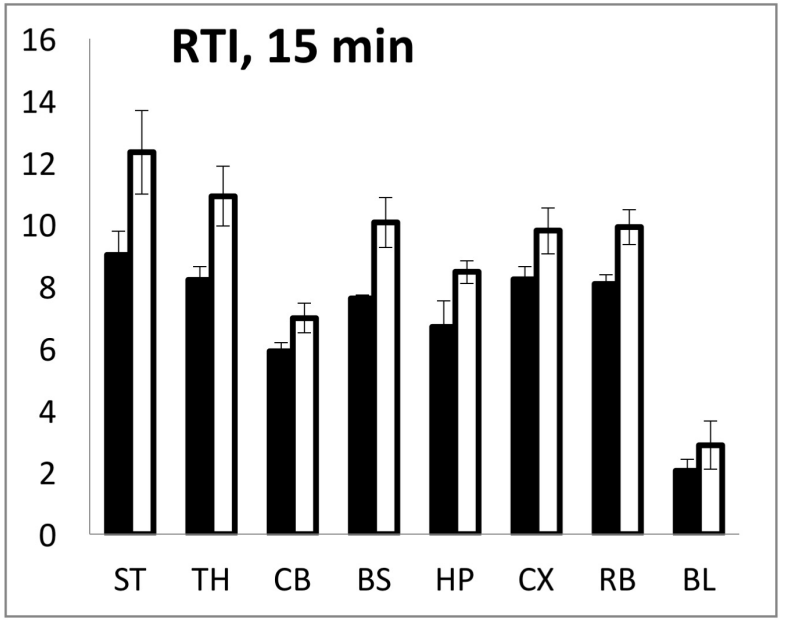
RTI, 15 min
16
14
12
10
8
6
4
2
0
ST
TH
CB
BS
HP
CX
RB
BL

Hu Fig 5 B

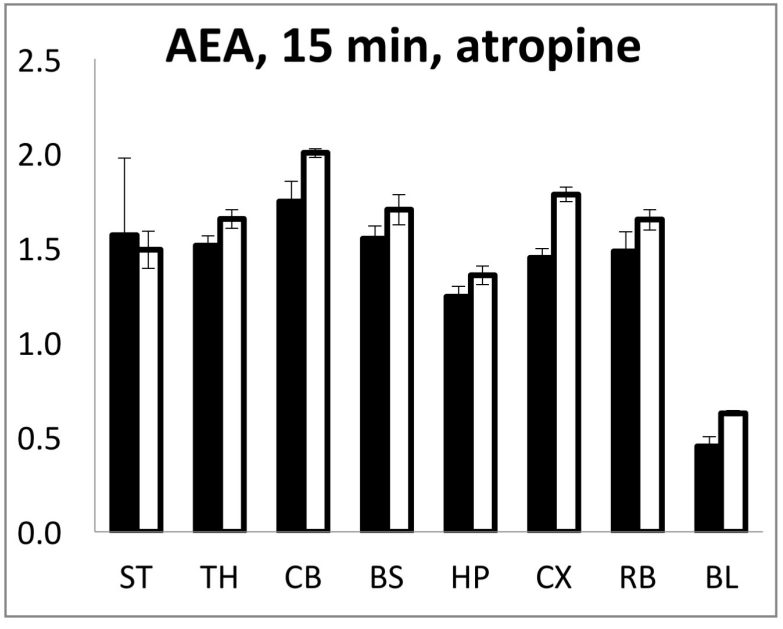
AEA, 15 min, atropine
2.5
2.0
1.5
1.0
0.5
0.0
ST
TH
CB
BS
HP
CX
RB
BL

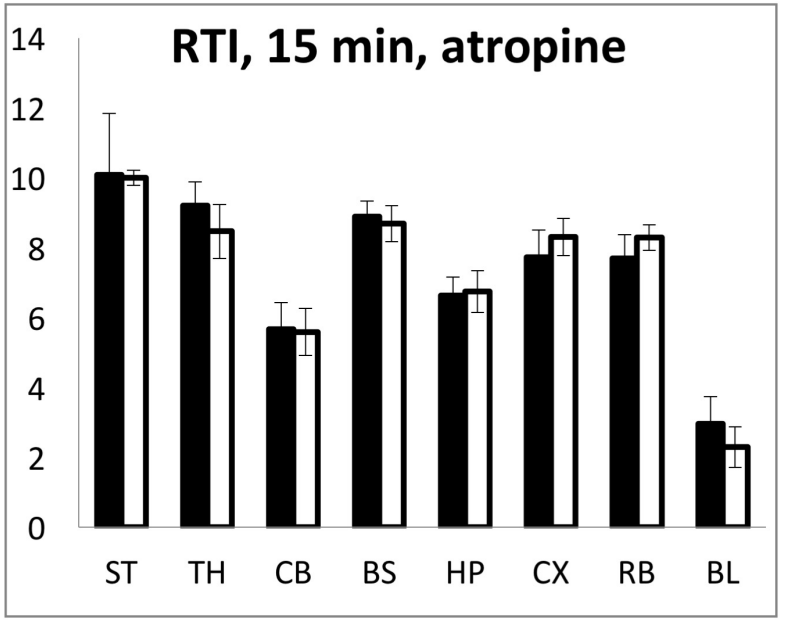
RTI, 15 min, atropine
14
12
10
8
6
4
2
0
ST
TH
CB
BS
HP
CX
RB
BL

Hu Fig 5 C

		Signal (DLU/mm^2/10^6/36d		
Region	Time	Arach.	Anand.	Ratio
Cortex	10min	1.97	9.45	4.79
	100min	2.26	11.0	4.87
Hippocampus	10min	1.33	5.84	4.38
	100min	1.52	7.06	4.65
Ventricular epithelium	10min	3.74	14.1	3.76
	100min	5.84	19.1	3.27
Thalamus	10min	1.89	8.25	4.36
	100min	2.11	9.92	4.69
Striatum	10min	1.47	6.66	4.53
	100min	1.76	8.26	4.70

Table 1. Quantification of the accumulation of radioactivity in various brain regions with OptiQuant. Values were averages from all the slices that contained the region of interest in each brain. The slices from the four mice injected with [^{14}C]arachidonic acid or [^{14}C-arachidonoyl]anandamide and euthanized 10 or 100 minutes later were apposed to the same phosphor imaging plate for 36 days (n =1).

Tracer	MW	PSA	HBD	HBA	clogP	clogD	pKa	FRB
Arachidonic acid	304	37	1	2	6.9	3.9	4.8	14
Anandamide	348	49	2	3	5.7	5.7	n/a	16
RTI-55	385	30	0	3	3.4	1.1	8.6[1]	3
Myristic acid	228	37	1	2	6.1	3.6	4.9	12
Myristoylethanolamine	272	49	2	3	5.0	5.0	n/a	14
Ethanolamine	61	46	3	2	-1.3	-3.4	9.5	1

[1]pKa value for cocaine

Table 2. Molecular metrics of radiotracers used in this study. Values are taken from Chemspider and other literature sources. MW – molecular weight (daltons); PSA = polar surface area (angstrom2); HBD = number of hydrogen bond donors; HBA = number of hydrogen bond acceptors; clogP = calculated log octanol/water partition coefficient; clogD = calculated log octanol/pH7.4 buffer partition coefficient; pKa = acidity; FRB = number of freely rotatable bonds.

S Sonti and SJ Gatley DRAFT

Uptake of synaptamide – *in vitro* and in vivo studies

Rationale: We wanted to explore the brain uptake of DHA and synaptamide both *in vivo* and *in vitro*. Previous work carried out by Kun Qian, demonstrates that the N-acylethanolamines of fatty acids are better taken up by the brain than the free fatty acids themselves. This was shown to be the case with the omega-6 fatty acid, arachidonic acid and its N-acylethanolamine, anandamide as well as with myristic acid (C14:0; not found in animal tissues but is analogous to AA) and its *N*-acylethanolamine, myristoylethanolamide. As DHA and synaptamide are structurally similar to AA and AEA, we wanted to investigate if a similar pattern will be observed with them. Performing *in vitro* uptake studies in parallel will probably uncover details about DHA uptake and synaptamide synthesis in neural cells alone and how relevant it may be to the brain uptake *in vivo*.

Method: *In vivo* brain uptake is determined by performing microdissection studies The dissolved tissues of various brain regions and culture medium from cell cultures are mixed with 5 ml of Scintillation cocktail and the amount of radioactivity in each sample is quantified by the liquid scintillation counter. Each sample will be counted for 30 minutes in order to eliminate background radiation and get more reliable counts. *In vitro* uptake studies are performed by incubating N27 cells with [C-14] DHA and synaptamide. Cell uptake is evaluated by determining the radiolabel content in the lipid extracts by radio TLC.

Data analysis: From the counts per minute (cpm) obtained from the beta-counter, absolute and relative uptake of the injected activity can be calculated. With use of two-tailed unpaired student's t test, comparisons of absolute and relative %IA/g values will be made. This will inform us of how the uptake differs within the brain regions and between *in vitro* and *in vivo* conditions. For *in vitro* uptake analysis, the average of atleast 3 experiments will be considered. An average of 8 animals will be considered for analysis of %IA/g values in *in vivo* uptake studies.

Results:

Regional brain uptake and distribution of exogenous synaptamide ([C-14] Synaptamide)

Regional brain uptake and distribution experiments were performed in mice using microdissection experiments. It is a simple technique which involves the administration of a tracer to the animals and after an appropriate interval, the animal is euthanized and the amount of radioactivity in various regions of the organ of interest can be quantified and subsequent distribution can be looked at. To look at the uptake and distribution of synaptamide, we will use [C-14] Synaptamide, synthesized in our lab. To our knowledge, we are the first to synthesize [C-14] labeled synaptamide and to perform an uptake and distribution study.

Labeled long chain fatty acids and their ethanolamides are stored in ethanol at -80^{o}C to prevent oxidation as they are extremely unsaturated and susceptible to oxidation. For injecting into the animals, the radiotracer solution is prepared fresh, just before starting each experiment, to limit its rearrangement or degradation. Ethanol is evaporated under argon air flow for protection against oxygen, and the tracer is re-dissolved in emulphor/ethanol/saline (1:1:18) vehicle. Before injecting into mice, 20 µl of the injection mixture will be tested, as a standard, with the scintillation counter for the amount of radioactivity injected for later calculation of IA%/g values. 0.1 µCi of [C-14] synaptamide in 200 µl emulphor/ethanol/saline (1:1:18) is injected into the mouse via tail vein injection. After 15 minutes, animals are euthanized by cervical dislocation, the brains removed immediately, and micro-dissected on a filter paper wetted with 0.9% saline.

The regions of interest, namely, hypothalamus, olfactory tubercle, frontal cortex, hippocampus, striatum, cerebellum, brain stem, mid brain, thalamus and rest of the brain are separated, weighed in scintillation vials, and soaked in solvable (tissue solubilizer). After tissue samples are completely dissolved, 5 ml of Scintillation cocktail is added to each vial, and the amount of radioactivity is quantified by the liquid scintillation counter. Blood samples are collected immediately after the mice are euthanized to prevent clotting of blood. Samples are dissolved in tissue solubilizer and bleached with 10% hydrogen peroxide before scintillation fluid is added.

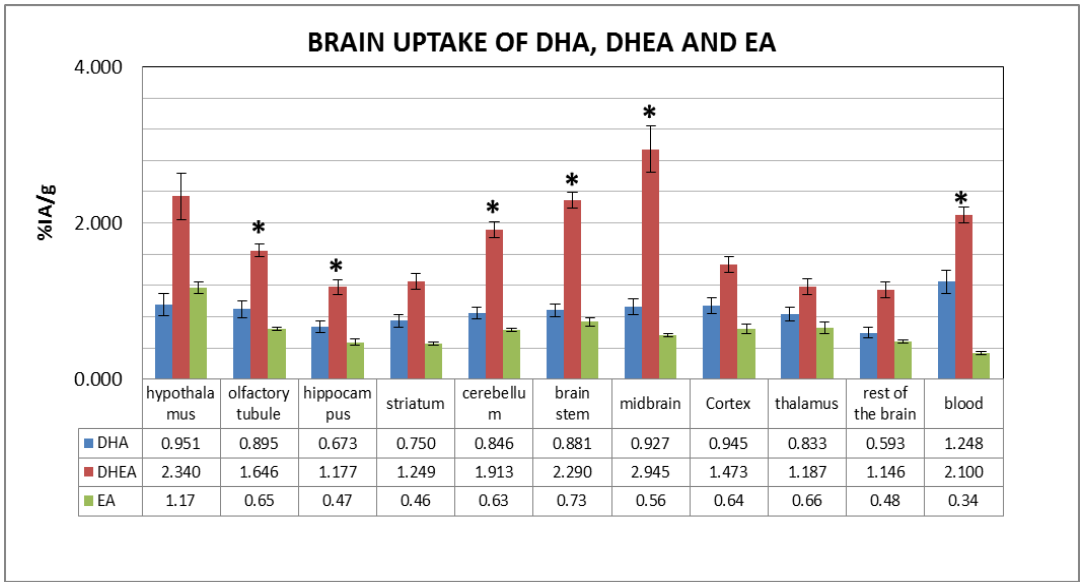

	hypothalamus	olfactory tubule	hippocampus	striatum	cerebellum	brain stem	midbrain	Cortex	thalamus	rest of the brain	blood
DHA	0.951	0.895	0.673	0.750	0.846	0.881	0.927	0.945	0.833	0.593	1.248
DHEA	2.340	1.646	1.177	1.249	1.913	2.290	2.945	1.473	1.187	1.146	2.100
EA	1.17	0.65	0.47	0.46	0.63	0.73	0.56	0.64	0.66	0.48	0.34

Fig 4 Results from microdissection studies in animals injected with 0.1µCi [^{14}C] Synaptamide, 0.1µCi [^{14}C] DHA and 1µCi [^{14}C] Ethanolamine (i.v.). Analysis of the regional distribution in the brain reveals that the pattern of synaptamide uptake is different from that of ethanolamine. %IA/g given as mean ± SD; error bars represent SEM; *N=3 (ethanolamine), N=8 (DHA and synaptamide)*.

The counts per minute (CPM) and H# obtained from the liquid scintillation counter will be used to calculate the percent of injected activity per gram (%IA/g) for the samples. The relative %IA/g values is calculated by dividing the absolute %IA/g value in each region of interest by the absolute %IA/g value of the whole brain. The percent injected activity per gram for synaptamide after 15 minutes is shown in Fig 4. In order to ensure that the pattern seen is due to the uptake synaptamide and rule out the possibility of synaptamide breakdown, we administered another set of animals with [C-14] ethanolamine. The pattern observed is quite different from that of synaptamide; thus confirming that synaptamide enters the brain without getting hydrolyzed into ethanolamine.

Previously done in our lab by Kun Qian, the autoradiography pattern of anandamide was quantified in terms of radioactive intensity (DLU/mm^2). Although anandamide is a structural analog of synaptamide; due to the difference in technique and output unit, we cannot compare the uptake of both anandamide and synaptamide; the pattern of their distribution can however, be compared. The pattern of anandamide distribution is different than that of synaptamide indicating a different uptake profile and its possible implications in functions quite different to that of anandamide (Fig 5).

Fig 5A and B

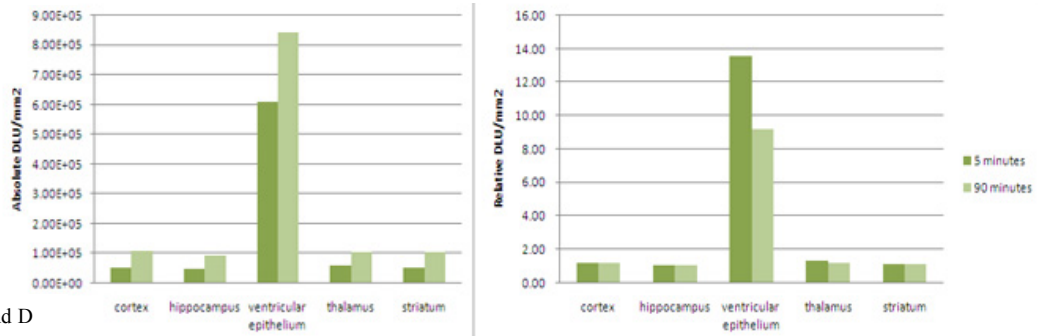

Fig 5 C and D

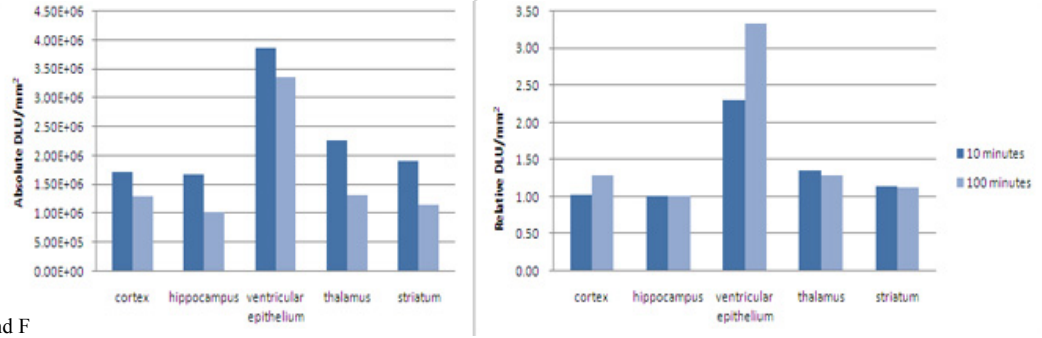

Fig 5 E and F

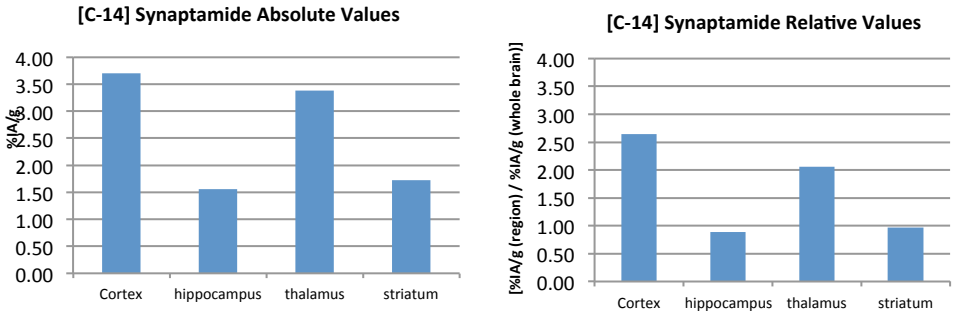

Fig 5. *A and B*. The pattern of distribution of ethanolamide as a control is evaluated by autoradiography (done by Kun Qian). The uptake pattern is uniform throughout except in ventricles. *C and D*. The pattern of distribution of Anandamide as observed with autoradiography (done by Kun Qian). The radioactivity in thalamus and striatum seem to be higher than the cortex and hippocampus. The increased radioactivity in the ventricular epithelium is probably due to the formation of ethanolamine due to hydrolysis. *E and F.* The pattern of synaptamide is quite different to the pattern of anandamide or ethanolamine. The uptake is high in cortex and thalamus.

Another notable observation made by Kun Qian from the autoradiography experiments was that the extent of uptake of anandamide was consistently higher than that of its corresponding acid, arachidonic acid (table 1). In autoradiography experiments, accumulation of radioactivity is shown as intensity (in DLU/mm^2) with the different levels of signal intensity reflecting the different amounts of radioactivity. The absolute values of signal intensity for each radiotracer in different brain regions are obtained after 36 days of exposing coronal brain slices. The signal intensity ratio revealed that the accumulation of radioactivity produced with [^{14}C] AEA is 3 to 5 fold higher than that produced with [^{14}C] AA (table 1).

		Absolute signal intensity (DLU/mm²) (36 days exposure)		Signal intensity ratios
Brain regions	Waiting time after injection	[¹⁴C] AA	[¹⁴C] anandmide	[¹⁴C] anandmide / [¹⁴C] AA
Cortex	10min	1.97E+06	9.45E+06	4.79
	100min	2.26E+06	1.10E+07	4.87
Hippocampus	10min	1.33E+06	5.84E+06	4.38
	100min	1.52E+06	7.06E+06	4.65
Ventricular epithelium	10min	3.74E+06	1.41E+07	3.76
	100min	5.84E+06	1.91E+07	3.27
Thalamus	10min	1.89E+06	8.25E+06	4.36
	100min	2.11E+06	9.92E+06	4.69
Striatum	10min	1.47E+06	6.66E+06	4.53
	100min	1.76E+06	8.26E+06	4.70

Table 1: absolute signal intensity ratios of radiotracer accumulation in the same brain regions reveal that accumulation of anandamide is higher than that of arachidonic acid.

Based on their structural similarity, we expected synaptamide and DHA to follow similar pattern. Indeed, we did find that brain synaptamide uptake was higher than that of DHA (table 2). The %uptake was evaluated using microdissection experiments. These observations may explain the potent action of synaptamide.

	%IA/g [^{14}C]DHEA	%IA/g [^{14}C]DHA	%IA/g [^{14}C]DHEA/[^{14}C]DHA
hypothalamus	**2.34**	**0.95**	**2**
olfactory tubule	**1.65**	**0.90**	**2**
hippocampus	**1.18**	**0.67**	**2**
striatum	**1.25**	**0.75**	**2**
cerebellum	**1.91**	**0.85**	**2**
brain stem	**2.29**	**0.88**	**3**
Cortex	**1.47**	**0.95**	**2**
thalamus	**1.19**	**0.83**	**1**
rest of the brain	**1.15**	**0.59**	**2**
midbrain	**2.95**	**0.93**	**3**
whole brain	**1.53**	**0.71**	**2**
blood	**2.10**	**1.25**	**2**

liver	**14.54**	**20.42**	**1**

Table 2: ratios of % DHA uptake and % synaptamide uptake in various brain regions. N=8.

***In vitro* uptake studies**

In order to extrapolate synaptamide uptake results observed *in vivo* and explain the functional effects observed *in vitro*, we want to perform uptake studies *in vitro* to determine the uptake of synaptamide and DHA as well as anandamide and arachidonic acid for comparison.

N27 cell line, used to evaluate the functional effects of DHA and synaptamide on neuritogenesis, was also used to perform the uptake studies. Since the functional effect was evaluated in cells differentiating under the influence of differentiating agents (dbcAMP and dehydroepiandosterone), we wanted to look at the uptake profiles in both undifferentiated and differentiating cells. We first performed these studies with anandamide as its uptake has been extensively studied in the past. We aimed to reproduce a linear range to look at its uptake to be able to compare it with that of arachidonic acid and in turn, extend this observation to understand the uptake of synaptamide and DHA.

Anandamide uptake is a saturable process and the saturation time depends on various factors such as cell density, concentration of anandamide added, accumulation of end products, presence of metabolizing enzymes, etc. Previous studies demonstrated that a linear uptake trend was observed within the first 10 minutes of substrate addition (Fowler, Tiger et al. 2004). We thus performed our uptake studies for 10 minutes – N27 cells were incubated with 200 nM [^{14}C – ethanolamine] Anandamide for 1, 2.5, 5 and 10 minutes. Cell pellets were harvested and lipids were extracted in chloroform. Anandamide is hydrolyzed by the membrane enzymes to release the [^{14}C – ethanolamine] which is water soluble and thus partitions into the aqueous phase The aqueous phase and an aliquot of the chloroform extract was used to quantify the radioactivity accumulated in the cell extracts using scintillation counting and another aliquot was used to perform a TLC to determine the chemical form of the radioactivity present in the cell extracts.

The scintillation counts from the aqueous phase of cell lipid extract revealed a time dependent accumulation of radioactivity – which indicates that the [**^{14}C** – ethanolamine] Anandamide is being hydrolyzed to release water soluble [^{14}C] ethanolamine in a time dependent manner (fig 6A and B). The scintillation counts from the chloroform extract also revealed a time dependent increase in radioactive accumulation in undifferentiated cells, but not in differentiating cells (fig 6A and B).

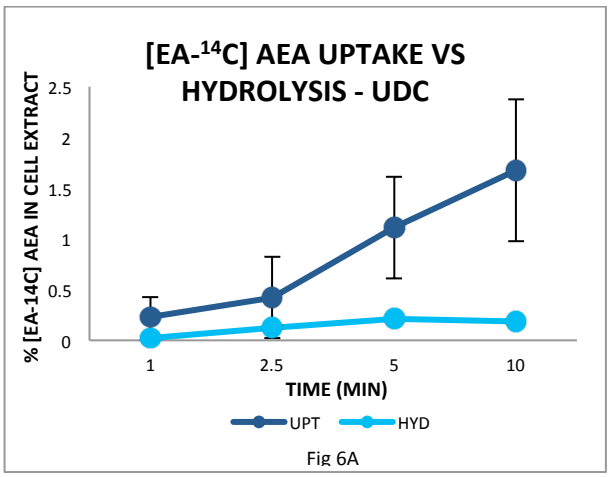

Fig 6A

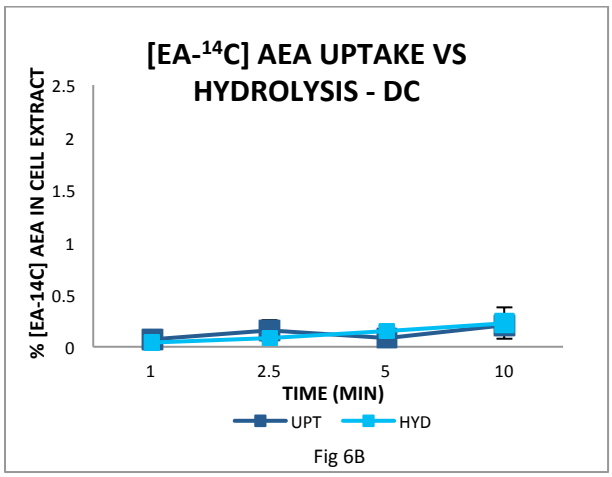

Fig 6B

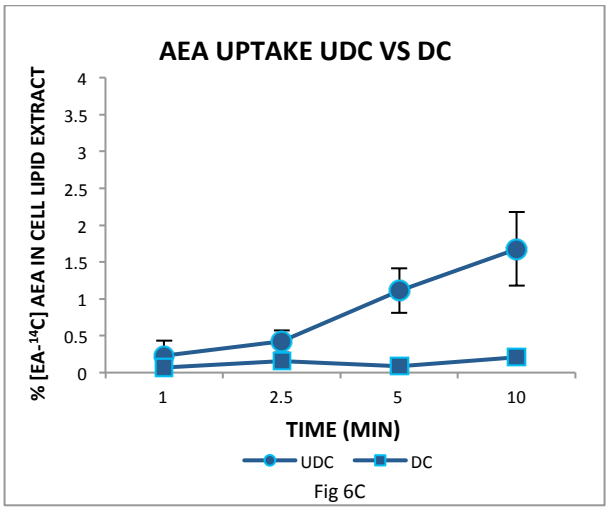

Fig 6C

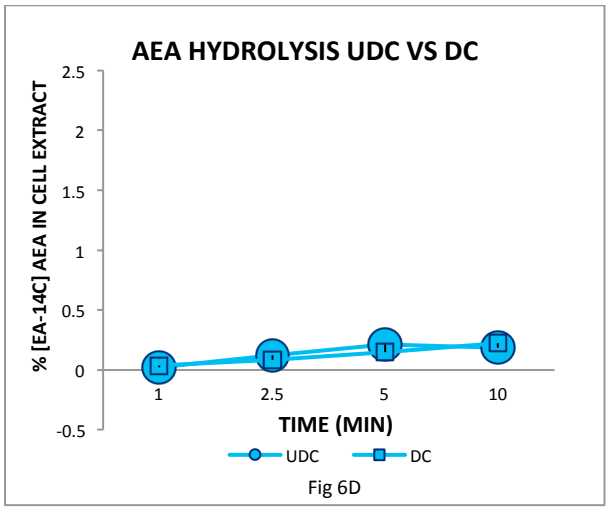

Fig 6D

Fig 6 *A*, [^{14}C] AEA uptake and hydrolysis in undifferentiated and *B*, differentiating N27 cells. Comparison of [^{14}C] Anandamide uptake *C*, and hydrolysis *D*, in undifferentiated and differentiated cells. Data is expressed in terms of % anandamide in cell lipid extract. *p<0.05; Error bars represent SD; *N=3.*

TLC analysis of the chloroform extract from undifferentiated cells showed that a part of radioactivity is intact anandamide. The chloroform extract was spotted against the standard radiotracer used to perform the uptake study. The RF values of the spots from the chloroform extract match with that of the standard indicating with some certainty that the part of radiotracer in the cell pellets is intact anandamide (fig 7A and B).

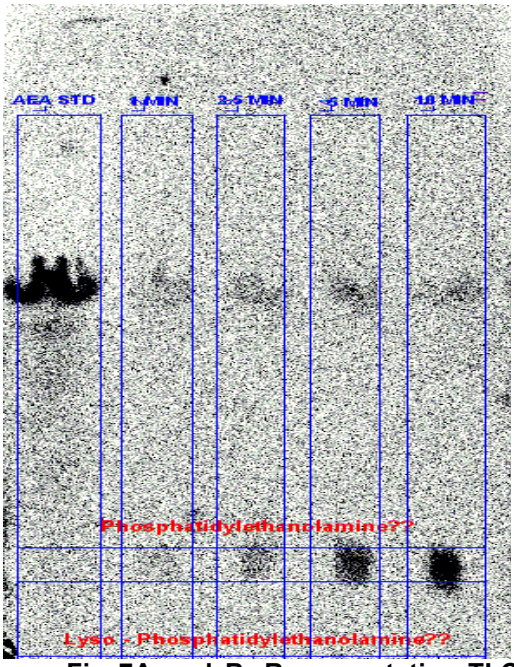

Fig 7A

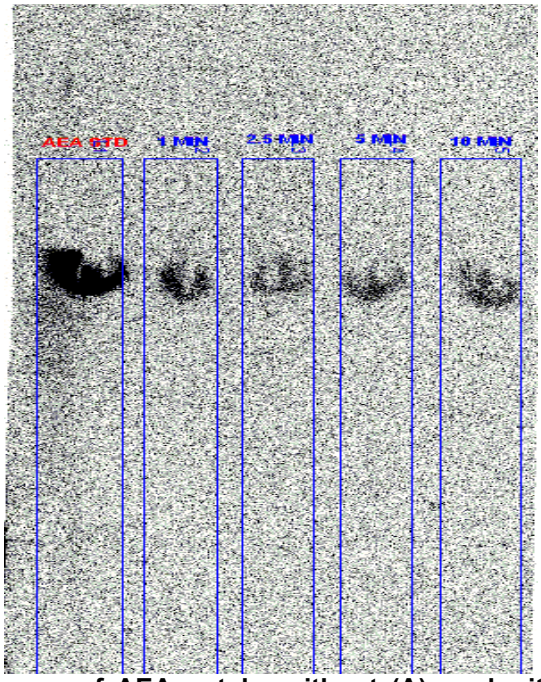

Fig 7B

Fig 7A and B. Representative TLC images of AEA uptake without (A), and with (B) inhibitor – PF3845 in undifferentiated N27 cells incubated with 200 nM [^{14}C] AEA.

Quantification of the spots shows that anandamide accumulation is time dependent (fig 8A). The chloroform extracts also revealed other hot spots. Since the radio tracer used was [**^{14}C** – ethanolamine] Anandamide, these spots are probably lipids – Phosphatidylethanolamine (PE), and lyso – Phosphatidylethanolamine (LYSO-PE) – that incorporated the radiolabelled ethanolamine (that was released upon anandamide hydrolysis) before it could escape into the aqueous phase (fig 7A). Quantification of the spots reveal a time dependent increase in intensity indicating increased incorporation of the label into the lipid with time (fig 8B).

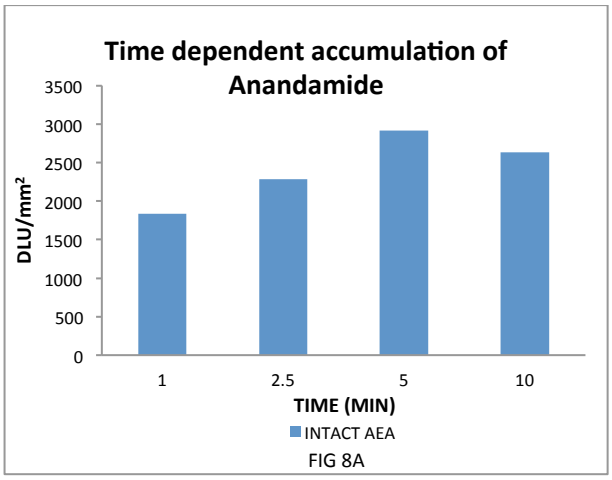

FIG 8A

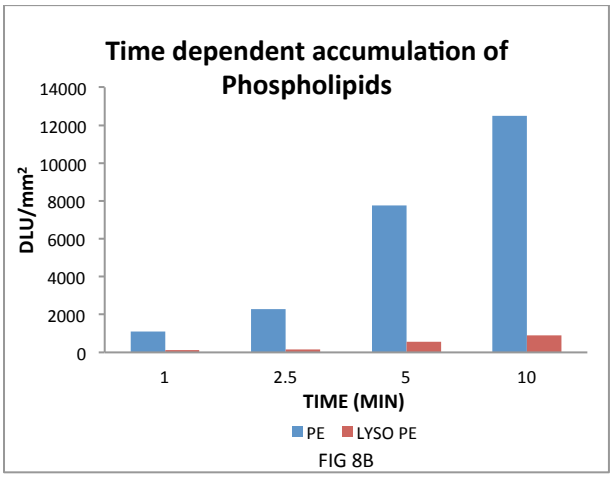

FIG 8B

Fig 8A and B. Quantification of hot spots from TLC images of chloroform extract of undifferentiated N27 cells incubated with 200 nM [C-14] AEA revealed a time dependent accumulation of AEA *A*, and phospholipids *B*.

As we noticed different uptake profiles for AA and AEA in vivo, we wanted to compare the same *in vitro*. So we repeated the uptake studies with 200 nM [C-14] AA and observed the uptake patterns in undifferentiated and differentiating cells (fig 9). TLC analysis showed that the radioactive content in cell extracts is not from free arachidonic acid, but from anandamide and other phospholipids that arachidonic acid might have incorporated into (fig).

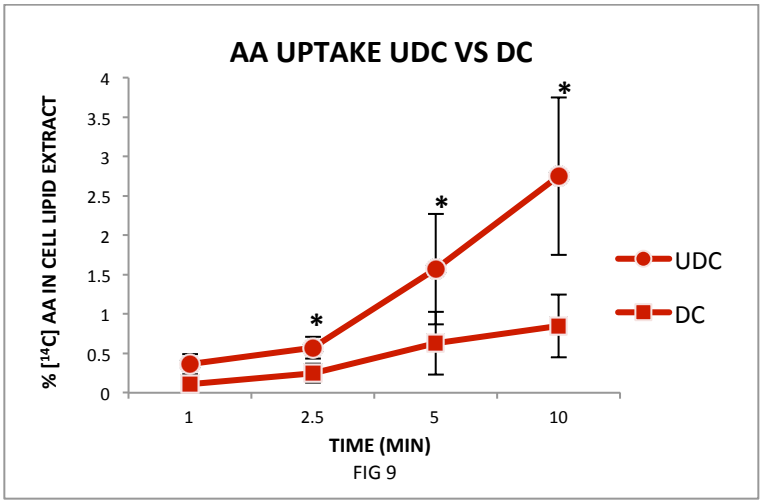

Fig 9. AA uptake in undifferentiated and differentiating N27 cells. Data is expressed in terms of % arachidonic acid in cell lipid extract. *p<0.05; Error bars represent SD; *N=3.*

To our surprise, we found that the uptake rate of arachidonic acid was similar to that of anandamide in undifferentiated cells (fig 10A). In differentiating cells, we observed that the uptake rate of arachidonic acid is higher than that of anandamide (fig 10B) which contradicts our observation *in vivo.*

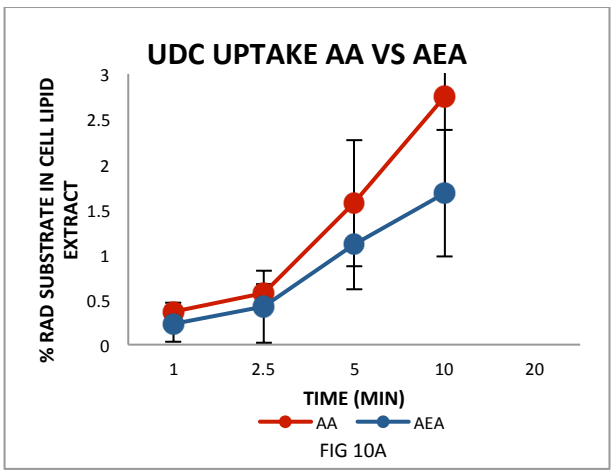

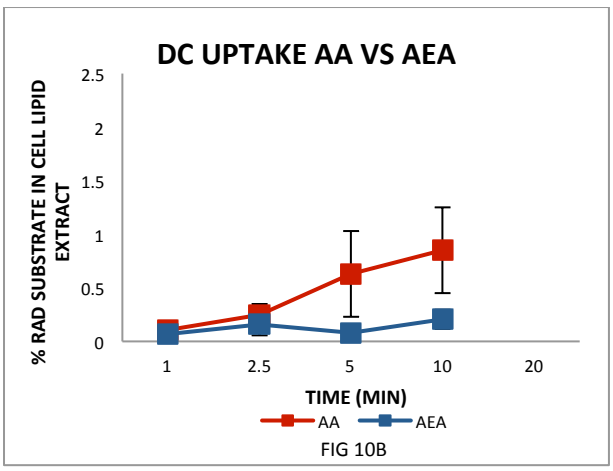

Fig 10. Comparison of [^{14}C] AA and [^{14}C] AEA uptake in undifferentiated, *A*, and differentiating, *B*, N27 cells. Data is expressed in terms of % radiotracer in cell lipid extract. *p<0.05; Error bars represent SD; *N=3.*

Anandamide uptake has been a subject of great controversy. Anandamide transport can be explained in a three step process – adsorption, transmembrane transport and desorption. The details of the transmembrane transport are not clear yet. There is a lot of evidence in support of as well as against the presence of an independent anandamide transporter. While some studies point to a FAAH (fatty acid amide hydrolase, major catabolic enzyme of endocannabinoids) independent transporter, others believe a variant of FAAH is responsible for its transport. Metabolism by FAAH into arachidonic acid and ethanolamine theoretically drives the uptake of anandamide into the cell. This again is a saturable, temperature dependent process. To understand the role of FAAH in determining the uptake pattern of anandamide in differentiating cells, we pre-incubated the cells with a specific FAAH inhibitor, PF 3845 and carried out lipid extraction and TLC analyses as before.

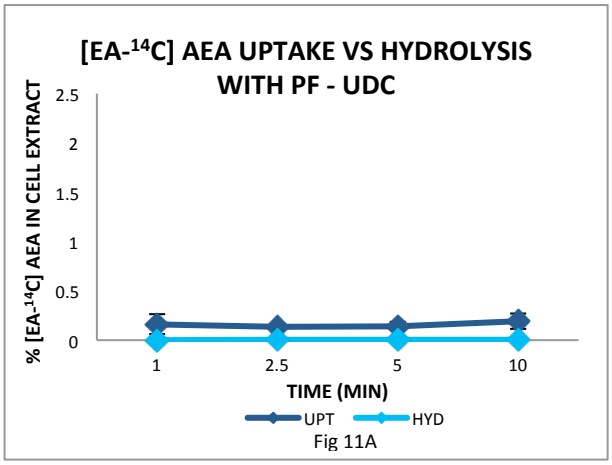

Fig 11A

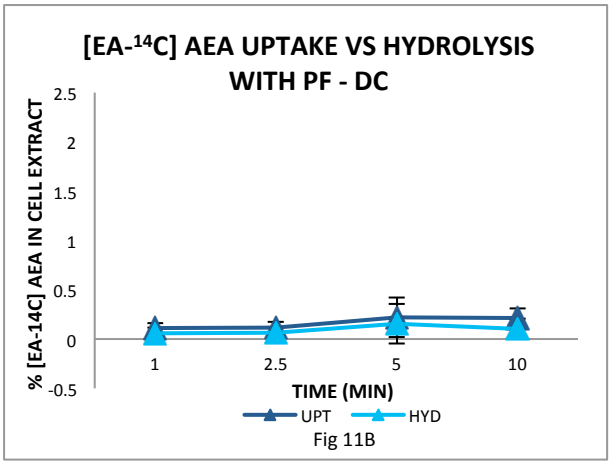

Fig 11B

Fig 11 Comparison of [^{14}C] AEA uptake and hydrolysis in undifferentiated, *A*, and differentiating, *B*, N27 cells pre-incubated with PF3845. Data is expressed in terms of % radiotracer in cell lipid extract. *p<0.05; Error bars represent SD; *N=3.*

With inhibitor pre-incubation, there was a significant decrease in anandamide uptake in undifferentiated cells suggesting that hydrolysis by FAAH is the major driving force for anandamide uptake (fig 11A and 12A). In differentiating cells FAAH inhibition did not seem to have an effect on AEA uptake or hydrolysis (fig 12C and 12D). This suggests that on differentiation, the N27 cells develop a FAAH independent uptake mechanism.

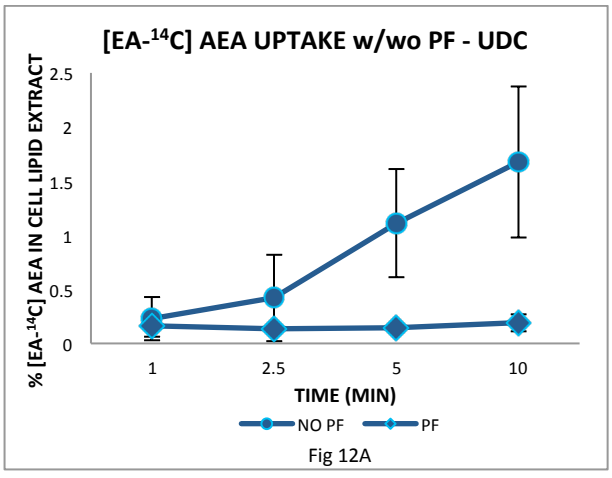

Fig 12A

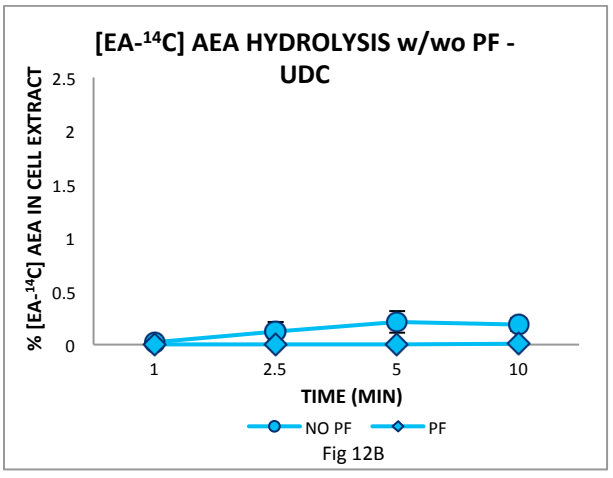

Fig 12B

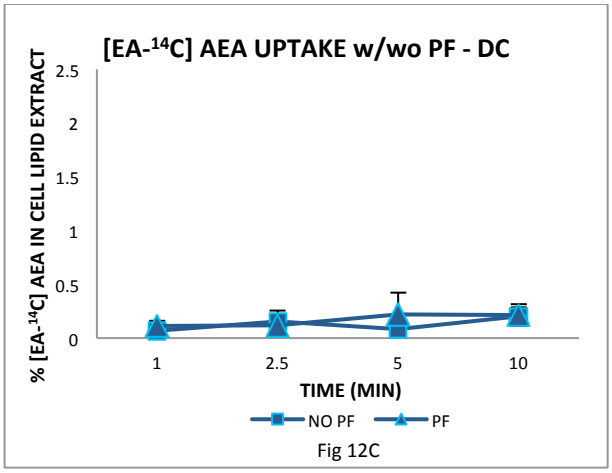

Fig 12C

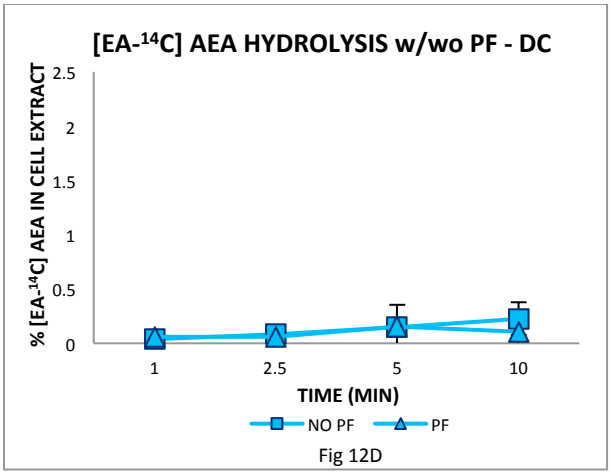

Fig 12D

Fig 12 Comparison of [^{14}C] AEA uptake (*A)* and hydrolysis *(B)* with or without PF3845 in undifferentiated (*A* and *B)* and differentiating (*C* and *D*) N27 cells. Data is expressed in terms of % anandamide in cell lipid extract. *p<0.05; Error bars represent SD; *N=3.*

Although the results for AA and AEA uptake are quite different from what were observed in vivo, we wanted to see if DHA and synaptamide uptake are similar to or different from in vivo studies and/or the *in vitro* AA – AEA uptake studies.

Since very little is known about synaptamide uptake, the same conditions used to determine AEA uptake were used to study synaptamide uptake and compare it with DHA uptake. Undifferentiated and differentiating N27 cells are incubated with 200 nM [EA-^{14}C] synaptamide for 1, 2.5, 5, 10 and 20 minutes. After incubation, the cell pellets are subjected to folch extraction and the collected organic and aqueous phases were analyzed for radiolabel distribution and quantification.

Scintillation analysis of both – organic and aqueous phases of undifferentiated cells shows that the radio label accumulation increases with time (Fig 13A). In contrast, in differentiating cells, the uptake seems to be independent of time (fig 13 B).

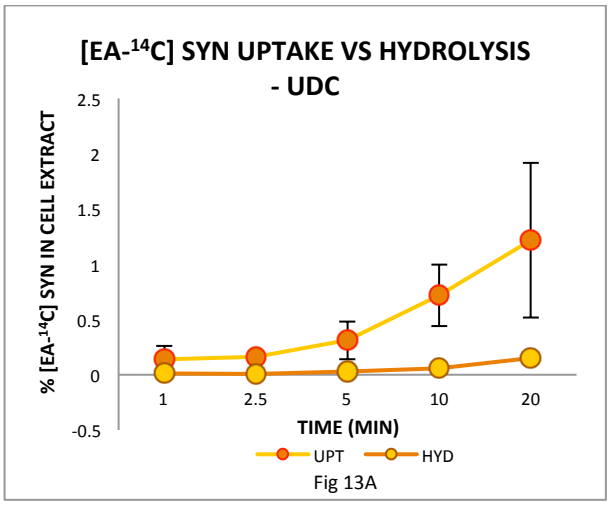

Fig 13A

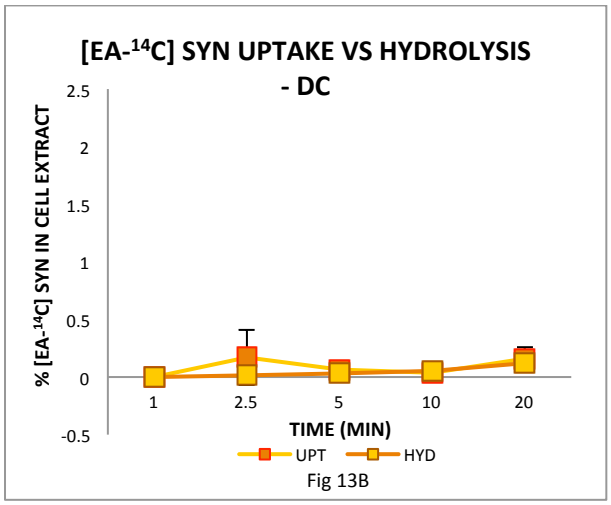

Fig 13B

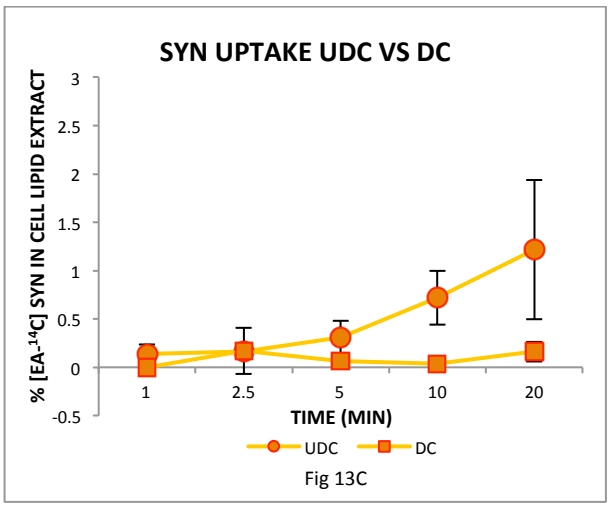

Fig 13C

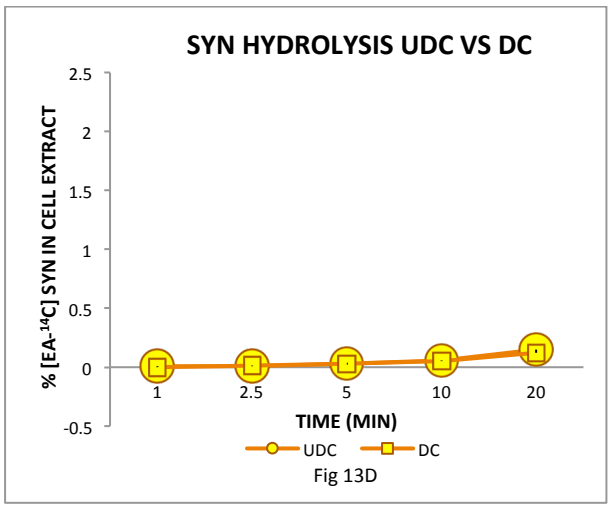

Fig 13D

Fig 13 Comparison of [^{14}C] synaptamide uptake and hydrolysis in undifferentiated (*A)* and differentiating *(B)* N27 cells. Comparison of synaptamide uptake (*C)* and hydrolysis (*D) in undifferentiated and differentiating N27 cells*. Data is expressed in terms of % synaptamide in cell lipid extract. *p<0.05; Error bars represent SD; *N=3.*

Synaptamide uptake pattern is similar to that of anandamide, but its uptake is lower in both undifferentiated and differentiating cells (fig 14 A and B). On comparing the hydrolysis of both anandamide and synaptamide, in undifferentiated and differentiating cells, the rate of hydrolysis of anandamide is significantly higher than that of synaptamide (fig 14 C and D; p<0.05). This suggests that the enzyme that hydrolyses NAEs hydrolyze anandamide preferentially.

The TLC analysis of synaptamide chloroform extract revealed a very similar profile to that of anandamide indicating that most of the synaptamide taken up was incorporated into phospholipids. This incorporation was time dependent.

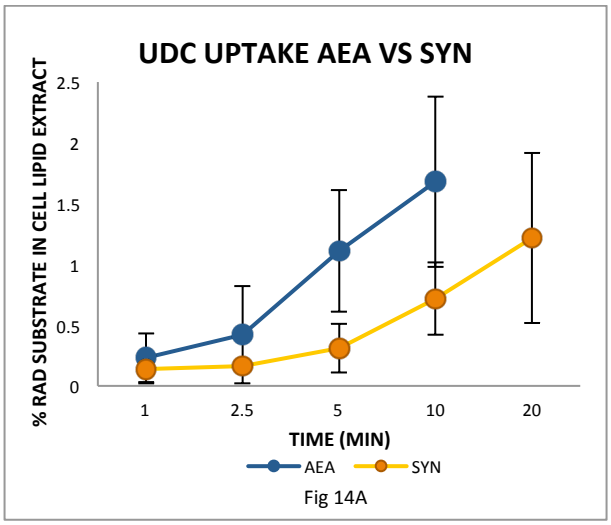

Fig 14A

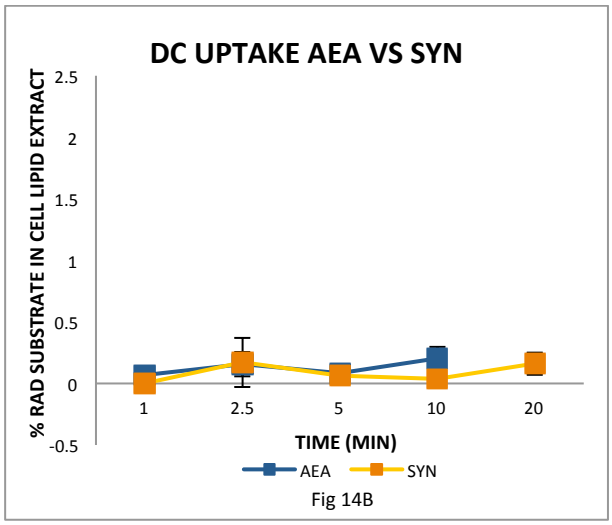

Fig 14B

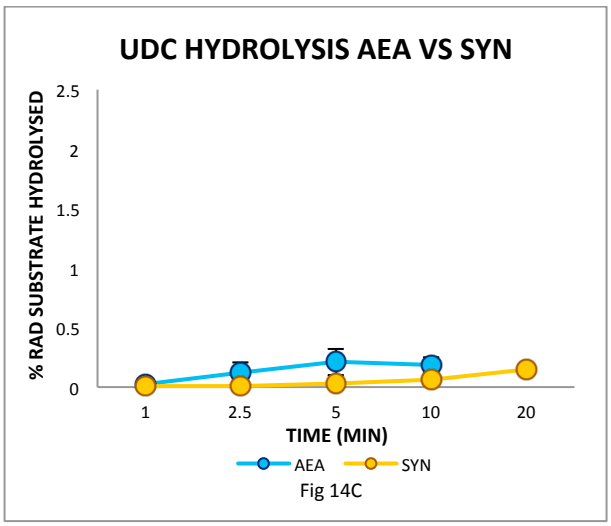

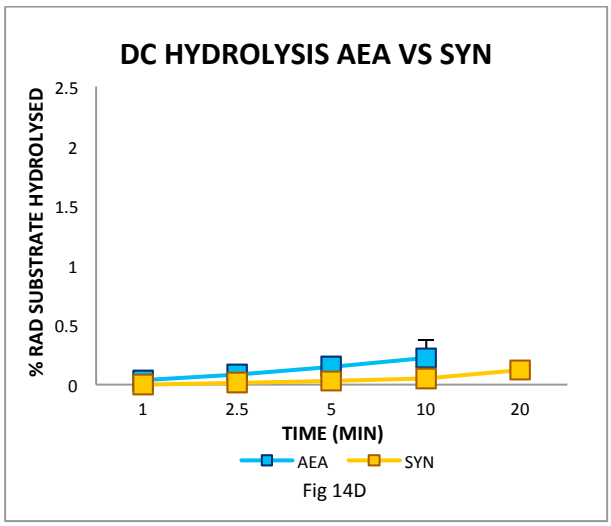

Fig 14 Comparison of [^{14}C] AEA and [^{14}C] synaptamide uptake (*A and B)* and hydrolysis *(C and D)* in undifferentiated (*A* and C) and differentiating (B and *D)* N27 cells. Data is expressed in terms of % radiotracer in cell lipid extract. *p<0.05; Error bars represent SD; *N=3.*

Uptake studies in N27 cells are repeated after pre-incubation with the FAAH inhibitor, PF3845. The results were similar to those observed with anandamide. In undifferentiated cells synaptamide uptake and hydrolysis rates are significantly lower when FAAH is inhibited, while in differentiating cells, there is no significant difference in both processes whether FAAH is present or inhibited (fig 15A and B).

This indicates that FAAH, which is known to hydrolyze various N-acylethanolamines, is responsible for hydrolyzing synaptamide into DHA and ethanolamine. The fatty acid released is quickly incorporated into phospholipids just as arachidonic acid. The TLC of organic phase from FAAH-inhibited cell pellets showed no label incorporation into phospholipids justifying the role of FAAH in hydrolyzing it into DHA and ethanolamine.

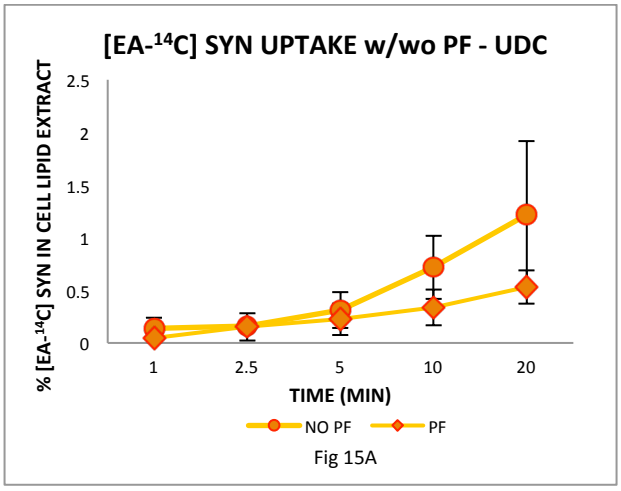

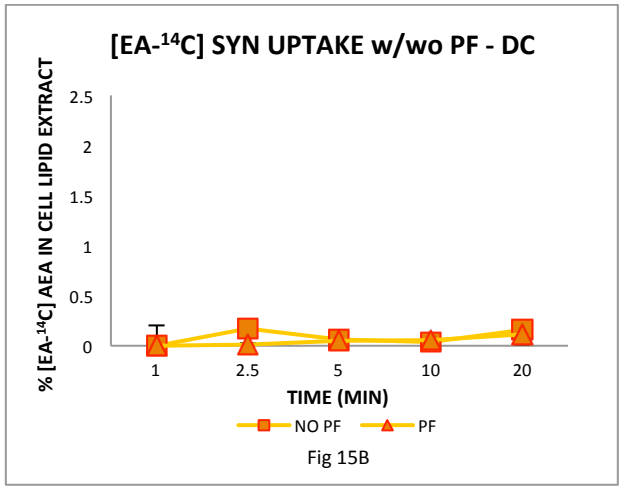

Fig 15: Comparison of [^{14}C] synaptamide uptake in undifferentiated (*A)* and differentiating *(B)* N27 cells pretreated with or without PF3845. Data is expressed in terms of % synaptamide in cell lipid extract. *p<0.05; Error bars represent SD; *N=3.*

In vivo uptake of DHA and synaptamide showed that synaptamide uptake is at least 2 fold higher than that of DHA. Similar profile was observed with AA and AEA. *In vitro* AA and AEA uptake studies resulted in opposite results where AA uptake was higher than that of AEA. In order to verify if the uptake of DHA is higher *in vitro* when compared to synaptamide, uptake studies are performed using [^{14}C] DHA.

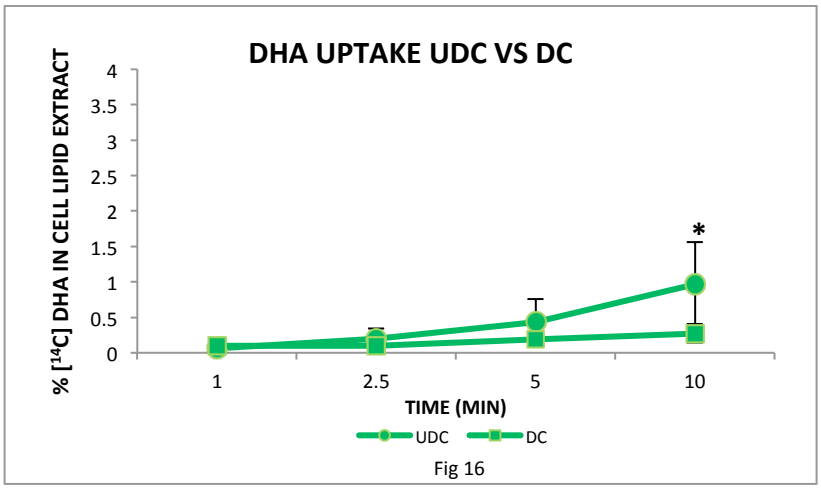

Fig 16: Comparison of [^{14}C] DHA uptake in undifferentiated and differentiating N27 cells. Data is expressed in terms of % DHA in cell lipid extract. *p<0.05; Error bars represent SD; *N=3.*

Like AA uptake, DHA uptake was higher in undifferentiated cells when compared with differentiating cells. While the uptake rate of DHA was lower than AA in both undifferentiated and differentiating cells (fig 17 A and B), it was similar to that of synaptamide in undifferentiated cells but higher in differentiating cells (fig 17 C and D).

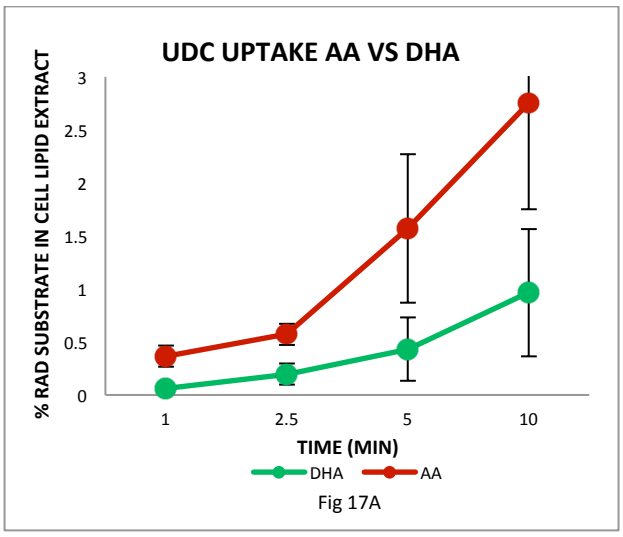

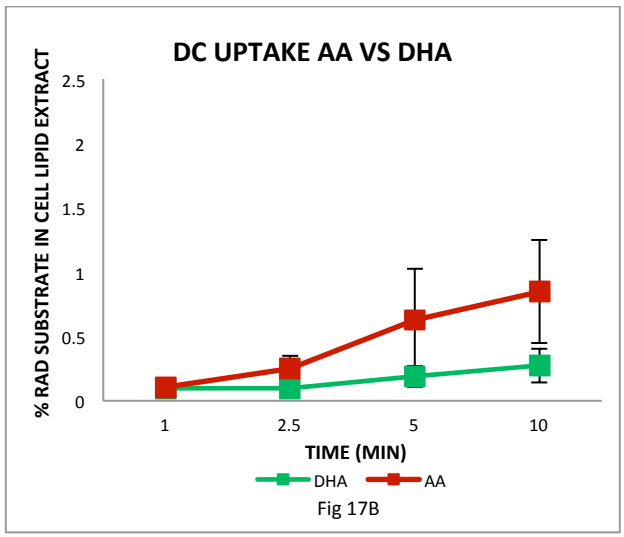

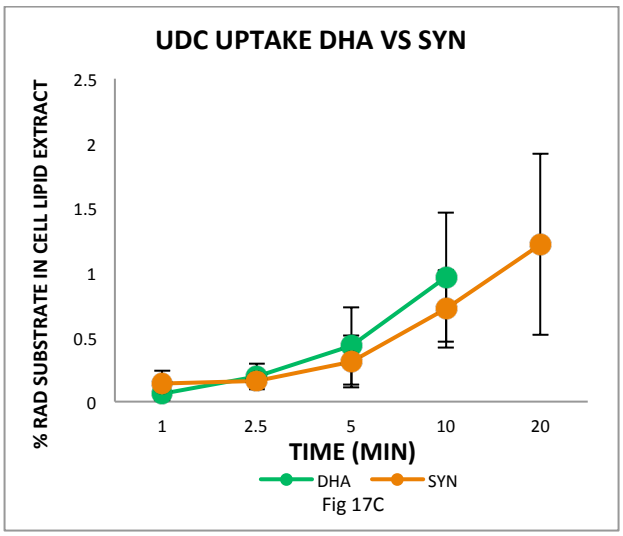

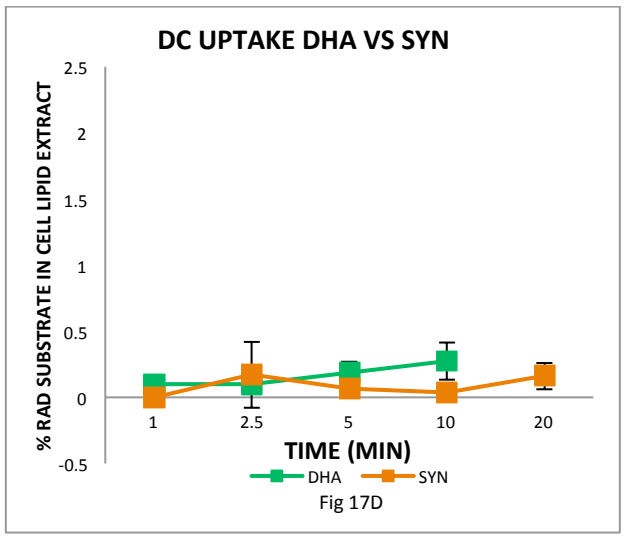

Fig 17: Comparison between [^{14}C] AA and [^{14}C] DHA uptake (A and B); and [^{14}C] DHA and synaptamide uptake (C and D) in undifferentiated (*A and C)* and differentiating *(B and D)* N27 cells. Data is expressed in terms of % radiotracer in cell lipid extract. *p<0.05; Error bars represent SD; *N=3.*

Discussion and relevance: Previous in vivo work using [C-14] AA and [C-14] anandamide from our lab demonstrate that the two tracers have similar uptake profiles in the brain. However, the accumulation of radioactivity with use of [C-14] anandamide is 3 to 5 fold higher than that produced with use of [C-14] AA. This phenomenon suggests that AA (a fatty acid with negative charge and higher polarity than anandamide) does not penetrate the blood brain barrier as well as anandamide. DHA (analogous to AA) and synaptamide (analogous to anandamide) are both expected to show a pattern similar to AA and anandamide respectively, and the pattern indeed was similar with synaptamide uptake being atleast 2 fold higher than that of DHA.

We failed to replicate this observation *in vitro*. The uptake rates of AA and DHA were found to be higher when compared with anandamide and synaptamide. This suggests that specialized uptake mechanisms present in *in vivo* environments are absent *in vitro*. As several studies established previously, *in vitro* fatty acid uptake is based on either the process of simple diffusion or the presence of transporter proteins, or a combination of both. The *in vitro* system is not a dynamic system – there is no blood flow that provides the cells with a concentration gradient or to remove the accumulated end points. This reinforces the fact that *in vitro* uptake is a saturable process because without continuous clearance of end products, there is a decrease in the corresponding uptake process.

AA and DHA have higher uptake in undifferentiated N27 cells; uptake of AA being higher than that of DHA. Fatty acid uptake in cells is driven by a combination of simple diffusion followed by their utilization (binding or metabolism) (Kamp and Hamilton 2006). Their utilization (and hence uptake) however depends on membrane enzymes such as the phospholipases and acyl-CoAs. These enzymes partition the available free fatty acids into different metabolic fates (Kalant D 2004). Phospholipases, specifically phospholipase A2s are responsible for releasing free AA and DHA from membrane phospholipids and Acyl Co-A synthase (ACS) enzymes are responsible for “fixing” the fatty acid in the cell (Mashek, Li et al. 2007). Consequently, the expression and activity of the specific phospholipases and ACS enzymes determine the fatty acid uptake and incorporation. The release of AA and DHA from membrane phospholipids is

mediated by two separate phospholipases – calcium dependent cPLA2 is responsible for the release of AA and calcium independent (inducible) iPLA2 specifically releases DHA (Strokin, Sergeeva et al. 2003). The expression of these enzymes establishes the required concentration gradient which drives the uptake of fatty acids. The released fatty acid is either incorporated into other phospholipids or triglycerides, or is metabolized by a set of enzymes (LOX, COX, CYP450s, etc.) which generate second messengers that can start a cascade of cellular functions (Rosa and Rapoport 2009). This consumption of fatty acids maintains their continuous influx simulating the "dynamism" of *in vivo* environments.

According to literature, 70% of PLA2 activity can be attributed to iPLA2 with its highest activity recorded in striatum followed by hypothalamus and hippocampus while cPLA2 is uniformly distributed all over the brain with a slightly increased activity in cerebellum (Yang, Mosior et al. 1999, Farooqui and Horrocks 2004). Among various ACS enzymes, ACS6 is highly expressed in brain tissues. This enzyme has a substrate specificity towards very long chain fatty acids (>C20), specifically to DHA (Marszalek, Kitidis et al. 2005). This translates to the fact that more DHA is preferentially incorporated into the membrane and very little is available to be metabolized. AA, in turn, is metabolized a little more and hence its accumulation into the membrane is slightly less than DHA. As a result, the turnover of AA is more than that of DHA. We observed a higher AA uptake over DHA in N27 cells which was lost with time. The relative expression of ACS6, PLA2 or COX and LOX in N27 cells is unknown and hence it is difficult to explain the higher AA uptake observed.

Anandamide and synaptamide have similar uptake profiles in N27 cells as their corresponding fatty acids. This is in contrast to what was observed in vivo where these ethanolamine containing fatty acid acids are taken up to a higher extent. Metabolism of these compounds inside the cells is expected to be the driving force of these compounds. However, when compared to anandamide, the uptake of synaptamide was pretty low suggesting that its metabolism in N27 cells is less than that of anandamide. It is a well-known fact that anandamide is the preferred substrate of fatty acid amide hydrolase (FAAH), a serine hydrolase which is usually associated with the inner cell membrane. In some cell lines it has been shown that anandamide transport was indeed mediated by modulating FAAH activity (Day, Rakhshan et al. 2001, Fowler, Tiger et al. 2004). We hypothesize that in N27 cells too, anandamide incorporates itself into the membrane by either a flip flop mechanism or some kind of a transporter making it accessible to the membrane associated FAAH which then hydrolyses it into its corresponding fatty acid (AA) and ethanolamine, thus creating a concentration gradient that drives the uptake of more anandamide into the cell. To confirm that it is indeed FAAH that is hydrolyzing anandamide and influencing its uptake, the cells were pre-incubated with a specific, irreversible FAAH inhibitor – PF3845. Blocking FAAH activity markedly decreased anandamide uptake as well as hydrolysis thus substantiating our hypothesis. Structurally similar to anandamide, it is expected that synaptamide undergoes a similar process. Combining the facts – synaptamide uptake being less than that of anandamide with a further decrease in synaptamide uptake with PF3845 administration – it can be suggested that synaptamide is a substrate for FAAH, albeit a poor substrate and thus its uptake profile can be explained.

Consistent with the above observations, analysis of chloroform extract of undifferentiated cells incubated with arachidonic acid and DHA did reveal synthesis of phospholipids as well as N-acylethanolamines but no free fatty acid suggesting that there is a rapid conversion of free fatty acids into their metabolites providing a concentration gradient for their uptake. Similar metabolism is noticed in cells incubated with the N-acyl ethanolamines. However, pretreatment of the cells with PF3845 decreased phospholipid formation from N-acylethanolamines indicating that less free fatty acid is available to be converted into phospholipids.

Differentiation of N27 cells was initiated by adding dibutrylcyclicAMP (dbcAMP) and dehydroepiandosterone to the cells. The uptake of fatty acids decreased considerably with the onset of differentiation. dbcAMP is one of the agents that catalyzes the activity of iPLA2 and increases the release of DHA (Strokin, Sergeeva et al. 2003). The decrease of DHA in the lipid extracts of differentiated cells when compared to undifferentiated cells may be explained by the fact that the amount of DHA released from the membrane is more rapid and consistent with addition of dbcAMP than the amount of DHA being reincorporated. Increase in dbcAMP has no effect on the activity of cPLA2 and the release of AA (Strokin, Sergeeva et al. 2003).

Under normal conditions, N27 cells have a small nucleus and large cytoplasm – Undifferentiated N27 cells are flat cells with high cytoplasm to nucleus ratio. On differentiation, the cells become more rounded, with decreased surface area and there is a large decrease in the cytoplasm to nucleus ratio. As the process of diffusion is proportional to the surface area of the cell, it may be suggested that the amount of fatty acid diffusing into the differentiating cell is less than that of the undifferentiated cell.

While the decreased uptake of DHA in differentiated cells may be explained based on above observations, it is still unclear why AA uptake is lower in differentiated cells. The drop in surface area of the cells may contribute a little, but is not sufficient to explain the drastic decrease.

The uptake profiles of both *N*-acylethanolamines in N27 cells decreased as the cells underwent differentiation. Uncertain of whether this decrease is because of the changes in morphology of the cells or because of the change in hydrolytic enzyme expression, experiments were repeated after pre incubating differentiated cells with PF3845. Surprisingly there was no difference in the uptake profiles when FAAH activity was blocked. It can thus be inferred that the onset of differentiation modulates the activity of FAAH in a way that the uptake of the *N*-acylethanolamines becomes FAAH independent. All the changes N27 cells undergo during differentiation have not yet been documented, and some light needs to be shed on that to explain the FAAH independent uptake process in differentiating cells.

References

1. Day, T. A., F. Rakhshan, D. G. Deutsch and E. L. Barker (2001). "Role of fatty acid amide hydrolase in the transport of the endogenous cannabinoid anandamide." Mol Pharmacol **59**(6): 1369-1375.
2. Farooqui, A. A. and L. A. Horrocks (2004). "Brain phospholipases A2: a perspective on the history." Prostaglandins Leukot Essent Fatty Acids **71**(3): 161-169.
3. Fowler, C. J., G. Tiger, A. Ligresti, M. L. Lopez-Rodriguez and V. Di Marzo (2004). "Selective inhibition of anandamide cellular uptake versus enzymatic hydrolysis--a difficult issue to handle." Eur J Pharmacol **492**(1): 1-11.
4. Kalant D, C. K. (2004). "Regulation of fatty acid transport." Curr Opin Lipidol **15**: 309-314.
5. Kamp, F. and J. A. Hamilton (2006). "How fatty acids of different chain length enter and leave cells by free diffusion." Prostaglandins Leukot Essent Fatty Acids **75**(3): 149-159.

6. Marszalek, J. R., C. Kitidis, C. C. Dirusso and H. F. Lodish (2005). "Long-chain acyl-CoA synthetase 6 preferentially promotes DHA metabolism." J Biol Chem **280**(11): 10817-10826.
7. Mashek, D. G., L. O. Li and R. A. Coleman (2007). "Long-chain acyl-CoA synthetases and fatty acid channeling." Future Lipidol **2**(4): 465-476.
8. Rosa, A. O. and S. I. Rapoport (2009). "Intracellular- and extracellular-derived Ca(2+) influence phospholipase A(2)-mediated fatty acid release from brain phospholipids." Biochim Biophys Acta **1791**(8): 697-705.
9. Strokin, M., M. Sergeeva and G. Reiser (2003). "Docosahexaenoic acid and arachidonic acid release in rat brain astrocytes is mediated by two separate isoforms of phospholipase A2 and is differently regulated by cyclic AMP and Ca2+." Br J Pharmacol **139**(5): 1014-1022.
10. Yang, H. C., M. Mosior, C. A. Johnson, Y. Chen and E. A. Dennis (1999). "Group-specific assays that distinguish between the four major types of mammalian phospholipase A2." Anal Biochem **269**(2): 278-288.